AD NUMBER

AD437911

LIMITATION CHANGES

TO:

Approved for public release; distribution is unlimited.

FROM:

Distribution authorized to U.S. Gov't. agencies only; Administrative/Operational Use; MAR 1964. Other requests shall be referred to Office of Naval Ressearch, Arlington, VA 22203.

AUTHORITY

ONR ltr 28 Jul 1977

AD 437911L

SU-SEL-64-022

Spatial Properties of Amplitude Fading of Continuous 17-Mc Radio Waves

by
John W. Ames

March 1964

Technical Report No. 87

Prepared under
Office of Naval Research Contract
Nonr-225(64), NR 088 019, and
Advanced Research Projects Agency ARPA Order 196-64

RADIOSCIENCE LABORATORY

STANFORD ELECTRONICS LABORATORIES

STANFORD UNIVERSITY • STANFORD, CALIFORNIA

SEL-64-022

SPATIAL PROPERTIES OF AMPLITUDE FADING OF CONTINUOUS 17-Mc RADIO WAVES

By

John W. Ames

March 1964

Technical Report No. 87

Prepared under
Office of Naval Research Contract
Nonr-225(64), NR 088 019, and
Advanced Research Projects Agency ARPA Order 196-64

Radioscience Laboratory
Stanford Electronics Laboratories
Stanford University Stanford, California

DDC AVAILABILITY NOTICE

All distribution of this report is controlled. Qualified DDC users shall request with certification of "Need-to-Know" from the cognizant military agency of their project or contract through:

Office of Naval Research
Department of the Navy
Washington 25, D.C.
Attn: Code 418

This document may be reproduced to satisfy official needs of U.S. Government agencies. No other reproduction authorized except with permission of:

Office of Naval Research
Department of the Navy
Washington 25, D.C.
Attn: Code 418

ABSTRACT

The experiment presented here was undertaken in order to contribute to the understanding of the mechanisms of radio-wave fading and to suggest possible improvements in present techniques of alleviating the undesirable effects of such fading.

Observations were made of the spatial distribution along the ground in the vicinity of a receiver of the magnitude of ionospherically propagated 17-Mc, cw, radio waves. To accomplish this the amplitude fluctuation, or fading, of cw signals transmitted 1840, 3741, and 5724 km from Texas, Hawaii, and Puerto Rico was observed at Stanford, California, on 12 dipole antennas evenly disposed in two perpendicular rows each about 20 wavelengths long. The number of ionospheric reflections experienced by the radio wave over the Texas- and Hawaii-to-Stanford paths was measured by means of a synchronized, oblique, step-frequency sounding system.

The spatial distribution of signal amplitude is found to exhibit a degree of periodicity that varies inversely with path length. Fading-null patterns, equivalent to optical diffraction patterns, consisting of nearly straight lines are observable 33 percent of the time on a signal propagated 1840 km and 10 percent of the time on a signal propagated 5740 km.

For a fixed path length the spacing along the ground between signal-amplitude minima decreases as the number of ionospheric reflections increases. The mean value of null spacing observed on signals propagated 3741 km from Hawaii varies from 1.4 km during periods of only one ionospheric reflection to 0.4 km during periods in which three ionospheric reflections are present. The observed fading nulls tend to lie diagonally across the great circle connecting the transmitter and receiver.

A mathematical model is constructed that shows how the spacing and orientation of signal nulls depends upon the angular elevations and bearings of the incoming rf wavefronts. This model correctly predicts the spacing and orientation of nulls in observed periodic fading

patterns if the arriving rf wavefronts are assumed to be deviated a few degrees to the south of the great circle by a small north-south downward tilt in the structure of the ionosphere.

Two observations made during periods of geomagnetic disturbance suggest that during the first 10 hours of the disturbance the ionospheric tilt is less than normal and that during the remainder of the storm the tilt is somewhat greater than normal. During one of the storms the small random variations in ionization density that cause irregular fading patterns appear to have been much smaller than normal.

The fact that average fading-null orientations can be predicted from a knowledge of the prevailing ionospheric tilt suggests a placement of space-diversity antennas that can be as much as twice as effective as present antenna layouts for moderate-length, east-west paths at no increase in equipment cost.

CONTENTS

CONTENTS (Continued)

TABLES

ILLUSTRATIONS

ILLUSTRATIONS (Continued)

ILLUSTRATIONS (Continued)

SYMBOLS AND ABBREVIATIONS

A, B, C	direction cosines of a wave normal
c	velocity of electromagnetic waves in free space (m/sec)
D	ground spacing between fading nulls (km)
e	electronic charge (coulombs)
1F,2F,etc.	ray designations
f	radio-wave frequency (cps)
F	single-antenna signal-fading rate
hf	high frequency--the range of radio frequencies between 3 and 30 Mc
i	angle of incidence of a wave normal
k_o	permittivity of free space--8.85×10^{-12} farads/meter
LPA	logarithmic periodic antenna
m_e	electronic mass (kg)
MOF	maximum observed frequency
N	electron density (electrons/m^3)
n	refractive index
P	length of ray path
V	apparent velocity along the ground of fading nulls (km/sec)
v_p	phase velocity of electromagnetic waves
β	phase constant of a wave
η	elevation angle of approaching plane wave
θ	bearing angle of approaching plane wave
λ	wavelength of rf waves
μ_o	permeability of free space--$4\pi \times 10^{-7}$ henry/meter

π	3.1416
ρ	perpendicular distance from an observer to an approaching plane wavefront
Ψ	direction of perpendicular to fading nulls as observed at the ground; $\Psi = 0$ is the direction from the receiver to the transmitter
ω	radian-wave frequency

ACKNOWLEDGMENT

The research reported here was supported entirely by Office of Naval Research Contract Nonr 225 (64) under ARPA Order 196-64, for which the author wishes to express his appreciation.

The author also wishes to acknowledge the assistance and encouragement of Professor O. G. Villard, Jr. in the planning of this experiment and the criticism of the manuscript. In addition, the nature of radio propagation experiments makes their success dependent on the generous assistance of a great number of people in widely separated parts of the world. The transmitting equipment was operated by Professor Braulio Dueño at the University of Puerto Rico, Professor Harold Spuhler at the Texas Technological College, and Mssrs. Gerry Hall and Arthur Weekly of Raytheon Company at Pahoa, Hawaii.

At Stanford, Mr. Lloyd Griffiths was a great help in reducing the raw data from Texas, as was Mrs. Kathy Shanahan in performing numerical computations and machine data plotting using the Stanford IBM 7090 computer, which was in part subsidized by NSF Grant GP 948. Professor Villard's office staff under the direction of Miss Myrna Kennady has shown great patience in typing and re-typing of the manuscript.

I. INTRODUCTION

A. BRIEF DESCRIPTION OF IONOSPHERIC RADIO WAVE PROPAGATION

The ionosphere is the region of the upper atmosphere that contains partly ionized gas and that extends from about 80 km above the earth's surface to a region of maximum ion density at about 300 km, above which the ion density decreases. The refractive index n of the region is given by

$$n = \frac{c}{v_p} = \left(\frac{\mu k}{\mu_o k_o} \right)^{1/2} \qquad (1)$$

where

c = free-space velocity of electromagnetic waves, 3×10^8 m/sec

v_p = phase velocity of electromagnetic waves in a region of refractive index n

μ_o = permeability of free space = $4\pi \times 10^{-7}$ henry/m

k_o = permittivity of free space = 8.85×10^{-12} farads/m

If the earth's magnetic field is neglected,

$$\mu = \mu_o$$

$$n = \left(\frac{k}{k_o} \right)^{1/2},$$

The motion of free electrons results in a modified permittivity,

$$k = k_o - \frac{Ne^2}{m_e \omega^2},$$

where

N = electron (or ion) density (electrons/m^3)

e = electronic charge = 1.60×10^{-19} coulombs

m_e = electronic mass = 9.11×10^{-31} kg

ω = radian wave frequency

Therefore,

$$n = \left(1 - \frac{Ne^2}{m_e k_o \omega^2}\right)^{1/2} \qquad (2)$$

Since N increases with height, the refractive index decreases with height and Snell's law of refraction, Eq. (3), shows that electromagnetic waves directed obliquely at the ionosphere are refracted down.

$$n_1 \sin i_1 = n_2 \sin i_2 \qquad (3)$$

where $i \triangleq$ angle of incidence on the interface between regions of refractive index n_1 and n_2.

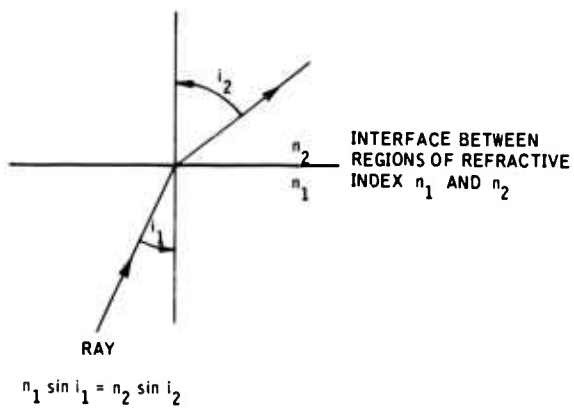

At appropriate frequencies, typically in the high-frequency (hf) or 3-to-30-Mc range, rays directed obliquely at the ionosphere are returned to earth where they can be reflected back up to the ionosphere for another hop, in this way traveling around the curvature of the earth. At the ionospheric reflecting point $i_2 = \pi/2$. Therefore,

$$n(\text{at reflection height}) = \sin i_o, \qquad (4)$$

where i_o = angle of incidence on the lower limit of the ionosphere.

Figure 1 is a schematic elevation view of representative ionospherically propagated radio rays as they commonly exist over one of the paths (Hawaii to Stanford, California) studied in the present experiment. The following features are significant.

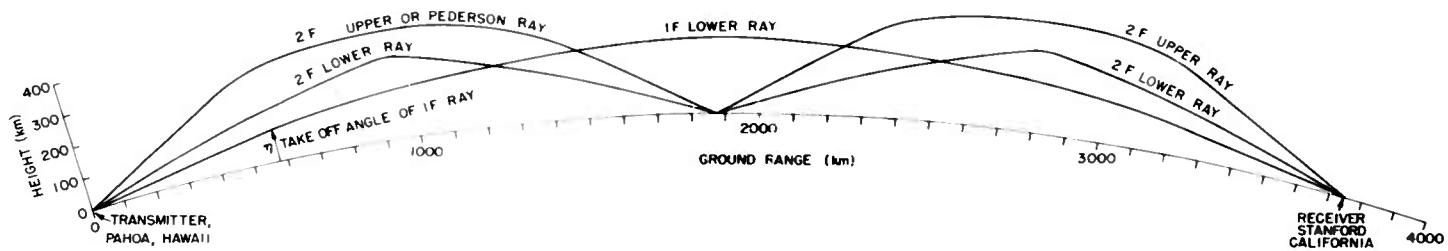

Fig. 1. SCHEMATIC ELEVATION VIEW OF REPRESENTATIVE IONOSPHERICALLY PROPAGATED RADIO RAYS.

The rays are gradually refracted or bent rather than reflected from a discrete surface. In spite of this fact, the term "reflection" or "hop" is usually used to denote an earth-ionosphere-earth segment of a ray path.

Energy can travel from transmitter to receiver by paths of different numbers of hops. Each such path is termed a mode--for example, a one-hop or two-hop mode. The group travel time for a ray over a two-hop path is about 0.5 msec greater than that over a one-hop path.

Rays with larger take-off angles γ_1 (smaller i_o), penetrate deeper into the ionosphere before they reach a refractive index that will return them to earth--see Eqs. (2) and (4). If a ray reaches the level of maximum electron density before it is turned down, it will continue upward and escape from the earth. Transition rays exist with take-off angles between that of the highest-order (two-hop in this case) lower ray and that of the lowest-angle escaping ray. Such transition rays are called "upper" or "Pederson" rays.

The region of the ionosphere at heights of about 100 km is termed the E region and that from about 200 to 300 km the F region. Rays are often refracted abruptly from the E region, though none were in the ionosphere represented by the electron-density profile from which Fig. 1 was computed.

A shorthand notation for a raypath includes the number of hops, the region of the ionosphere in which the ray turns back to earth, and whether the ray is upper or lower. Thus Fig. 1 includes a 1F lower ray, a 2F lower ray, and a 2F upper ray.

Since the complete expression for ionospheric refractive index is a complicated function of many factors, such as solar-ultraviolet and X-radiation, and the earth's magnetic field, it is in a constant state of flux, leading to considerable variability of mode configurations. For example, the modes over the paths studied in this experiment often changed from two or three hops to no propagation at all in a period of a few hours.

The earth's static magnetic field has the effect of making the ionosphere birefringent--that is, a particular volume of ionosphere has two values of refractive index. The practical effect of this is

to split each of the rays previously described into two components of slightly different phase and group velocities. The time-delay difference between the magnetoionically split components is much less than that between the geometrical modes.

This description of ionospheric radio-wave propagation is necessarily brief and can be expanded by reference to various texts on the subject such as Budden [1961],* Ratcliffe [1959] or Circular 462 [1948] of the U. S. Bureau of Standards.

B. REVIEW OF PREVIOUS STUDIES AND UNDERSTANDING OF HF RADIO FADING

When a radio wave in the high-frequency range is propagated by means of reflections from the ionosphere over distances ranging from a few hundred to many thousands of kilometers, it is found to fade, that is, to fluctuate in magnitude over a wide range. See Grisdale, Morris and Palmer [1957]. The first-order characteristic of hf fading is the fluctuation of the magnitude of the signal, often by tens of decibels and usually with a period on the order of 1 sec. One effect of fading is to impose a large-amplitude, low-frequency modulation on the signal being transmitted. This is not too serious an effect, since such fluctuations in signal magnitude can be smoothed out by automatic-volume-control devices. The most harmful effect of fading is the reduction of the signal amplitude below the local noise or interference level, making it impossible to recover useful information from the transmitted signal.

As first suggested by Brown, Martin, and Potter [1926], signal-envelope fading as observed on an antenna appears to be due to the movement of a pattern of varying field strength along the ground past the antenna.

The object of the present work is to describe this pattern and present a mechanism for its production. The term "fading pattern" is used to describe such spatial distributions of field strength. A random fading pattern could be produced by small-scale focusing resulting from

*See Bibliography at the end of this document.

irregularities in the ionosphere. Such effects have been considered by Ratcliffe [1948] and Booker, Ratcliffe, and Shinn [1949]. A periodic pattern similar to an optical diffraction pattern could be caused by destructive interference between two rays traveling different paths, such as one-hop and two-hop F-layer rays. See, for example, Banerjee and Mukerjee [1948]. Either kind of pattern would be stationary if the ionosphere were not varying with time. However, any temporal variation in the structure of the ionosphere would cause a motion of either kind of pattern. Since it is clear that both effects can occur, the question remains, which predominates in the case of hf, oblique, continuous-wave (cw) transmissions. Rays reflecting from different parts of the ionosphere would be expected to produce a detectable periodic interference (or diffraction) pattern if their amplitudes were similar, but random focusing and defocusing effects or random variations in ionization density could completely mask such a periodic pattern if the random effects were large enough. Conversely, the random effects might simply be small modulations on periodic diffraction patterns.

As background for the present investigation, the current understanding of the fading of obliquely transmitted, high-frequency waves can be summarized as follows. High-frequency waves that are transmitted in pulses short enough in duration (100 μsec or less) to separate the different geometrical modes fade with a period of approximately 20 sec to 1 min. This fading can be due either to destructive interference between the two magnetoionically propagated components, as found by Hedlund and Edwards [1958], or a random scattering process as described by Balser and Smith [1962], who found spatial correlation distances of about 40 wavelengths in a direction perpendicular to the ray path when propagation was via a single mode.

Continuous wave signals, for which the received signal voltage is the sum of voltages propagated by all the active modes, usually fade much faster, with a period on the order of 1 or 2 sec. The amplitude of fading cw signals has generally been found to follow a Rayleigh probability distribution except at special times, such as when upper and lower rays are interfering near the MOF (maximum observable frequency). Grisdale, Morris, and Palmer [1957] discuss this effect and also report

that the spatial correlation of signal strength falls significantly at a distance of about 200 or 300 meters. A random variable s has a Rayleigh distribution if its cumulative distribution function is $P(s) = 1 - \exp[-(s/s_o)^2]$.

Bixby [1953] has given a theoretical derivation of the fading at and near the MOF based on a nontilted ionosphere with a smooth, parabolic, ion-density distribution.

The slow magnetoionic fading described above rotates the polarization of individual modes and, since the receiving antennas are horizontally polarized, has the effect of removing a particular geometrical mode for periods of about 20 sec from the summation contributing to the cw signal. For example, if 1F and 2F horizontally polarized rays were being received, a spatial fading pattern would be observed. If then, one ray became vertically polarized, the interference pattern would disappear and a strong, nonfading signal would remain.

The various space-correlation measurements have generally suffered from a lack of sample points. That is, attempts were made to measure space correlation using two or three antennas, often arranged in a triangle. A resulting weakness has been the necessity to characterize the spatial properties of high-frequency fading with a single number, such as the distance beyond which the signal strength becomes uncorrelated. This approach implies the assumption of the existence of a pattern of field strength consisting of a random or perhaps a circular shape. No attempt has previously been made to actually observe the pattern of field strength as it exists at the ground. In addition, it has only very recently become possible to compare specific instances of fading with a firm knowledge of the specific propagation modes present at the time of observation.

A review of individual papers in the literature of radio-wave fading pertaining to the present experiment is included in Appendix A.

C. PURPOSE OF THIS EXPERIMENT

The first goal of this experiment is to measure the spatial properties of the distribution along the ground in the vicinity of a receiver

of the signal magnitude of high-frequency, ionospherically propagated, continuous radio waves. A number of the papers cited (Grisdale, and others in Appendix A) have reported a signal-strength correlation distance on the order of a few hundred meters. They have not described the extent to which spatial fading patterns show a regularity or periodicity or what the nature of this periodicity is, if and when it is present. There have been no reports describing either the orientation or the velocity of motion along the ground of periodic field-strength patterns associated with obliquely propagated, hf, cw waves. The experiments that describe the size of patterns in terms of a correlation distance are limited in that they can not be precise without a knowledge of the shape of the pattern that they are measuring.

The second major aim of this experiment is to attempt to describe the mechanism of production of the observed fading patterns. The relation between the orientation of periodic fading patterns and ionospheric tilts is explored. The dependence of fading-pattern-null spacing on propagation mode structure is investigated.

D. OUTLINE OF THE EXPERIMENT AND ITS PRINCIPAL RESULTS

The experimental arrangements and observations are described in detail in later sections; however, a brief outline in the form of a chronology should prove useful in relating the various results to each other and to the model developed.

Twelve dipole antennas arranged in an "L" 300m on a side were sequentially connected to a receiver whose output was recorded as intensity on moving film. A simple analysis of the recorded receiver output yielded the dimensions, orientation, and motion of the signal fading patterns.

The first observations were made on a 17.8-Mc, cw signal transmitted from Mayaguez, Puerto Rico, and received at Stanford, California. If the propagating rays had been exactly in the vertical great-circle plane between the transmitter and receiver, considerations of symmetry would have led to the expectation of fading patterns consisting of parallel nulls lying perpendicular to the great circle. As shown later, however,

if fading is caused by destructive interference between modes, and if the ray paths of the different modes deviate by only a few kilometers or fractions of a degree from the great-circle path, the resulting fading pattern can be rotated by tens of degrees.

The observed fading patterns were, in fact, rotated about 60 deg from the perpendicular to the great circle in a direction that could have been caused by the small prevailing North-South downward tilt in the ionosphere over the path.

In order to verify the hypothesis that the orientation of the fading nulls was due to the ionospheric tilt, cw transmissions at 17.8 Mc were instituted from Hawaii to Stanford. Since the propagation from Hawaii was in approximately the opposite direction to that from Puerto Rico while the North-South ionospheric tilt was assumed to be about the same, the fading patterns were expected to lie at an angle to the propagation path of about the same magnitude as before but of opposite direction. The subsequent observation of this correlation of fading-pattern characteristics with ionospheric tilts and propagation-mode identity lent support to the simple interference theory that had been proposed to account for the periodic fading patterns observed.

An additional reason for studying the Hawaii-Stanford path was the availability of a Granger Associates step-frequency, synchronized, oblique sounder that was already in operation at the Raytheon site at Pahoa, Hawaii. The use of the oblique sounder made possible, at least part of the time, the definite determination of the identity of the modes of propagation, which, as will be seen, aided in the interpretation of fading patterns.

After the completion of the Hawaii measurements the opportunity was taken to operate an oblique sounder and a cw transmission from Lubbock, Texas, to Stanford, thus providing data over a short path to complement that over the previous, relatively long ones.

II. PREDICTION OF CHARACTERISTICS OF SPATIAL FADING PATTERNS

The hypothesis that periodic fading patterns result from destructive interference between waves following discrete ray paths will be examined by predicting the types of fading patterns to be expected for various propagation configurations and then comparing these predictions with observed fading patterns.

A. FADING PATTERN MODEL

The model described predicts the null spacing and direction in fading patterns resulting from the destructive interference of two sets of equal-strength wavefronts that are described by their bearings and elevations with respect to an observer. Figure 2 shows the geometry of the incoming plane waves, an example of which is the plane wave front shown at a range ρ, bearing θ, and elevation η with respect to an observer at the origin o. The description of a particular wave front must include ρ but θ and η are sufficient to describe an incoming wave in general. The point P at (ρ, θ, η) or (x,y,z) is the foot of a perpendicular from the plane to the origin.

Figure 3 defines the parameters of a fading pattern resulting from the destructive interference of two incoming rays. The orientation or

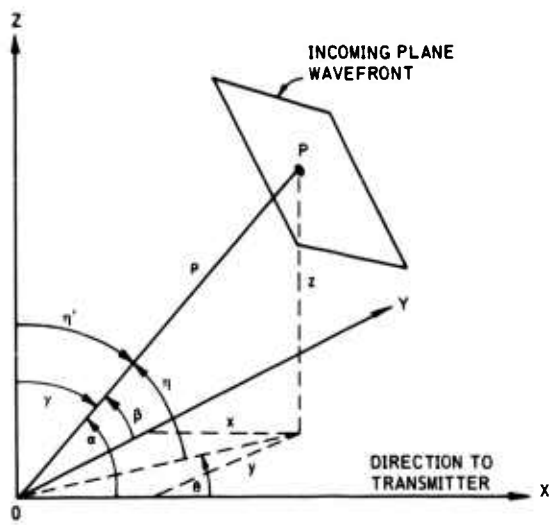

Fig. 2. DEFINITION OF GEOMETRY OF INTERFERING WAVES NEAR A RECEIVER.

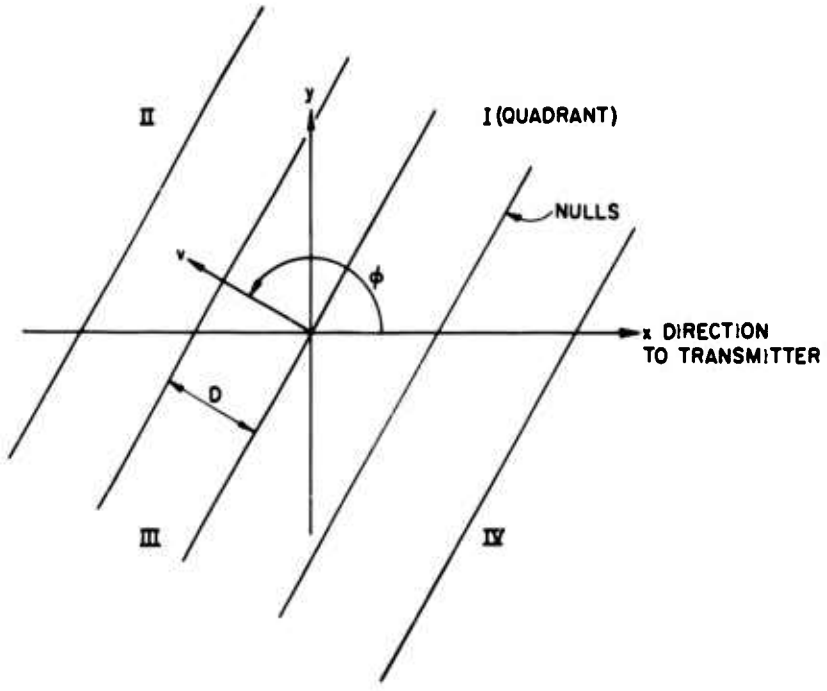

Fig. 3. DEFINITION OF SPATIAL FADING-PATTERN PARAMETERS.

direction of the fading pattern is defined as ψ, which is the perpendicular to the signal minima, or nulls; $\psi = 0$ is the direction from the receiver to the transmitter; D is the perpendicular spacing along the ground between nulls; the X-Y plane in both figures represents the ground.

Equations (5), (6), and (7) are the result of a complete derivation in Appendix B.

$$\psi_A = - \tan^{-1}\left[\frac{\cos \gamma_1 \cos \theta_1 - \cos \gamma_2 \cos \theta_2}{\cos \gamma_1 \sin \theta_1 - \cos \gamma_2 \sin \theta_2}\right] + \frac{\pi}{2} \qquad (5)$$

$$\psi_B = \psi_A + \pi \qquad (6)$$

$$D = \lambda / \left[(\cos \eta_1 \cos \theta_1 - \cos \eta_2 \cos \theta_2)^2 + (\cos \eta_1 \sin \theta_1 - \cos \eta_2 \sin \theta_2)^2 \right]^{1/2} \quad (7)$$

This derivation yields a static pattern, since the directions of the incoming waves are assumed constant. φ_B is computed along with φ_A for comparison with the observed data, which include the motion of the nulls and which exhibit approximate 180 deg symmetry; λ is the wavelength of the rf waves. The subscripts 1 and 2 refer to the two waves interfering to cause the fading pattern. The earth's curvature in the vicinity of the receiver is neglected.

B. PREDICTION OF FADING PATTERNS

In order to examine the equations for φ and D it is convenient to fix one ray in azimuth and elevation and let the other vary in both these quantities. The mode configurations examined in greatest detail will be those for the Hawaii-Stanford path since more data are available for it than for the others.

Ray tracings such as Fig. 1 have been computed by the method of Croft and Gregory [1963] for the Hawaii-to-Stanford path based on ionospheric-electron-density profiles measured by vertical-incidence pulse soundings at Hawaii and Stanford. From these and other ray tracings based on a hypothetical ion-density profile derived in part from rocket soundings at Wallops Island, Virginia, estimates can be made of typical values of ray elevation angle η_1. For the Hawaii-to-Stanford path the elevation angles of the received F-layer propagated rays are expected to be: 1F - 2 deg to 12 deg, 2F - 14 deg, 3F - 22 deg. The two- and three-hop E-layer rays are expected to have elevations of 2 deg and 7 deg when present.

It is also necessary to obtain an estimate of the expected deviations from the great circle that will be experienced by the rays traversing the path. Wright, Wescott, and Brown [1961] published, as part of a series, contours of mean electron density along the 75th meridian. For the present purpose these data should be sufficiently accurate to be

useful in predicting the ionospheric tilt at the midpoint of the Hawaii-to-Stanford path 65 deg to the west. Figure 4 is a representative plot of daytime ion-density contours as a function of height and latitude.

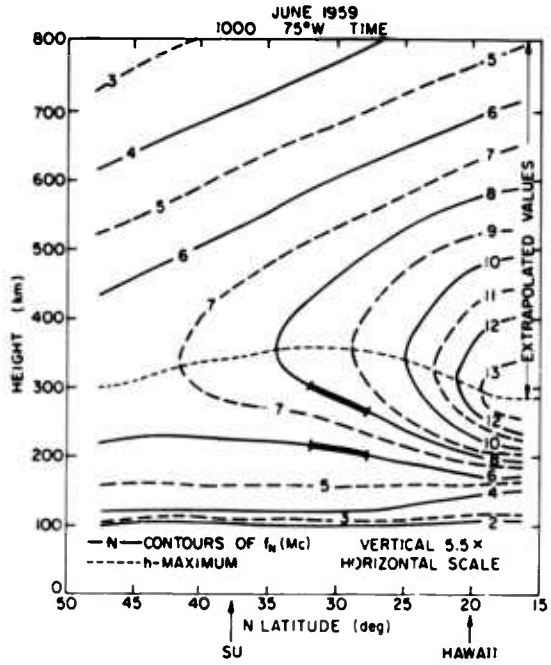

(From Wright et al [1961])

Fig. 4. REPRESENTATIVE DAYTIME PLOT OF ION-DENSITY CONTOURS.

Midway between the Stanford and Hawaii latitudes two segments of curves of constant ion density are emphasized by heavier lines. The lower one can be taken to represent the lateral tilt of the reflecting region encountered by relatively low-angle rays while the upper one shows the larger tilt corresponding to the reflection region for higher-angle rays. Taking into account the vertical-scale expansion it can be seen that the lower contour has a tilt toward the south of 1.9 deg and the upper one a tilt of 4.7 deg.

Figure 5 shows that a ray in traveling from a transmitter to receiver by means of a reflection from a tilted ionosphere is reflected from a point in the ionosphere deviated out of the vertical great-circle plane. In the simple case treated here the ray must deviate enough so that it lies in a plane perpendicular to the tilted layer.

Figure 6 illustrates the estimation of lateral deviations expected for rays assumed to make mirror-like or metallic reflections from the

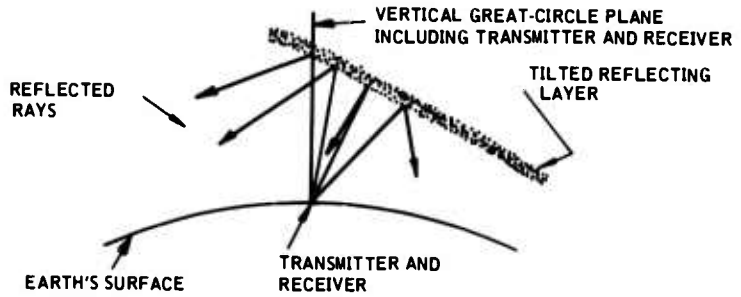

Fig. 5. ILLUSTRATION OF RAY DEVIATION.

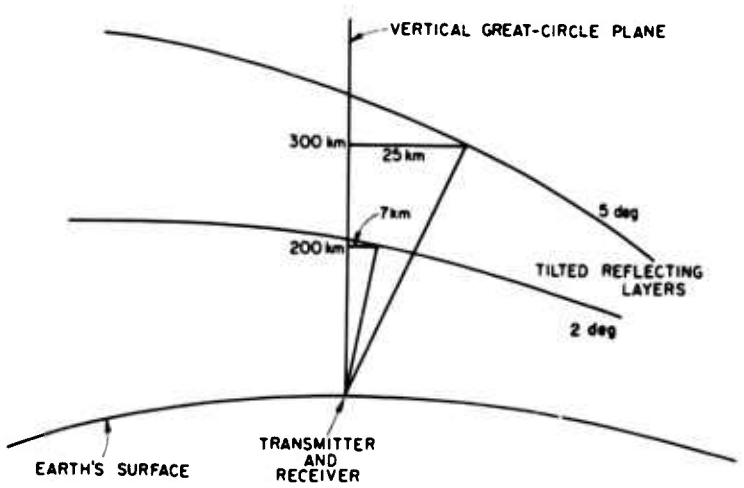

6a. End View of Propagation Path

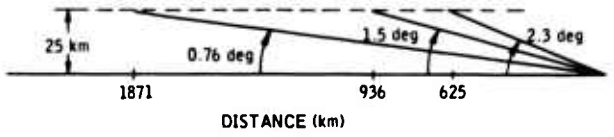

6b. Plan View

Fig. 6. ESTIMATION OF RAY DEVIATION FROM GREAT CIRCLE.

layers of Fig. 4. It is also assumed that the deviation of the ray results only from the tilt of the layer from which it reflects and is not affected by tilted lower layers. Figure 6a is an end view of the tilted planes of propagation containing rays reflecting from layers with a 2-deg tilt at 200-km height and a 5-deg tilt at 300-km height. The resulting lateral deviations out of the great circle are 7 km for the ray reflecting from the lower layer and 25 km for the higher ray. The fact that rays of two or more hops make intermediate ground reflections out of the great circle is neglected since inclusion of this spherical-geometry effect would complicate the estimation of lateral deviations more than is justified by the accuracy desired. The effect of these ground-reflection deviations would clearly be to increase the total lateral-ray deviation, probably by an amount on the order of 50 percent. It can be seen that the angular-bearing deviations as observed at the receiver for 1-, 2-, and 3-hop rays propagated 3741 km from Hawaii and deviated 25 km out of the great circle will be about 0.76, 1.5, and 2.3 deg to the south of the great circle (Fig. 6b).

It is perhaps appropriate to comment here that, as shown in Fig. 1, rays do not actually make mirror-like reflections from the ionosphere. Such an approximation is justified for the estimation of ray deviations performed above since the estimated ray heights are obtained from calculations (Croft and Gregory, [1963]) not employing the metallic-reflection assumption.

Hayden [1961] finds that 5-Mc waves transmitted from east to west at 40-deg north latitude have their ordinary magnetoionic component deviated an average of 9 deg to the north of the great circle while the extraordinary component is deviated an average of 4 deg to the south. This effect, however, is not expected to be as pronounced in the present experiment at 17.8 Mc since, as is shown by Scott [1950] in a derivation from the complete magnetoionic equations, the amount of deviation of rays by interaction with the earth's magnetic field is approximately inversely proportional to the square of the wave frequency. In any event, the tilted layers of Fig. 4 would be expected to have the effects described in the previous paragraphs since they will impart a net southward deviation to higher-angle rays. Figure 4 and others from Wright

et al [1961] suggest that the tilted-layer effects expected in the present experiment would not have been observed by Hayden since, at his latitude, the layer tilts are not as large.

Since the derivation of expected ray deviations given here is based on average values of electron-density profiles observed at a different longitude and in an earlier year than the present experiment, and includes many simplifying assumptions, it can establish only approximate values. The important result is that higher-angle rays over both the paths studied in this experiment can normally be expected to arrive at the receiver deviated up to 2 or 3 deg to the south of lower-angle rays.

The curves of Fig. 7 describe the interference patterns expected when 2F is the highest-order mode present. The undeviated reference ray is a 2F lower ray at an elevation η of 14 deg. The interfering rays are both higher and lower with varying deviations. A number of observations can be made with the aid of Fig. 7.

The fading-pattern parameters (as defined in Fig. 3) that are expected during times of interference between laterally undeviated

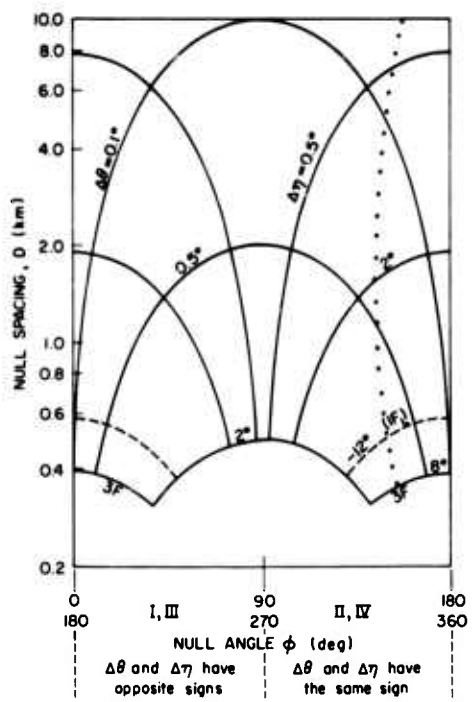

Fig. 7. PARAMETERS OF SPATIAL FADING PATTERNS EXPECTED WHEN THE HIGHEST-ORDER MODE PROPAGATING IS 2F.

rays appear in Fig. 7 along the lines $\varphi = 0$ and 180 deg (where $\Delta\theta = 0$). The null spacing D in this case is simply an inverse function of the vertical angular separation $\Delta\eta$ of the incoming wavefronts.

As one of the rays deviates from the great circle the fading pattern undergoes considerable variation both in φ and D. For propagation from Hawaii, $\Delta\eta$ and $\Delta\theta$ will have the same sign, since rays higher than the reference will be deviated further south, while rays lower than the reference will be deviated less far south than the reference ray. For a particular elevation separation, as the bearing separation increases from 0 deg, the null spacing is reduced and φ tends toward 90 deg from 180 deg or toward 270 deg from 360 deg.

It is thus apparent that, as a result of the lateral tilts, the null angle for the Hawaii path will lie in quadrants II and IV defined in the usual geometrical manner. That is, 90 deg $< \varphi <$ 180 deg or 270 deg $< \varphi <$ 360 deg. Since the direction of the ionospheric tilt as seen from the receiver is reversed for the Puerto Rico and Texas paths, φ for them should lie in quadrants I and III. The 180-deg ambiguity in each case arises because the geometrical wave-interference derivation used to find φ predicts only the orientation and not the motion of the fading patterns.

The curve marked 3F ($\Delta\eta$ = 8 deg) sets one lower limit on the value of D for two-hop F propagation since higher elevation angles correspond to three-hop propagation. Another lower limit to D is set by the maximum expected value of $\Delta\theta$, which has been estimated above as about 2 deg for the two-hop ray. The $\Delta\theta$ = 2 deg and $\Delta\eta$ = 8 deg lines intersect, giving an approximate minimum expected value of D = 0.3 km for 2F propagation. Figures 8 and 9 show that the corresponding minimum values of null spacing are about 0.5 km and 0.2 km for the cases in which 1F and 3F are respectively the highest-order rays.

The dashed curve marked 1F in Fig. 7 represents the fading patterns caused by interference between the 2F lower and 1F lower rays. The maximum value of D in all cases is essentially unlimited.

The time variation of φ and D during simple special events, such as the appearance at the operating frequency of the two-hop ray,

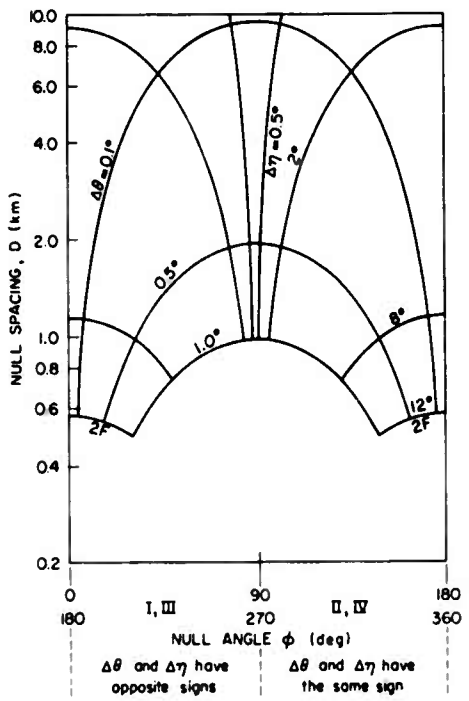

Texas and Puerto Rico Data Expected in Quadrants I and III; Hawaii Data Expected in Quadrants II and IV.

Fig. 8. PARAMETERS OF SPATIAL FADING PATTERNS EXPECTED WHEN 1F IS THE HIGHEST-ORDER PROPAGATING MODE.

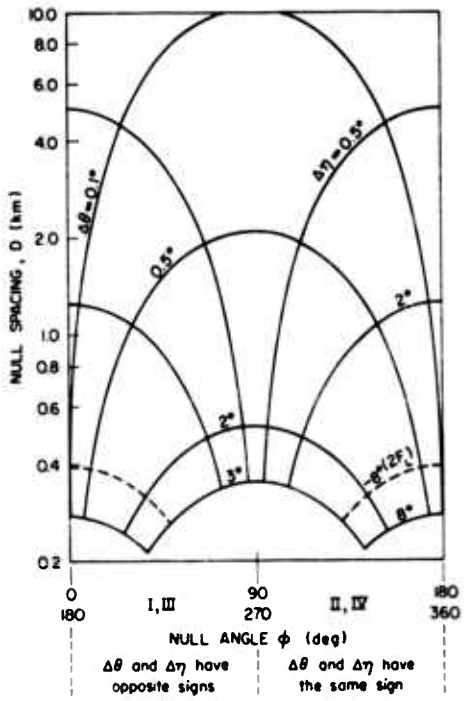

Fig. 9. PARAMETERS OF SPATIAL FADING PATTERNS EXPECTED WHEN 3F IS THE HIGHEST-ORDER PROPAGATING MODE.

can be predicted. The difference in elevation angle of the two 2F rays in Fig. 6a is approximately

$$\Delta\eta = \tan^{-1}\frac{\text{diff. in reflection height}}{\text{range to reflection point}} = \tan^{-1}\frac{100\text{ km}}{935\text{ km}} = 6\text{ deg}$$

If it is assumed, as in Fig. 6a, that the difference in bearing angles, 1.1 deg, is proportional to the difference in elevation, then $\Delta\theta = 0.18\,\Delta\eta$. When 2F energy first appears, the upper and lower rays will be nearly identical and the fading will be indeterminate. However, as the MOF for the two-hop ray increases, the upper and lower rays will separate in both elevation and bearing, as shown by the vertical dotted line in Fig. 7. The values of D and ϕ along this line show that the fading patterns would be expected to maintain an

approximately constant bearing (depending on $\frac{\Delta \theta}{\Delta \eta}$) but to decrease in spacing. Of course, if the 2F upper ray is weaker than the 1F lower ray, the elevation angles of the strongest interfering rays will come closer together as the 2F lower ray decreases in elevation, and the null spacing will start at a relatively small value and increase.

It should be noted that Fig. 7 was actually derived for the case where both rays are deviated equal amounts but in opposite directions from the great circle. The error introduced by this shift is very small, however, because the largest effect on ϕ is from the difference in bearing of the interfering waves. If both rays are equally shifted a few degrees, the fading patterns rotate only the amount of the shift, which is much less than the change in ϕ that would be caused by relative bearing changes of the same magnitude.

To summarize this discussion, it is expected that, for signals propagated from Hawaii, the fading nulls will have velocity bearings ϕ in quadrants II and IV and the null spacing will decrease as the order of the propagating modes increases. The signals from Puerto Rico and Texas are expected to have null directions in quadrants I and II as a result of the opposite relation between propagation direction and ionospheric tilt over those paths.

C. NULL VELOCITY

The null velocity is given by

$$V = DxF, \tag{8}$$

where D is expected to lie in the approximate range of 0.2 to 2 km and F is the fading rate in cps observed on any individual antenna. The signal fading rate observed on a single antenna is equivalent to the beat frequency between the radio-frequency voltages of two rays that have experienced different doppler shifts as a result of vertical ionospheric-layer motion or electron-density variation. This phenomenon has been studied by a number of investigators. Davies et al [1962] give a clear exposition of the various mechanisms resulting in such

frequency shifts. Fenwick [1960] finds doppler shifts on the order of 0.1 to 2 cps over paths similar to those studied here.

The null velocity will adjust itself according to Eq. (8) to accommodate the fading rate determined by the difference in doppler shifts of the interfering waves and the null spacing determined by the static ray geometry. The average value of V can therefore be expected to be near the geometrical mean of the range 0.02 to 4 km/sec, or about 0.3 km/sec.

III. EXPERIMENTAL ARRANGEMENTS

A. CW RECEIVING ARRAY

The spatial signal-strength fading patterns are observed by means of a group of antennas (Fig. 10) consisting of two perpendicular rows of horizontal dipoles each tuned to 17.8 Mc. One row of seven dipoles is on a line at 96 deg east of North (the bearing from Stanford to Puerto Rico, where the transmitter was originally located). The other row of five dipoles is perpendicular to the first. The individual antennas are 9 meters (one-half wavelength) above ground and are spaced 61 meters (3.6 wavelengths) center to center. During the course of the Hawaii experiment an extra dipole was added between No. 6 and No. 7, to facilitate interpreting very closely spaced fades.

Individual coaxial cables connect each antenna to an electronic commutator in the receiver building. The commutator, consisting of diode gates driven by multivibrators, samples each antenna in numerical order for 5 msec, repeating a cycle every 85 msec. The commutated signal then goes to a Collins R-390A communications receiver with a bandwidth of 2 kc and a modified AGC time constant of about 2 sec.

The i-f output of the receiver modulates the beam intensity of an oscilloscope whose sweep is synchronized with the commutator cycle.

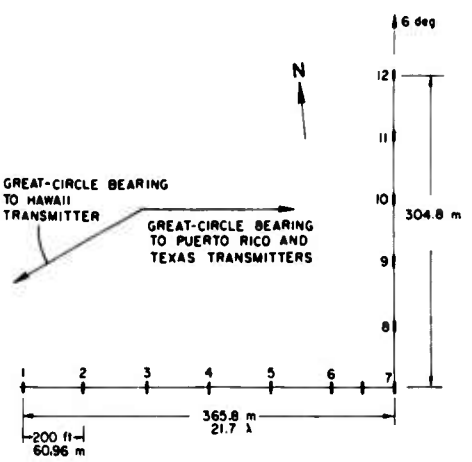

Fig. 10. PLAN VIEW OF FADE-SAMPLING ARRAY.

When this intensity-modulated sweep is photographed by a film moving perpendicular to the trace at constant speed, a record such as Fig. 11 is produced. The dark regions correspond to signal minima, the light ones to signal maxima.

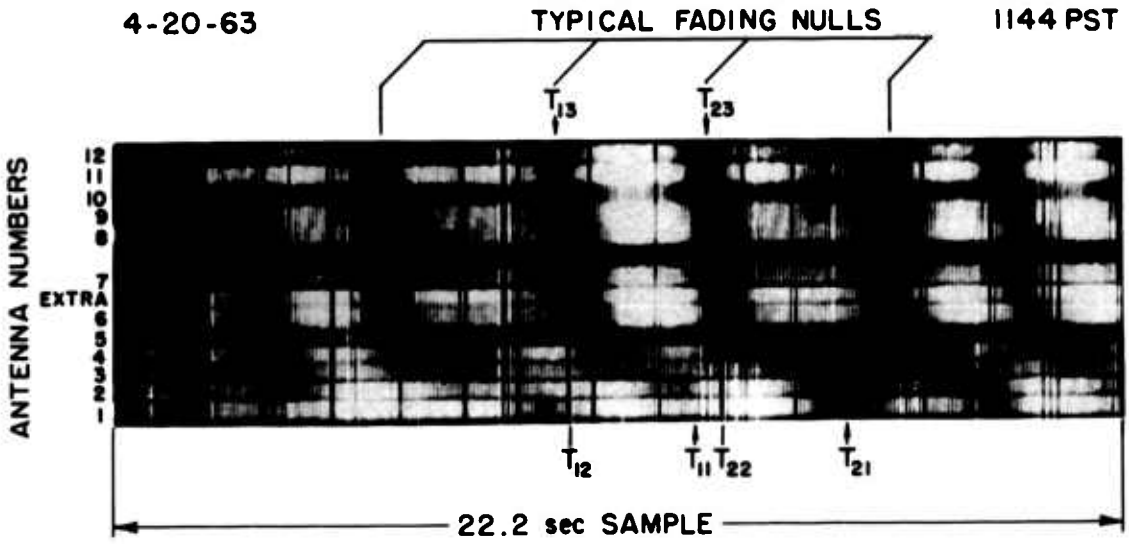

Fig. 11. TYPICAL RECORD FROM FADE-SAMPLING ARRAY.

If a series of straight-line signal nulls moves across the array, the direction, spacing, and speed of the nulls can be obtained by measuring the times when adjacent fades cross antennas 1, 7, and 12. No numerical measurement is made on the remaining antennas, although the information from them is essential to identify the presence of straight fades, their gross direction, and their spacing. For example, the two idealized null pattern records superimposed in Fig. 12 would be indistinguishable from each other if observed on antennas 1, 7, and 12 only. The shape and motion of small-scale curved fades could, in principle, be deduced, but the reduction problem would be formidable and the results would be ambiguous.

Data, as in Fig. 11, are recorded for approximately 20-sec periods at 2-min intervals throughout the day. The information describing two

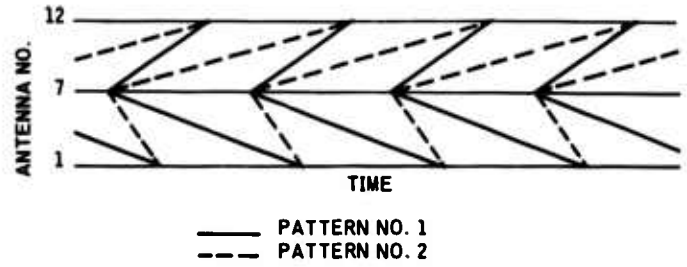

Fig. 12. TWO HYPOTHETICAL FADING-PATTERN RECORDS SHOWING INADEQUACY OF MEASUREMENTS USING ONLY THREE ANTENNAS.

adjacent nulls out of each 2-min period is transcribed from the film onto punched IBM cards by means of a Benson-Lehner Corp. Boscar film reader. The choice of which particular null pair to record is subjective, with the object being to pick one that is fairly representative of that 20-sec period and that is also clear enough to read accurately. After the data are on cards, they are analyzed by means of a computer program that yields the direction ψ of the perpendicular to a null, the perpendicular spacing D along the ground between the nulls, the apparent velocity V of the nulls in the direction perpendicular to their length, and the single-component fading rate F, which is the fading rate that would be observed on a single antenna if the measured pattern were the only fading present.

The following is a sample calculation of fading parameters from the measured times in Fig. 11. Velocity V and direction ψ are computed separately for each of the two nulls, and then an average value of each parameter is obtained. The fading rate is simply the reciprocal of the average time between nulls as measured on each of the three antennas. The null spacing is the average velocity divided by the fading rate. The null configuration deduced by means of these calculations is shown in Fig. 13.

$t_{11} = 9.08$ sec $\qquad t_{21} = 12.40$ sec

$t_{12} = 6.40$ sec $\qquad t_{22} = 10.25$ sec

$t_{13} = 6.16$ sec $\qquad t_{23} = 10.23$ sec

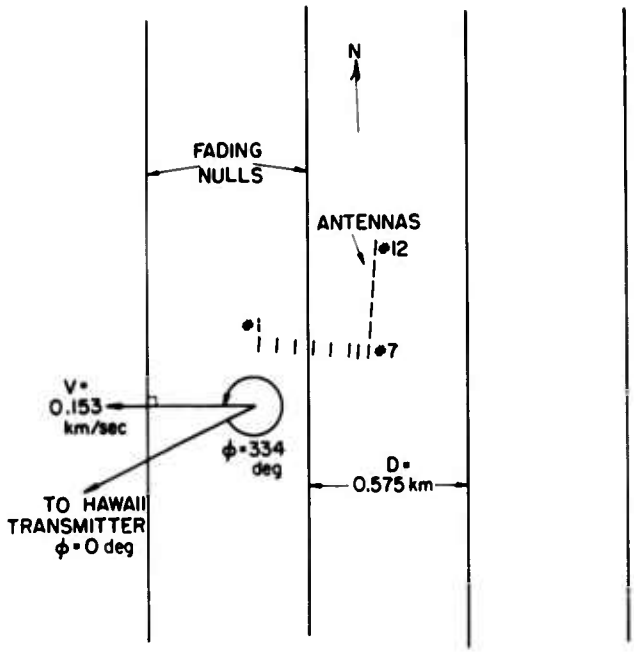

Fig. 13. PLAN VIEW OF NULL CONFIGURATION DEDUCED FROM FIG. 11.

d_x = 0.3658 km (spacing between antennas No. 1 and 7)

d_y = 0.3048 km (spacing between antennas No. 7 and 12)

The component of null velocity along each leg of the antenna array is computed first.

$$v_{x_1} = \frac{d_x}{t_{12}-t_{11}} = -0.1361 \text{ km/sec}$$

$$v_{y_1} = \frac{d_y}{t_{13}-t_{12}} = -1.27 \text{ km/sec}$$

$$v_{x_2} = \frac{d_x}{t_{22}-t_{21}} = -0.1698 \text{ km/sec}$$

$$v_{y_2} = \frac{d_y}{t_{23}-t_{22}} = -15.25 \text{ km/sec}$$

The component velocities are used to determine the direction of motion of the null (perpendicular to the null itself).

$$\phi_1 = \pi + 151 + \tan^{-1}\frac{v_{x_1}}{v_{y_1}} = 337 \text{ deg}$$

π is added in this example because both component velocities are negative; 151 deg are added to rotate the coordinates so that a null traveling toward the transmitter (Hawaii) will have $\phi = 0$ deg.

$$\phi_2 = \pi + 151 + \tan^{-1}\frac{v_{x_2}}{v_{y_2}} = 332 \text{ deg}$$

The average of the two values is obtained.

$$\phi = \frac{\phi_1+\phi_2}{2} = 334 \text{ deg}$$

$$V_1 = \frac{v_{x_1} v_{y_1}}{\left[v_{x_1}^2+v_{y_1}^2\right]^{1/2}} = 0.1351 \text{ km/sec}$$

$$V_2 = \frac{v_{x_2} v_{y_2}}{\left[v_{x_2}^2+v_{y_2}^2\right]^{1/2}} = 0.1698 \text{ km/sec}$$

$$V = \frac{V_1+V_2}{2} = 0.153 \text{ (average velocity of the nulls) km/sec}$$

$$F = 3/[(t_{23}-t_{13})+(t_{22}-t_{12})+(t_{21}-t_{11})] = 0.266 \text{ cps}$$

$$D = \frac{V}{F} = 0.575 \text{ km}$$

The fading-pattern measurements have the following limitations.

The smallest null spacing that can be reliably measured is about 0.1 km as a result of the spacing between the elements of the sampling array.

The largest null spacing that can be measured is limited by the 20-sec sample time and is a function of null velocity. For a typical null velocity such as 0.5 km/sec the maximum measurable spacing would be 10 km.

The slowest fade that can be readily measured is one that takes the entire 20-sec sample time to cross the array. This corresponds to a velocity of 0.015 km/sec.

A null traversing the entire array in two or three sampling sweeps of 85 msec each would have a velocity of about 1.5 km/sec which would be the maximum velocity observable. Faster nulls would appear to strike the entire array at once.

The angular resolution depends on the sharpness of the nulls; however, values of ϕ are frequently observed to have a spread, over several measurements, of about 5 deg, which is probably a reasonable estimate of the resolution.

A small error in measurement of ϕ is contributed by the uneven terrain on which the antennas are situated. For rays at an elevation of 5 deg the error in ϕ is about 10 deg, but for elevations of 10 deg or more the error is less than 2 deg. Since most of the waves observed arrive with elevation angles greater than 10 deg, this error is negligible.

B. CW TRANSMISSIONS AND PATHS

Three paths were studied during the course of the experiment. The parameters of the cw transmissions are presented in Table 1.

C. OBLIQUE SOUNDERS

1. Description

A Granger Associates, synchronized, oblique, ionosphere sounder was operated over the paths from Hawaii and Texas to Stanford in order to be able to identify the modes propagating at any given time. Briefly, this system operates by transmitting from one end of the path a short (50-μsec) pulse that is received on a synchronized receiver at the other

TABLE 1. CW TRANSMISSION PARAMETERS

Path	Great-Circle Bearing from Stanford, Calif. (deg)	Range (km)	cw Frequency (Mc)	cw Power (w)	Height of Transmitting Antenna (3-element yagi) (m)	Dates of Operation
Mayaguez, P.R., to Stanford, Calif.	96	5724	17.8825	700	14	5-14-62 to 6-1-62
Pahoa, Hawaii, to Stanford, Calif.	247	3741	17.8625	700	21	11-2-62 to 6-8-63
Lubbock, Texas, to Stanford, Calif.	96	1840	17.7385	50-500	15	8-1-63 to 10-23-63

end and intensity displayed on 35-mm film. The presence of more than one path of propagation splits the pulse into a number of components spread in time by up to 2 or 3 msec. After sending up to 10 pulses on one frequency, both the transmitter and receiver shift to a higher frequency, spaced (according to the frequency band) by 100 to 800 kc and the process is repeated, sweeping in this manner from 4 to 64 Mc, thus covering the entire high-frequency range of interest.

The peak pulse power from both oblique sounders was 30 kw, pulse width was 50 μsec, and PRF 20 pps. The Stanford end of the sounder paths was instrumented with a Granger model 902 transmitter-receiver that had been modified to perform a number of experiments simultaneously, of which this was only one. The Stanford sounder antenna was a Collins 237B-1 rotatable logarithmic periodic antenna 30 m above a 55-m-high knoll. It therefore had a much greater sensitivity to low-angle radiation than the cw array.

The sounder system was used only for the Hawaii and Texas paths. A Granger model 904 transmitter was located at Pahoa, Hawaii, feeding a 21-m-high rhombic antenna 122 m long on each leg. Ten pulses per channel were transmitted. The transmission direction was reversed for

Texas. Six pulses per channel were transmitted from Stanford to a Granger model 903 receiver at Lubbock, which used a Hy-gain LPA 24-m high for reception.

2. Interpretation of Sounder Data

Figure 14a shows an oblique ionogram for the Hawaii-to-Stanford path. Figure 14b is a tracing of the sounder signal. The solid vertical lines are interfering signals and should be disregarded. Four basic phenomena produce the most noticeable characteristics of oblique ionograms.

1. The travel time of rays increases with the number of ionospheric reflections.
2. The maximum observable frequency (MOF) of a mode decreases as the number of hops increases.
3. The upper ray associated with a particular mode has its greatest amplitude near the MOF of that mode.
4. An upper ray has a greater travel time than its associated lower ray. Both, of course, merge at the MOF.

These characteristics are used to identify the propagation modes contributing to the received 17.8-Mc, cw signal on which the fading pattern measurements are made. As will be seen later in the data, not all ionograms are as readily interpreted as Fig. 14a, which merely indicates that the ionosphere does not always fit a simple model. In Fig. 14 the 1F, 2F, and 3F rays have MOF's of about 31, 19, and 13.5 Mc respectively. 2 and 3 hop E layer rays appear with MOF's of 23 and 16 Mc.

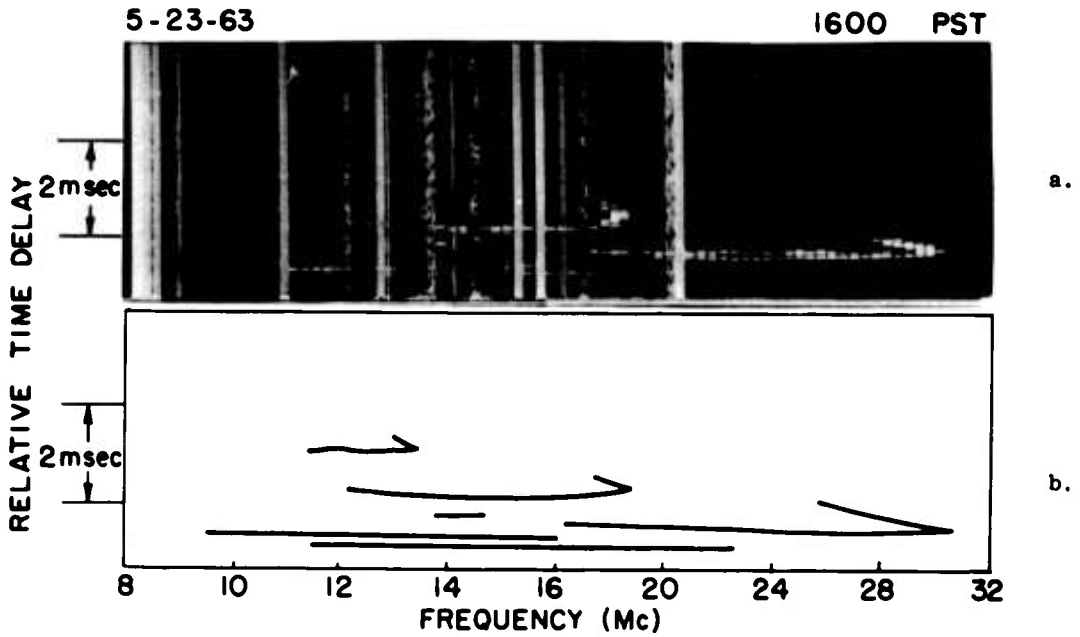

Fig. 14. OBLIQUE IONOGRAMS.

IV. OBSERVATIONS AND INTERPRETATIONS

A. AMOUNT OF PERIODIC FADING OBSERVED

1. Definition of Periodicity

One of the primary results desired from this experiment is a knowledge of the degree of regularity or periodicity exhibited by the observed fading patterns.

Two semi-objective standards of periodicity are established. The fading patterns are considered "periodic" if they appear at least as regular as the samples in Fig. 15. The patterns are considered "measurable" if they appear as regular as the samples in Fig. 16. Though it is difficult to establish purely objective criteria for these categories, it is readily apparent that the "measurable" patterns in Fig. 16 show a greater degree of irregularity than the "periodic" ones of Fig. 15. It is equally clear that the "measurable" patterns exhibit enough tendency toward regularity for measurements made on appropriate adjacent fades to be characteristic of the fading during the sample period.

The samples of Fig. 17, though strictly speaking not all random, do not have enough regularity to make meaningful pattern measurements. For example, adjacent nulls in the center frame on the left in Fig. 17 appear to be moving in opposite directions. The irregular patterns usually have sizes and shapes similar to the regular ones, indicating that they probably are a result of similar but more complex mechanisms, such as interference between three or more raypaths of comparable intensity, or between raypaths that have been subjected to random focusing or ion-density variations of sufficient magnitude to obscure their regularity.

2. Dependence on Path Length

The periodicity of the observed fading patterns decreases with path length, with "periodic" patterns present on 20 percent of the signals received from Texas but on only 2 percent of those from Puerto Rico. These results are shown in Fig. 18. Early in the course of the

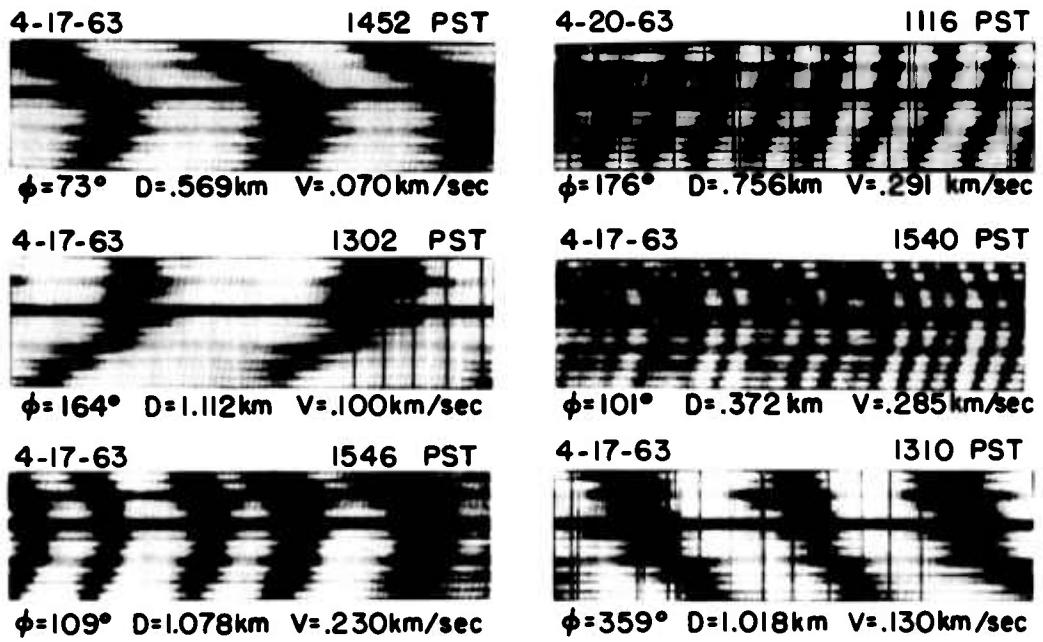

Fig. 15. SAMPLE FADING RECORDS SHOWING "PERIODIC" FADING PATTERNS.

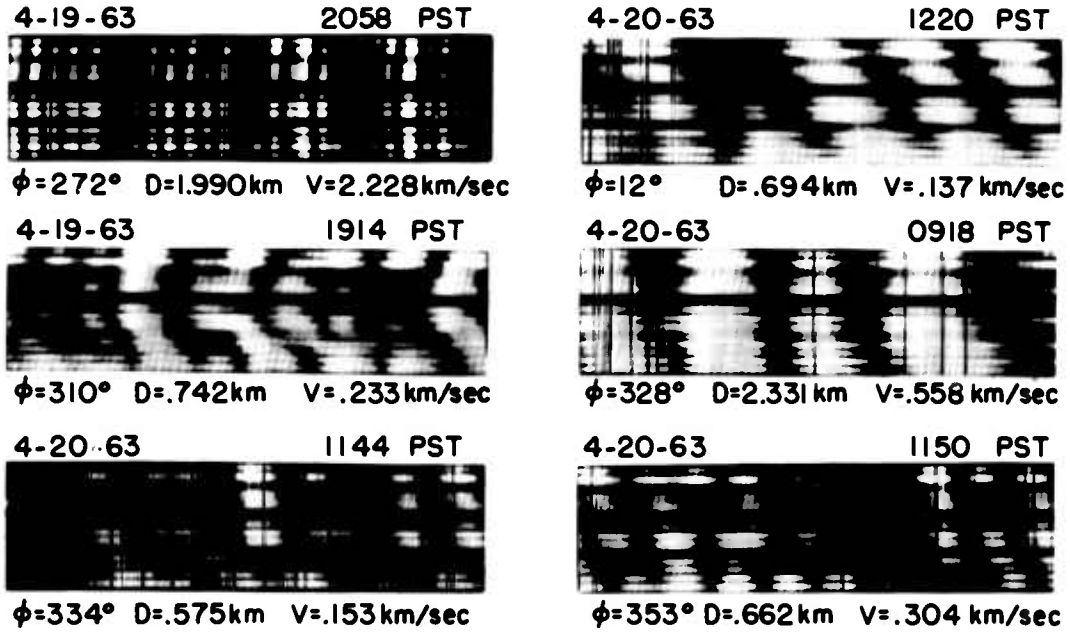

Fig. 16. SAMPLE FADING RECORDS SHOWING "MEASURABLE" FADING PATTERNS.

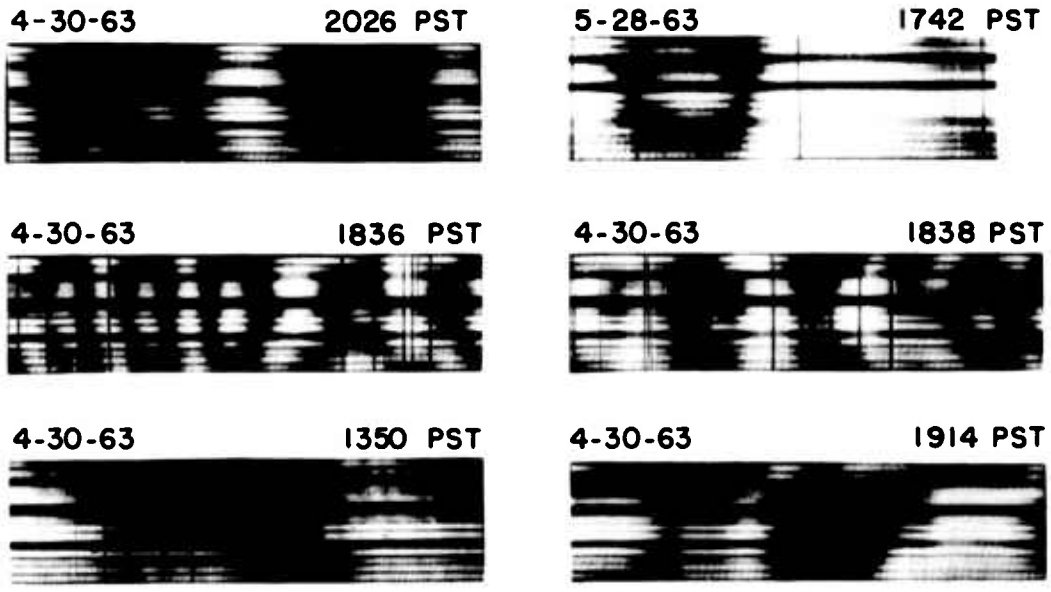

Fig. 17. SAMPLE FADING RECORDS SHOWING "RANDOM" OR NONMEASURABLE PATTERNS.

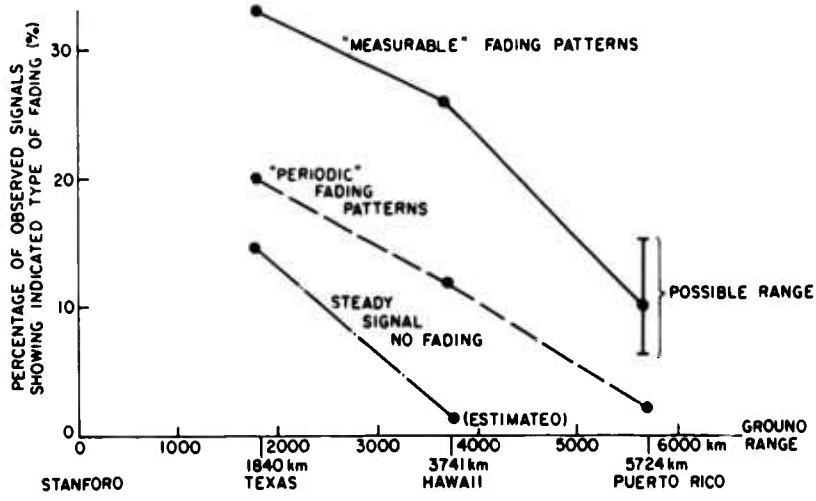

Fig. 18. PERIODICITY OF FADING PATTERNS AS A FUNCTION OF PATH LENGTH.

experiment, when the Puerto Rico data were being analyzed, a somewhat more flexible standard existed for the classification of patterns as "measurable," resulting in the range of uncertainty shown.

3. Maximum Random Ionization Possible during Periods of Periodic Fading

It is interesting to consider the maximum amount of random variation in electron density that can be present along two raypaths that are interfering to form a periodic fading pattern. A 1-radian random variation of the phase of the signal following one path with respect to that of one following the other during one fading period would certainly destroy a periodic pattern. The following development establishes the percentage change in ionization necessary to produce such a phase shift.

Consider destructive interference between one- and two-hop F-layer rays on a 3741-km path such as Hawaii to Stanford. The rays travel about 2000 km in the ionized region between heights of 140 and 250 km (see Fig. 1). The approximate average ionization density in this region during periods of two-hop, 17-Mc propagation is $N = 30 \times 10^{10}$ electrons/m^3. At an instant of time the phase of a wave is defined by the voltage equation $V = e^{-j\beta x}$, where $\beta = \omega/v_p$ is the phase constant expressed in radians/meter. For simplicity, β is assumed constant in the ionized region and the magnetic field is neglected. With these restrictions,

$$\beta = \frac{\omega}{v_p} = \frac{\omega}{c} n = \frac{\omega}{c}\left[1 - \frac{Ne^2}{\omega^2 m_e k_o}\right]^{1/2}$$

If the physical path length in the ionized region is denoted P, the total phase path length in the region is $P\beta$.

$$\frac{d(P\beta)}{dN} = -\frac{Pe^2}{2c\omega m_e k_o\left[1 - \frac{Ne^2}{\omega^2 m_e k_o}\right]^{1/2}}$$

let $\Delta(P\beta) = 1$ radian. Then

$$\Delta N = - \frac{2c\omega m_e k_o \left[1 - \frac{Ne^2}{\omega^2 m_e k_o} \right]^{1/2}}{Pe^2}$$

$$\frac{\Delta N}{N} = -0.33 \times 10^{-4} = -0.003 \text{ percent.}$$

As noted above, $N = 3 \times 10^{11}$ electrons/m^3

$P = 2 \times 10^6$ m

$\omega = 2\pi \times 17.8 \times 10^6$ radians/sec.

The remaining parameter values appear with Eqs. (1), (2). We thus have the result that, if a measurable fading pattern is present, the ionization-density difference between the two paths must not change randomly by more than 0.003 percent during a fading period, typically about 2 sec. Since the random difference variation is less than 0.003 percent, the random variation of ionization along each path can not exceed 0.003 percent by any large amount because this would require the ionization along both paths to vary in the same random manner.

Examination of fading-pattern data reveals that, though a pattern may persist for periods of an hour or more, the spatial phase variation of the nulls seldom remains uniform for longer than 10 or 20 sec. That is, if a tracing is made of a 10-sec period of fading-data film and is then translated to the following 10-sec period, the nulls, though quite similar, are not congruent.

It can be concluded from these results that the random variation in electron density along an ionospheric raypath during periods of periodic fading is approximately 0.003 percent in a 10-sec period. During periods of random fading patterns, which include the majority of signals, the random fluctuations in ion density are greater than 0.003 percent in a 1- or 2-sec period.

These results are in good agreement with results from vertical-incidence-sounding data obtained by Wright, Wescott and Brown [1961],

which show that, following layer formation, the average diurnal variation in electron density is about 10 percent/hr, or about 0.003 percent/sec. This figure is taken from an average electron-density-vs-time curve for a fixed height of 200 km. Actual hourly variations are therefore smoothed and are probably somewhat larger.

B. TYPICAL FADING PATTERN AND PROPAGATION MODE OBSERVATIONS

1. 1 May 1963

Figure 19 displays for a typical day a series of plots (to the same time scale) of null spacing, direction, velocity, and propagation mode structure. Each point on the D, ϕ, and V plots represents a measurement of the fading pattern observed during a separate 20-sec sample period. The propagation-mode structure is represented in simplified form by a delay-time-vs-time-of-day plot that was synthesized from the sweep-frequency oblique-sounder records. Samples of the latter along with fading patterns observed at the same time are shown in Fig. 20 and are identified by the circled numbers in Fig. 19.

At 0900 PST, Fig. 19 (1), only two-hop, E-layer propagation was present. No signal was observed on the cw receiver, because of the low angle of arrival (2 deg) of the 2E rays. The sweep-frequency sounder was more sensitive to low-angle rays than the cw receiver. See Chapter III for details.

By 0950 PST, Fig. 19 (2), the one-hop, F-layer signal had appeared on both the sounder and cw receivers. The 1F ray can arrive at angles from 2 deg up to about 12 deg, the latter occurring during periods of layer formation and decay when the upper and lower rays follow similar trajectories. The fading pattern is broad and diffuse as a result of the low and nearly equal arrival angles of the interfering 1F upper and 1F lower rays.

At 1110 PST, two- and three-hop, E-layer rays were visible on the sounder but no cw signal was visible. When the 1F ray reappeared at 1115 PST on the oblique sounder the cw signal reappeared with large values of null spacing. As the MOF of the 1F ray increased and the angle of arrival of the upper and lower rays diverged, the null

spacing decreased as expected (Chapter II-B). Figure 19 (3) shows the propagation modes and fading patterns during this period.

Figure 19 (5) illustrates a weak cw signal with diffuse, irregular, fading patterns observed during a period when only the 1F lower ray was present. The E-layer rays are presumed to remain at about the same arrival angle and so do not contribute to the cw signal.

At about 1730 PST the two-hop F ray appeared, the cw signal strength increased, and the null spacing decreased, implying that the fading was then a result of interference between 1F and 2F rays as opposed to the 1F upper-lower ray interference observed from 1500 to about 1700. Figure 19 (8) illustrates the modes and the fading.

From about 1900 PST to signal fade-out the mode structure became ambiguous. Detailed ray tracings in Appendix C show, for example, that at extreme one-hop ranges such as the 3741 km from Hawaii to Stanford, it is possible to have three separate and distinct one-hop, F-layer rays with appreciable separations in time delay as a result of partial E-layer bending.

At 2000 PST, Fig. 20 (10), the first half of the fading-pattern data is obscured by the transmitter identification keying, which occurred on each hour and half-hour. Other fading-data frames in Figs. 20 and 22 that are nominally on the hour or half-hour are actually 2 min later.

The ϕ-vs-time plot of Fig. 19c displays the predicted concentration of values in quadrants II and IV characteristic of signals propagated from Hawaii. Another typical feature is the reversal of direction of ϕ with a period on the order of 2 hr. The reversal of the direction of motion of the nulls is thought to be a result of reversal of the difference in ionospherically caused frequency shifts of the two interfering waves (Chapter II-C).

The smaller variations in null angle ϕ are probably a result of small scintillations in θ, the bearing angle of the individual arriving waves. Figure 7 shows that very small θ variations can lead to much larger changes in ϕ. Bramley [1956] measured random bearing fluctuations of single rays at 11 Mc of about 2 deg about the mean bearing. Waterman and Strohbehn [1963] have described small-amplitude wave motions in a reflecting medium that can cause scintillations in

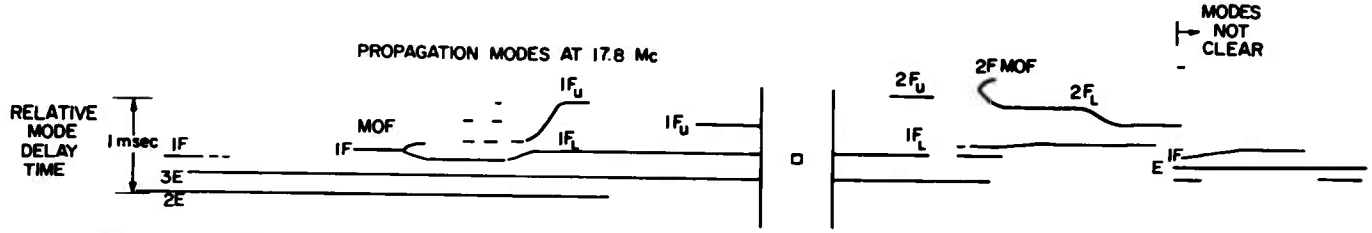
PROPAGATION MODES AT 17.8 Mc
MODES NOT CLEAR
RELATIVE MODE DELAY TIME
1 msec
IF
3E
2E
MOF
IF_U
IF_L
$2F_U$
$2F_L$
2F MOF
E

a.

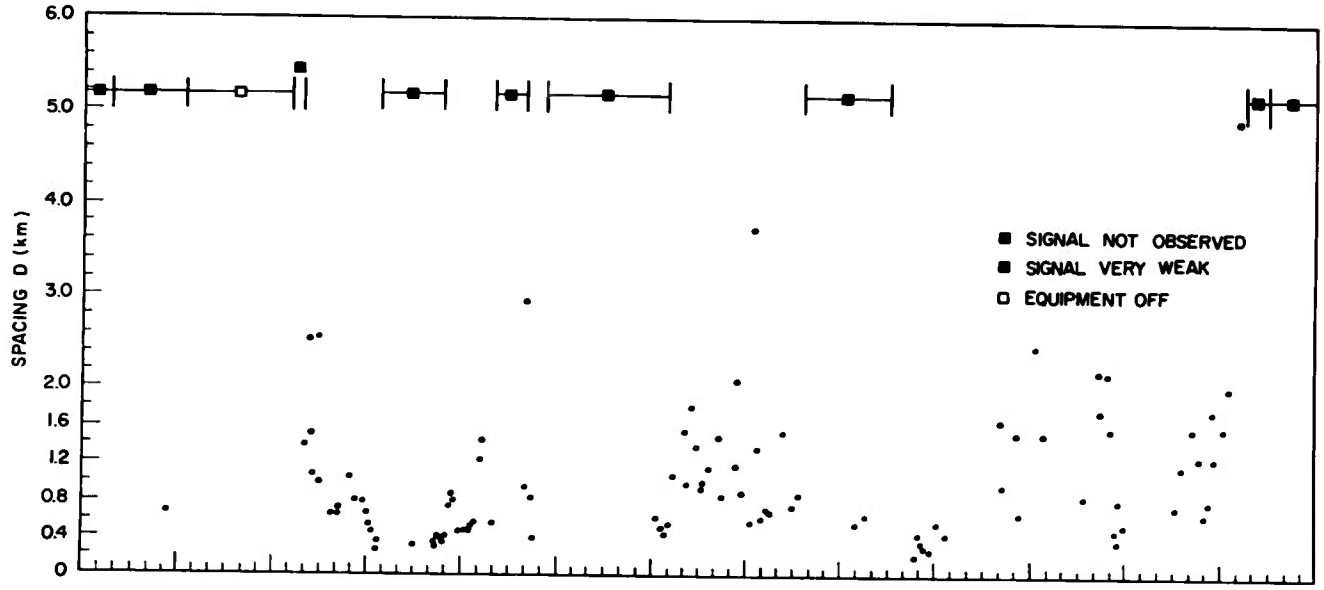
SPACING D (km)
6.0
5.0
4.0
3.0
2.0
1.6
1.2
0.8
0.4
0
SIGNAL NOT OBSERVED
SIGNAL VERY WEAK
EQUIPMENT OFF

b.

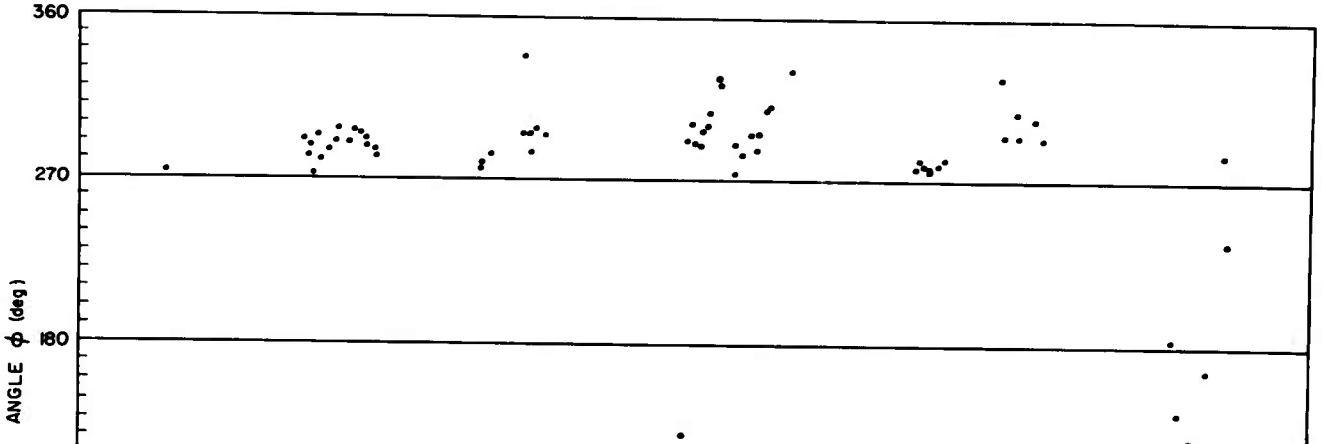
ANGLE ϕ (deg)
360
270
180

c.

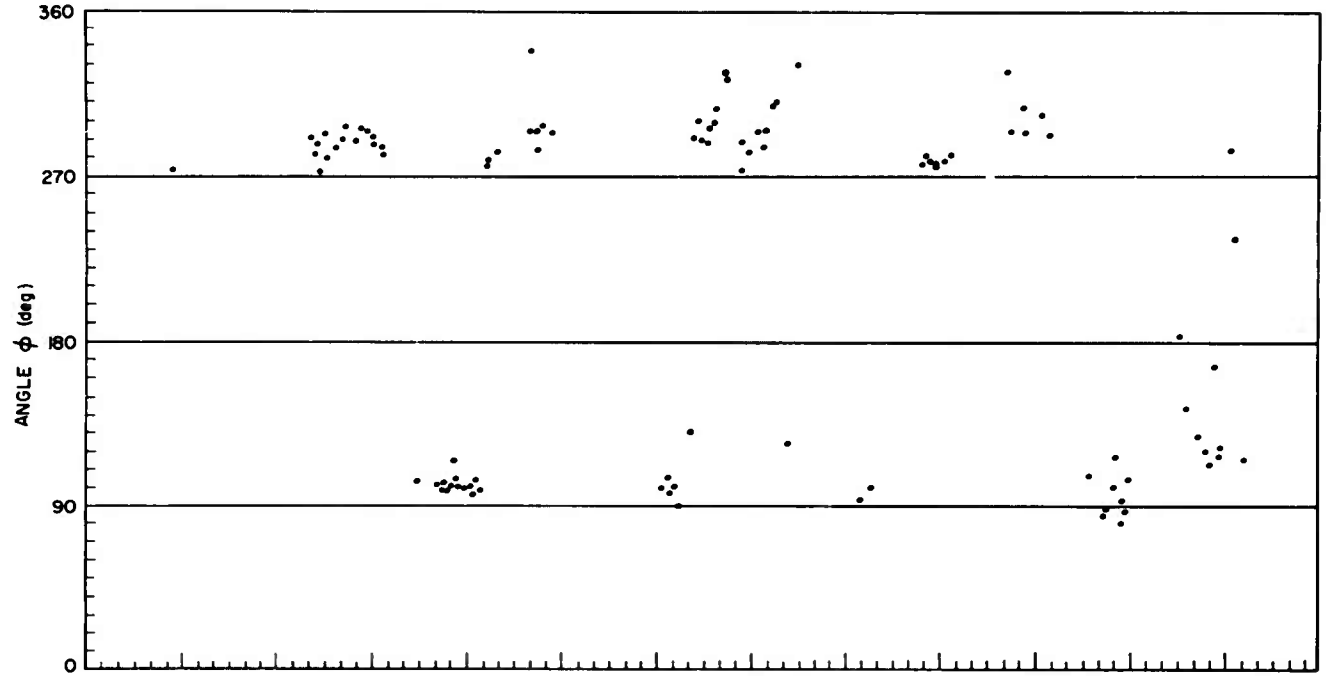

c.

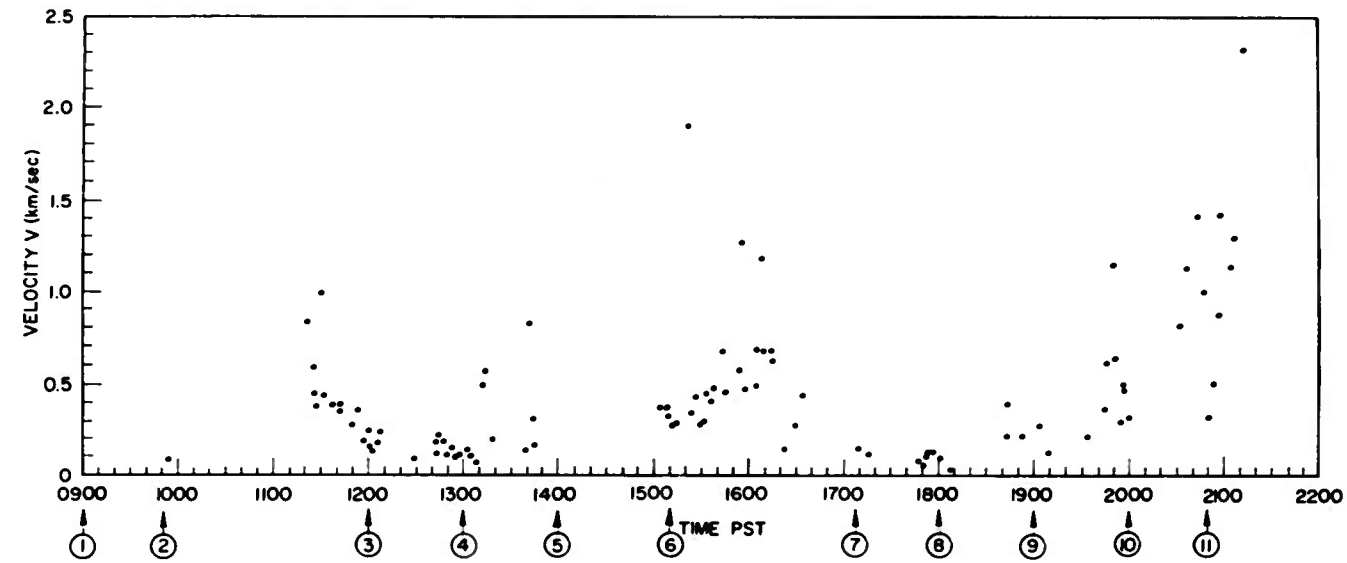

d.

Fig. 19. PLOTS OF NULL SPACING, DIRECTION, VELOCITY, AND PROPAGATION-MODE STRUCTURE FOR 1 MAY 1963.

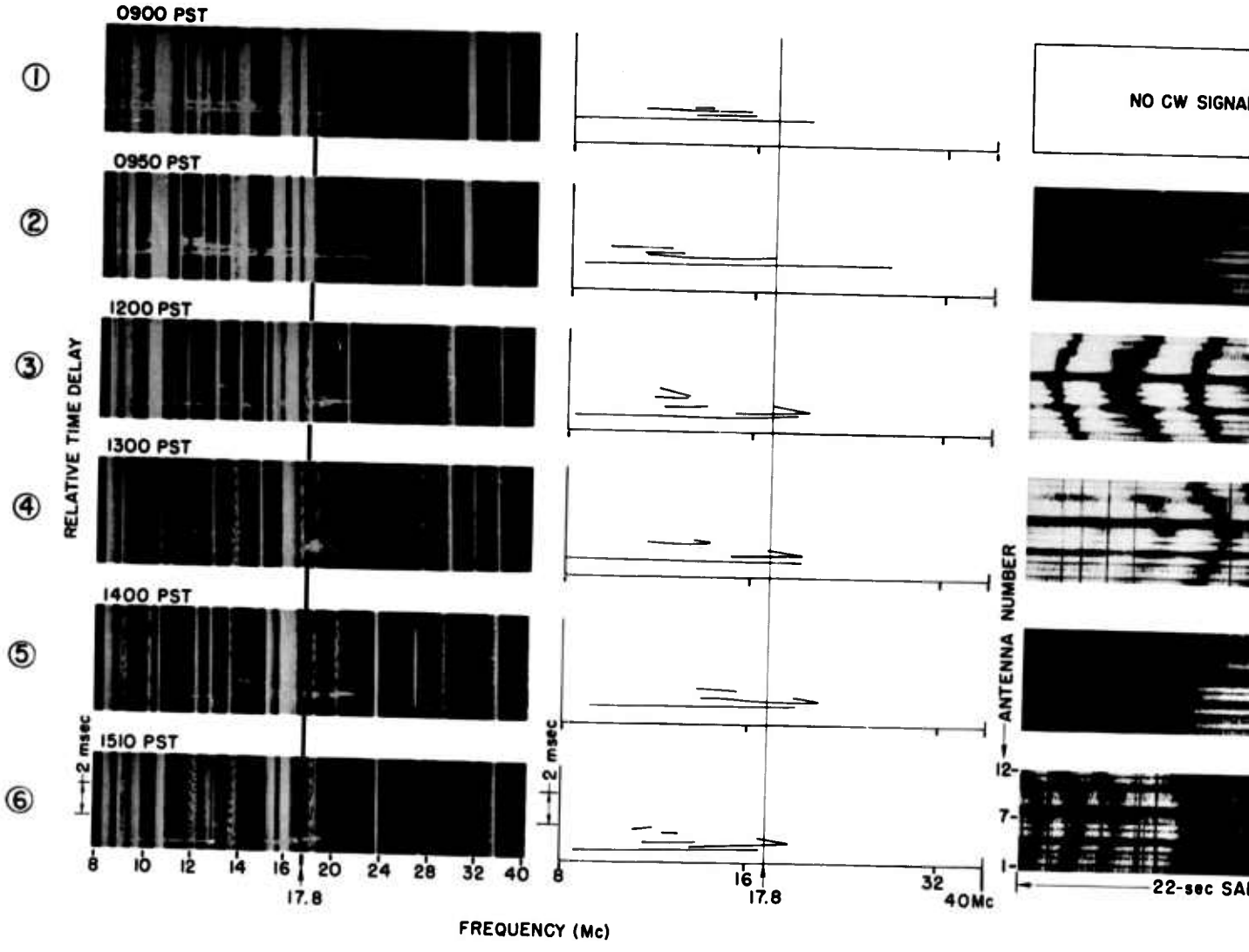

Fig. 20a.

Fig. 20. COMPARISON OF cw FADING PATTERNS AND PR
RECORDS OF 1 MAY 1963.

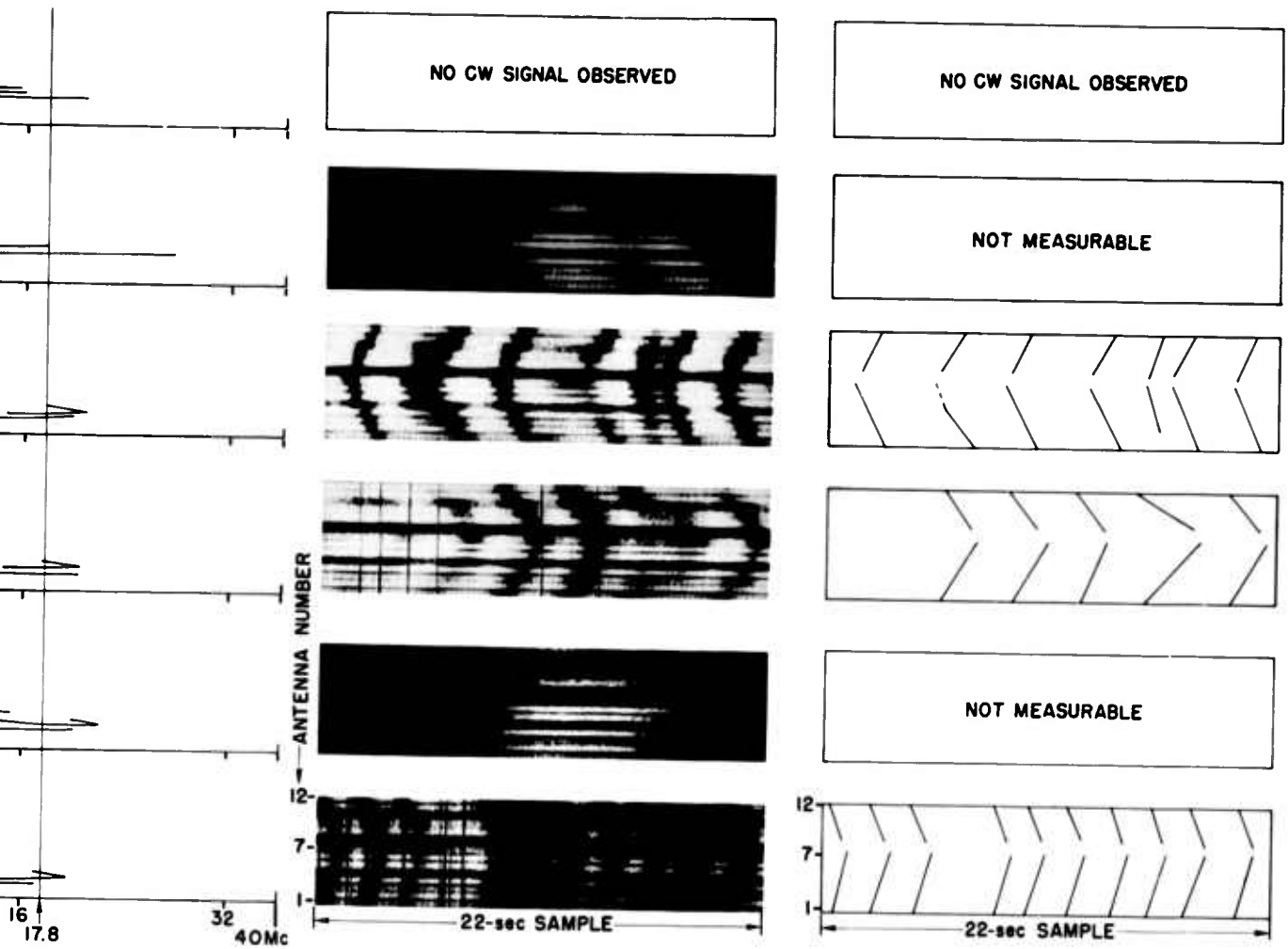

Fig. 20a.

30. COMPARISON OF cw FADING PATTERNS AND PROPAGATION MODE RECORDS OF 1 MAY 1963.

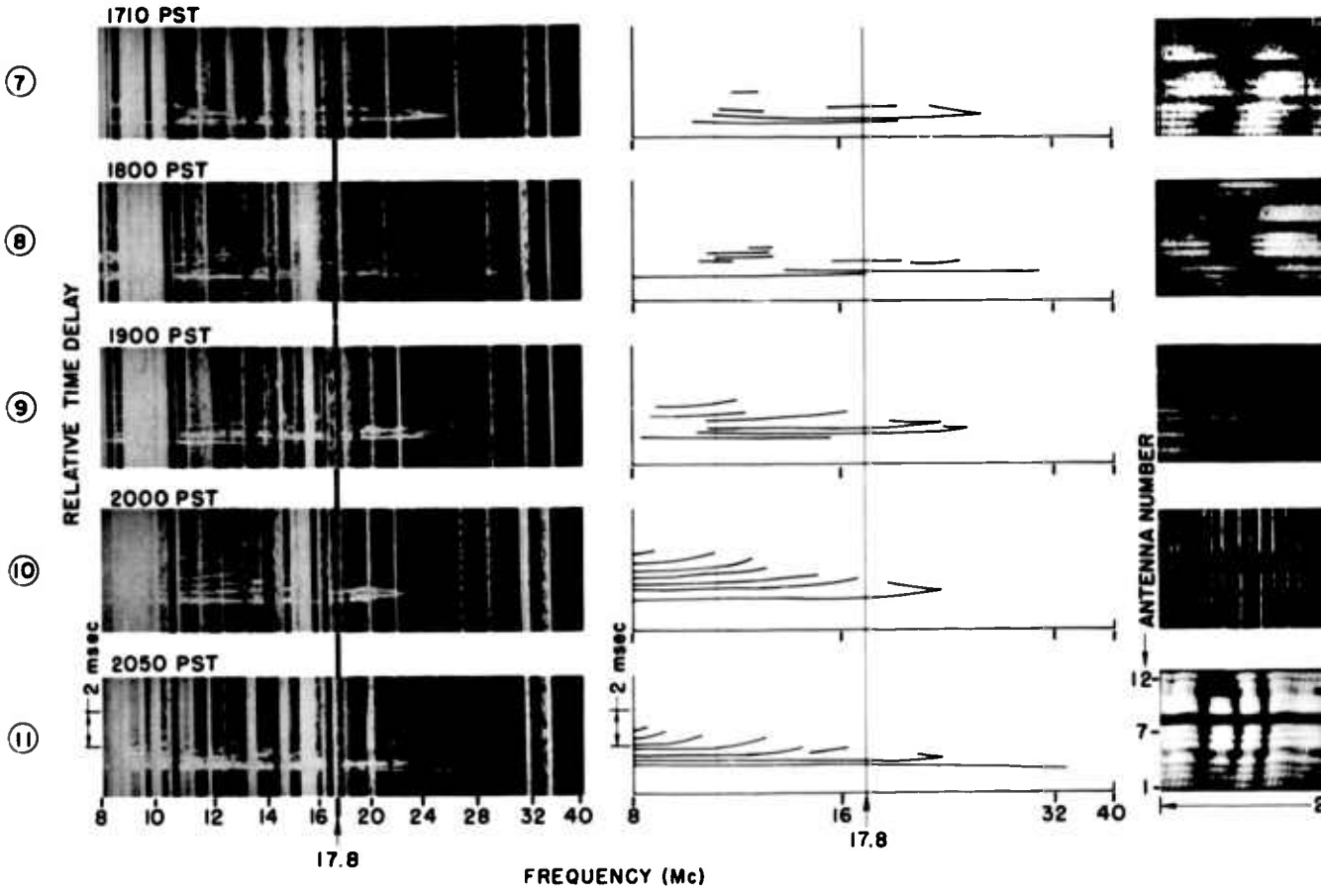
1710 PST
1800 PST
1900 PST
2000 PST
2050 PST
⑦
⑧
⑨
⑩
⑪
RELATIVE TIME DELAY
2 msec
8 10 12 14 16 20 24 28 32 40
17.8
8 16 32 40
17.8
FREQUENCY (Mc)
ANTENNA NUMBER
12
7
1

Fig. 20b.

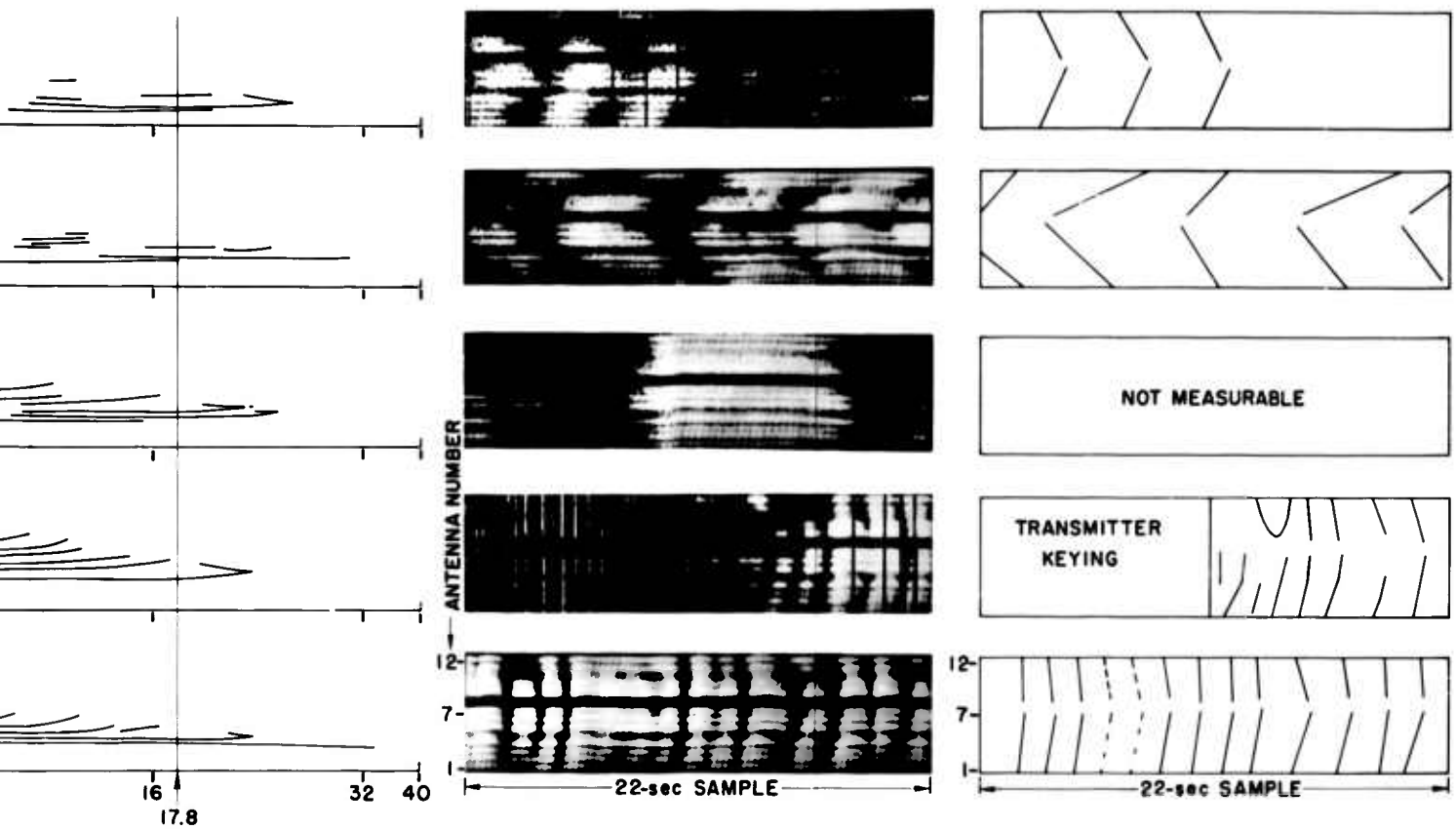
16
17.8
32
40
ANTENNA NUMBER
12
7
1
22-sec SAMPLE
NOT MEASURABLE
TRANSMITTER
KEYING
12
7
1
22-sec SAMPLE

c)

Fig. 20b.

the angle of arrival of radio waves reflected obliquely from such a surface. Though their experimental work was at a wavelength of 10 cm, the mechanism they describe should be generally applicable.

2. 18 April 1963

Figures 21 and 22 show more typical mode configurations and associated fading patterns for 18 April 1963. The fading during the appearance of the two-hop ray is interesting. The rays must have been in the vertical great-circle plane at this time since ϕ was 0 deg. During the course of the establishment of the two-hop ray, the null spacing increased from 0.35 to 0.6 km, implying that the interfering rays were coming closer to each other in angle of arrival. For this reason the interference must have been between the 1F and 2F lower rays rather than between 2F upper and lower rays.

Later, at 1500, a three-hop, F-layer reflection appeared, and with it periodic fading with characteristically small spacing between nulls.

C. CORRELATION OF OBSERVED FADING-PATTERN PARAMETERS WITH KNOWN MODE CONFIGURATIONS

1. Hawaii Data

The parameters of fading patterns observed during periods of known propagation-mode structure are compared in Fig. 23 with values predicted to occur as a result of various typical propagation conditions. This comparison is one of the most fruitful in demonstrating the effects of the relative elevation and bearing of radio waves interfering to form spatial fading patterns on null spacing and orientation. As before, the discussion will deal in detail primarily with results observed on signals from Hawaii, since more data are available for this path than for the others.

Oblique-sounding records such as are shown in Fig. 20 were examined for instances during which the mode structure was relatively unambiguous and readily interpreted. One-hundred-and-eleven hours of such data were found on 22 days between 19 March and 6 June 1963. During these times it was, of course, also required that the cw transmitting and

receiving equipment be operating properly, and that the ionosphere be dense enough to support a signal at 17.8 Mc.

The fading data were sorted into three groups in which the highest-order propagating mode observed on the coincident oblique ionograms was either 1F, 2F, or 3F. The static fading parameters for these three groups were then plotted in Fig. 23, superimposed on grids of values predicted for typical ray elevations for the different modes. The grids are calculated from Eqs. (5), (6), and (7) and are in fact the same as those in Figs. 7, 8, and 9, except that they show ϕ values in quadrants III and IV separate from those in I and II and that they include more detailed values of $\Delta\theta$ and $\Delta\eta$.

It is clear at once from examination of Fig. 23 that the bulk of values of ϕ lie in quadrants II and IV and that interference between higher-order modes results in decreased values of null spacing. In general, the observed data agree quite well with the values predicted by the interference model and expected ionospheric tilt discussed in Chapter II. In view of the approximate 180-deg symmetry of the data, two centroids (shown as circled crosses) were calculated for each of the scatter plots of D vs ϕ. The logarithmic D scale makes the centroids appear slightly high, and the scarcity of points on the 3F plot makes the centroids in that case somewhat ambiguous. In addition, values of D greater than 10 km were plotted as 10 km, but the centroids were calculated using the full values.

A number of interesting additional phenomena, not all of which are understood, appear in the D-vs-ϕ scatter plots.

In Fig. 23a there are two quite symmetrical groups of points clustered about ϕ = 100 deg and ϕ = 280 deg, with values of D between 0.4 and 2.0 km, corresponding to values of $\Delta\theta$ (bearing separation) between 0.5 and 2.0 deg and elevation separation $\Delta\eta$ up to about 6 deg. These points probably correspond to interference between 1F upper rays and either 1F lower rays or 3E rays.

There is another group of points in Fig. 23a, with values of ϕ between 330 and 360 deg, that is not balanced by a corresponding group near 180 deg. These points have values of $\Delta\theta$ up to about 1 or 2 deg and values of $\Delta\eta$ over 8 deg. They seem to result from

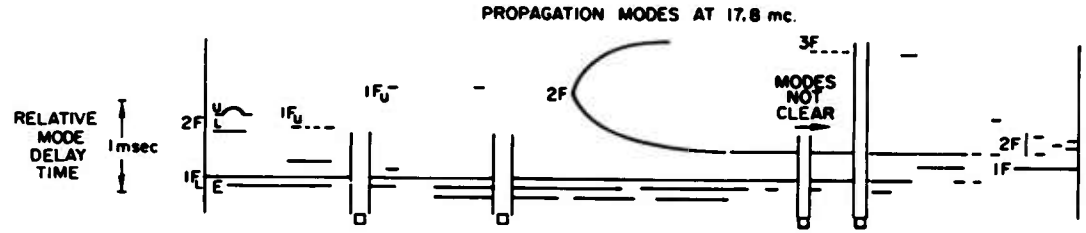
PROPAGATION MODES AT 17.8 mc.
RELATIVE MODE DELAY TIME
1msec
2F
1F
MODES NOT CLEAR
3F

a.

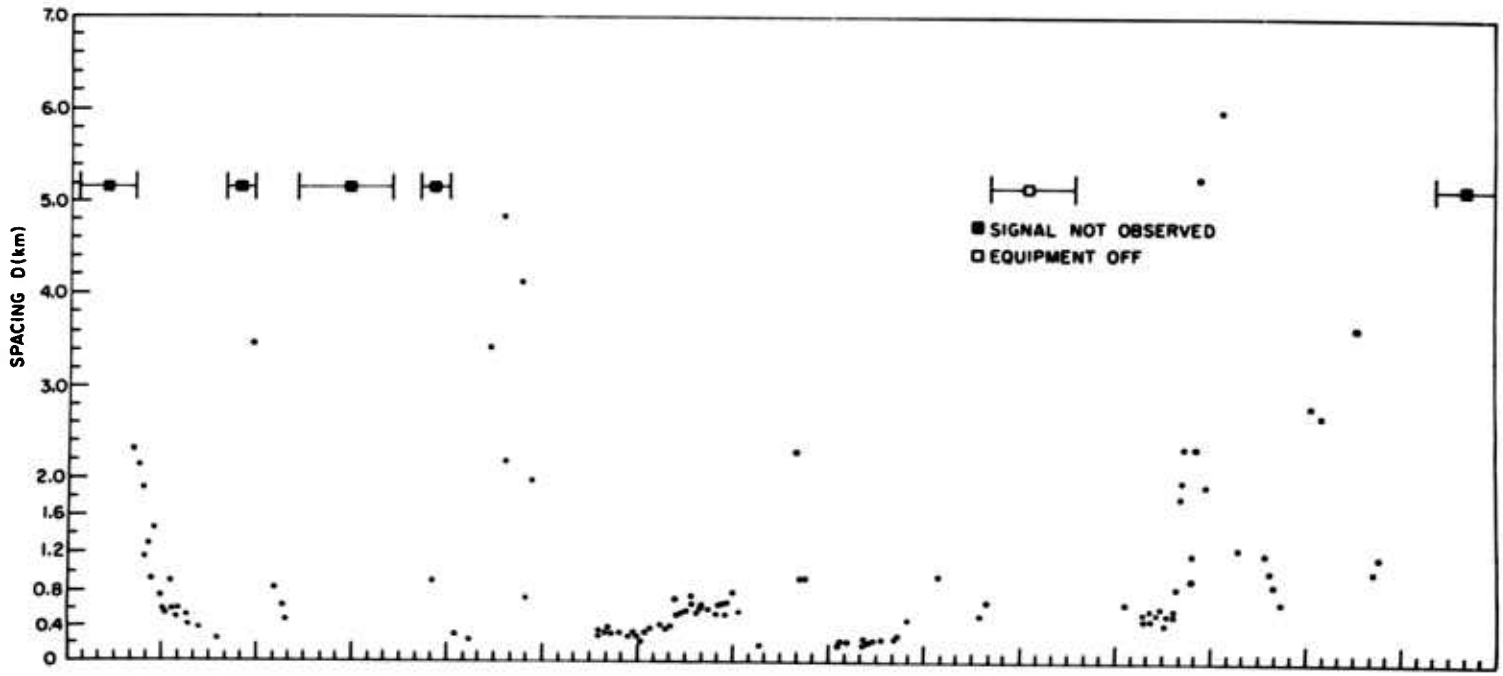
SPACING D(km)
7.0
6.0
5.0
4.0
3.0
2.0
1.6
1.2
0.8
0.4
0
SIGNAL NOT OBSERVED
EQUIPMENT OFF

b.

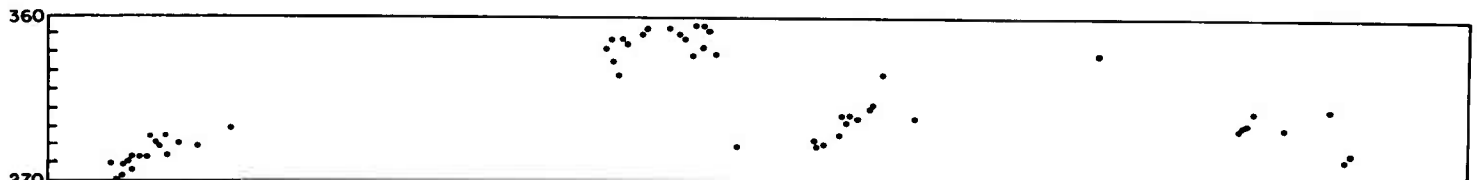
360
270

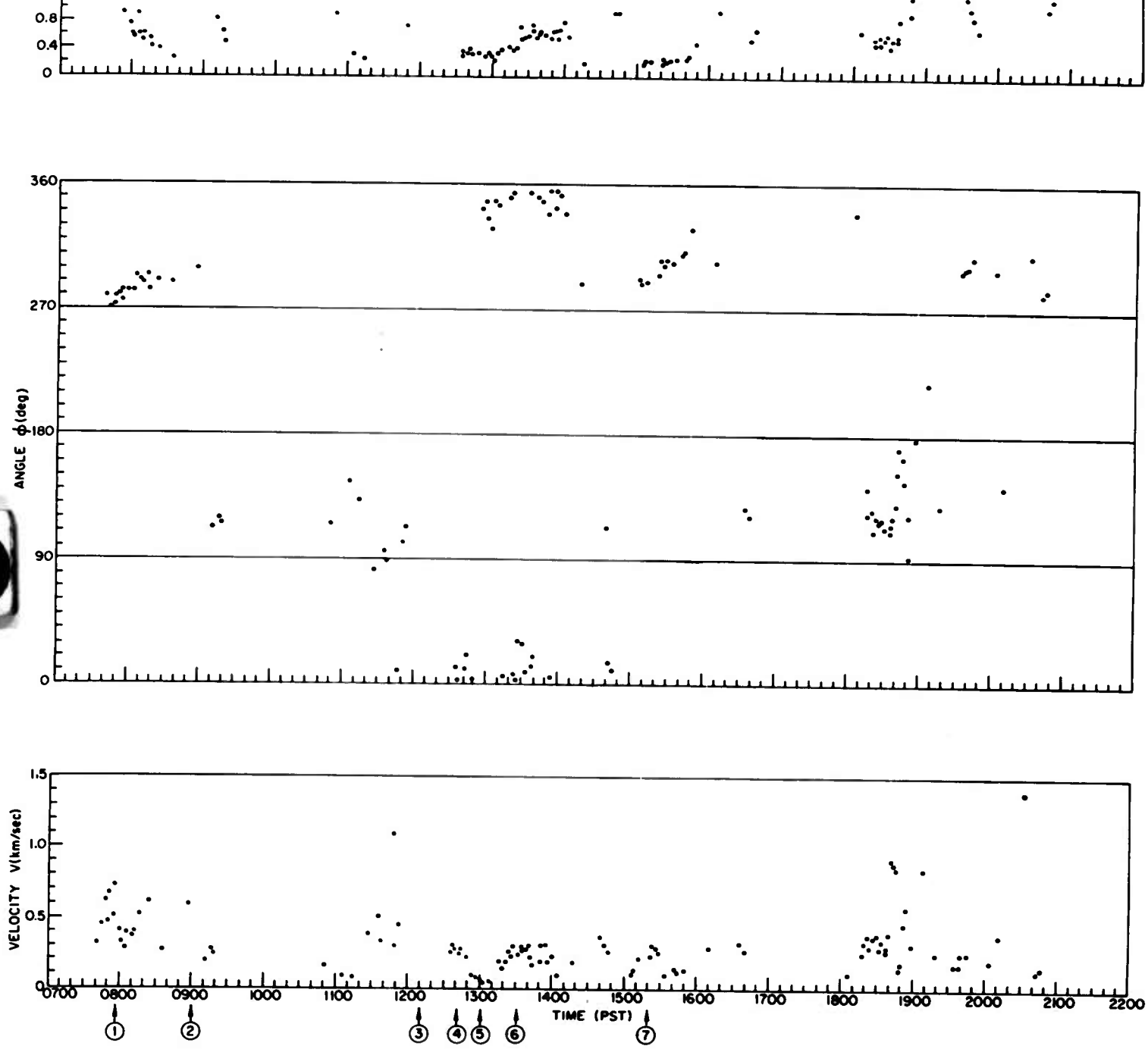

Fig. 21. PLOTS OF NULL SPACING, DIRECTION, VELOCITY AND PROPAGATION MODE STRUCTURE FOR 18 APRIL 1963.

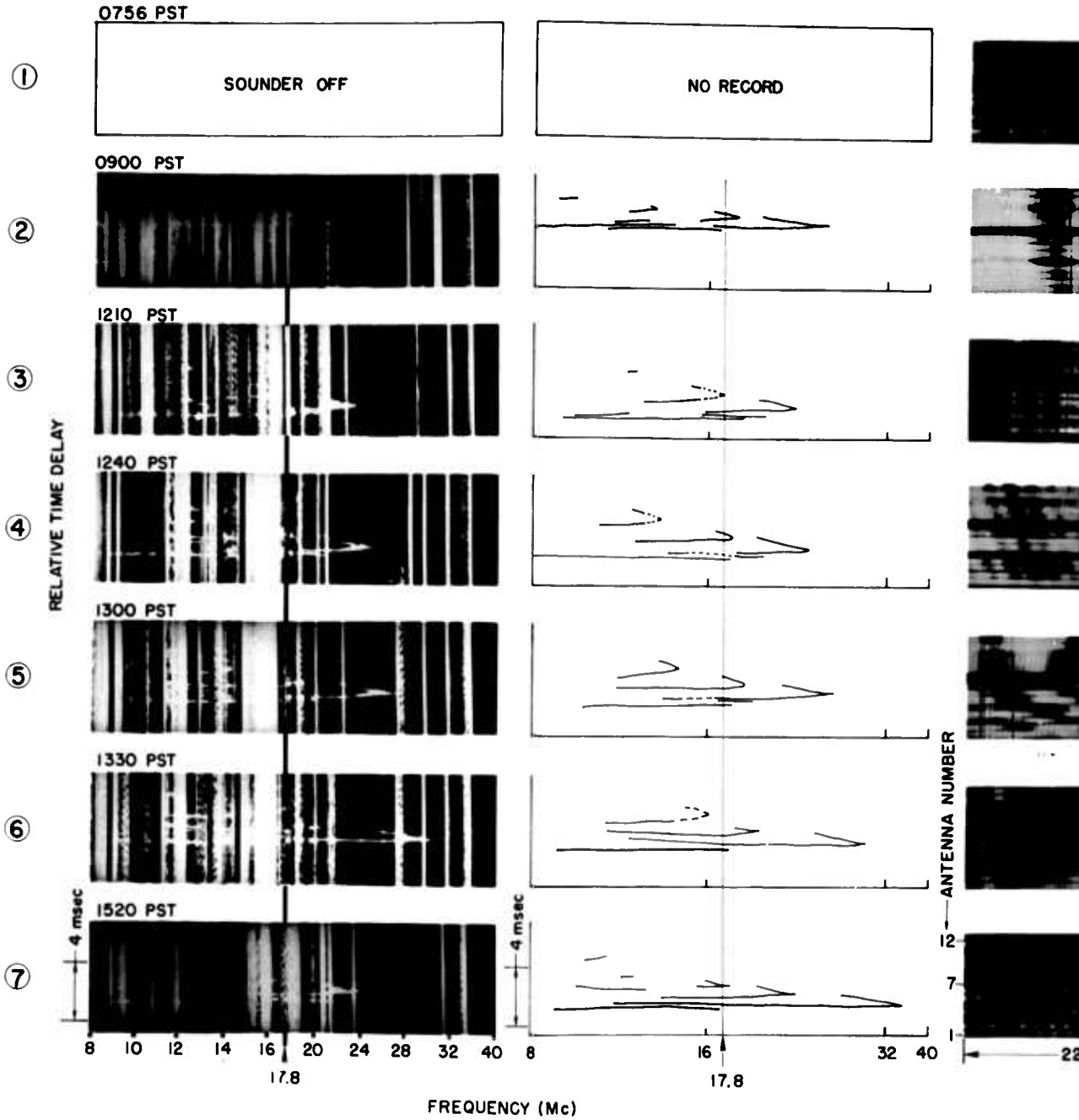

Fig. 22. COMPARISONS OF cw FADING PATTERNS AND P
RECORDS FOR 18 APRIL 1963.

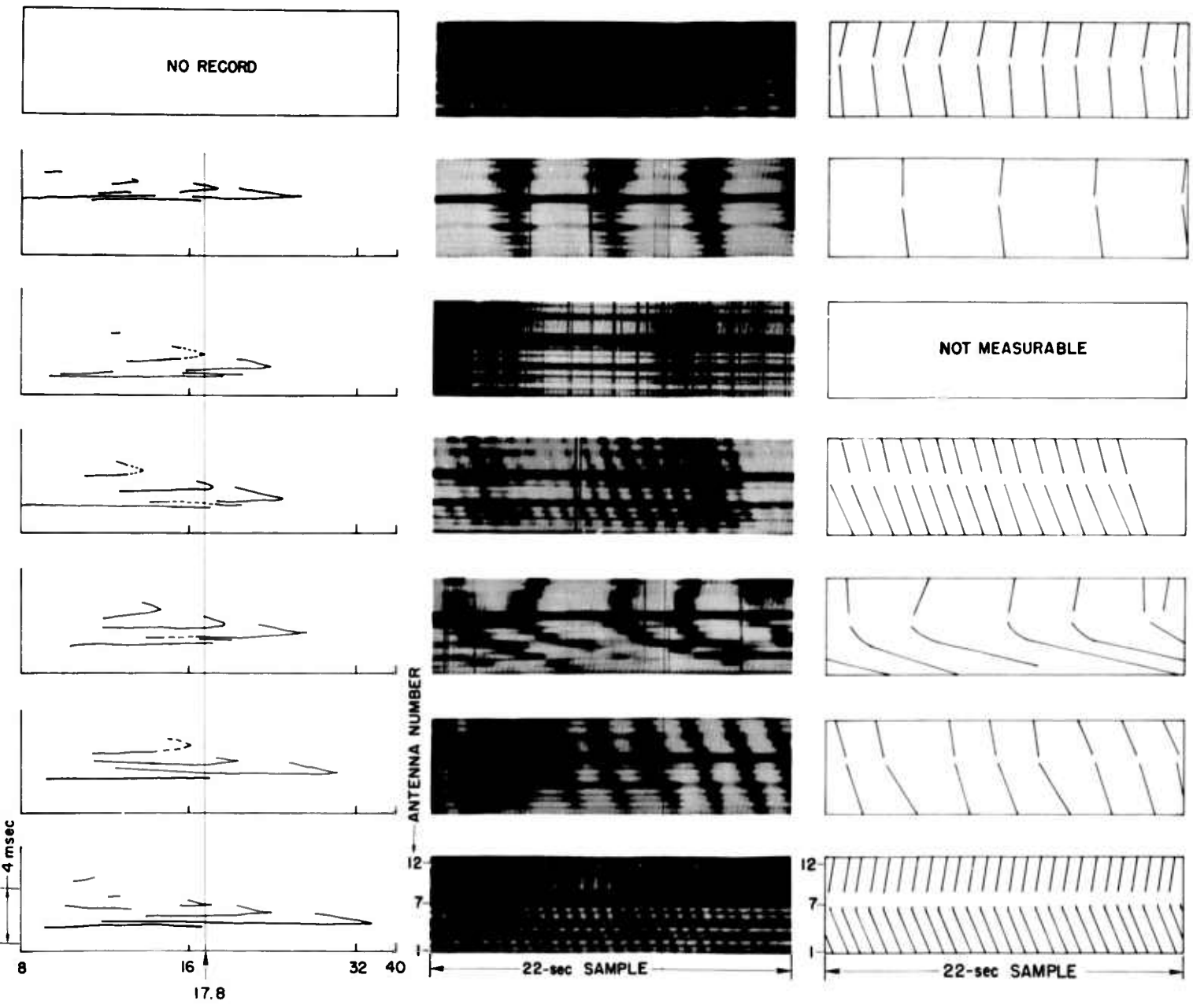

Fig. 22. COMPARISONS OF cw FADING PATTERNS AND PROPAGATION-MODE RECORDS FOR 18 APRIL 1963.

2

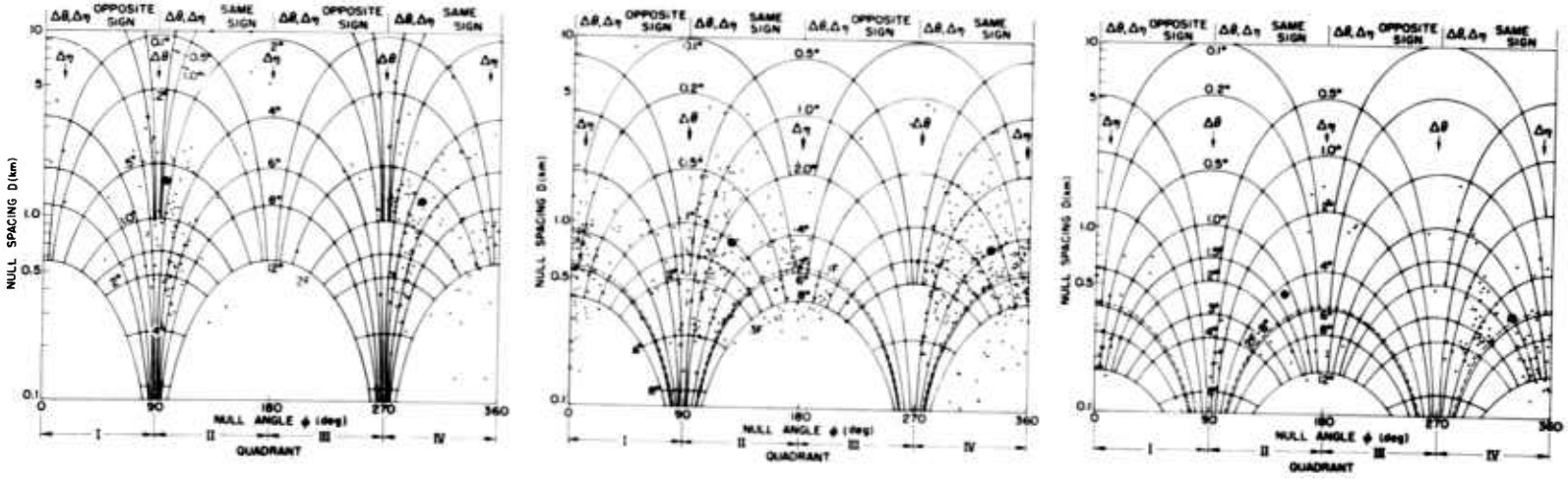

23a. 1F Propagation

23b. 2F Propagation

23c. 3F Propagation

Fig. 23. PREDICTED AND OBSERVED FADING-PATTERN PARAMETERS DURING PERIODS OF DIFFERENT-LAYER PROPAGATION FROM HAWAII.

interference between rays that are both close to the great-circle bearing and that never come close to each other in elevation, such as perhaps different-order E-layer rays. The fact that Φ for this group is near 360 deg means that the nulls are moving in the approximate direction of the transmitter. Such motion would result if the frequency of the higher-elevation-angle ray had a larger positive value of doppler shift than the lower-elevation-angle ray. The 3E ray would, of course, be expected to have a larger doppler shift than the 2E ray, though it is not so obvious why the 3E value should always appear to be positive with respect to the 2E shift.

Figure 23b, showing fading parameters during times when 2F was the highest-order mode observed, contains the largest number of points of the three D-vs-Φ plots and is the most nearly symmetrical.

The points in this case fairly evenly fill quadrants II and IV and also show a grouping around Φ = 0 deg that has a number of points in quadrant I. The bearing deviation $\Delta\theta$ is generally between 0.5 and 4 deg, and the elevation difference varies from 0 deg up to about 8 or 10 deg. The elevation difference may in this and Fig. 23c be negative corresponding to 1F or E rays, in which case the bearing difference is generally negative also. All that is required for Φ to lie in quadrants II or IV is that $\Delta\theta$ and $\Delta\eta$ have the same sign, which will result from a general north to south downward tilt of the reflecting layers.

The 3F scatter diagram, Fig. 23c, has, as expected, the smallest average values of null spacing and also shows a concentration of Φ values in the second and fourth quadrants. The splitting of the points in quadrant IV into two groups, leaving the centroid in a region of few points, may have the same significance as in Fig. 23b. It should be kept in mind that 1F, 2F, or E rays can contribute to the effects observed in the 3F plot, since the criterion for selection was simply the identity of the highest order mode. The laterally deviated rays during times of 3F propagation appear to cluster about $\Delta\theta$ = 3 deg and $\Delta\eta$ = 4 deg.

2. Puerto Rico and Texas Data

Scatter diagrams of D vs ϕ for the Puerto Rico and Texas observations are shown in Figs. 24 and 25.

Lower rays from Puerto Rico could have arrived with elevation angles from 5 deg (2F) to 23 deg (5F) and upper rays to about 30 deg. Since no oblique ionograms were available for the Puerto Rico path, the data are not separated by mode. The primary conclusion to be drawn from Fig. 24 is that the null patterns have values of ϕ primarily in quadrants I and III, as expected from the prevailing lateral ionospheric tilts over the path.

The values of D and ϕ observed on the signals from Texas were much more concentrated in value about approximate means of D = 0.7 km and ϕ = 11 and 222 deg. Only the 1F lower and upper rays at estimated elevation angles of from 13 up to 31 deg were observed over the Texas-to Stanford path. The elevation angles were estimated from ray tracings by Croft and Gregory [1963] for a representative daytime ionosphere over an 1840-km path. Both groups of points have mean ϕ and D coordinates that correspond to elevation differences of 4 deg between the rays. The bearing separations between the rays are significantly different, however. The group in quadrant III has a value of $\Delta\theta$ of -1.0 deg, which is about what would be expected from the ionospheric tilt, but the mean value of the group in quadrant I corresponds to a $\Delta\theta$ of only -0.2 deg. The origin of this asymmetry is not well understood, though it seems not to be an equipment effect. Such an asymmetry would occur if the nulls are curved, rather than straight, and if the curvature is different for opposite directions of null motion.

The $\Delta\theta$, $\Delta\eta$ grid is the same one used in Fig. 23b for η_o = 14 deg but the difference is negligible for the measurements made here.

D. AVERAGE VALUES OF FADING PARAMETERS

1. Orientation of Fading Nulls

Histograms of the distribution of ϕ as measured on signals propagated over the three paths studied are shown in Fig. 26 and are summarized in Table 2. For each path about 70 percent of the nulls lie

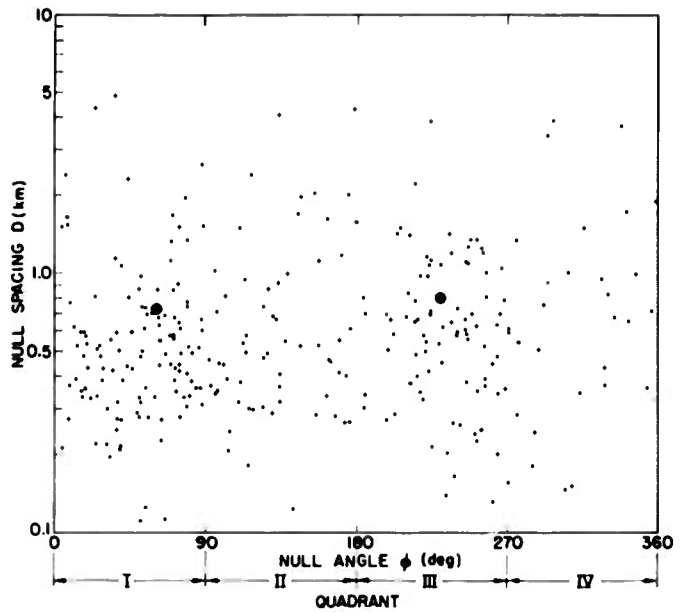

Fig. 24. OBSERVED FADING-PATTERN PARAMETERS (D vs ϕ) FOR ALL PROPAGATION FROM PUERTO RICO.

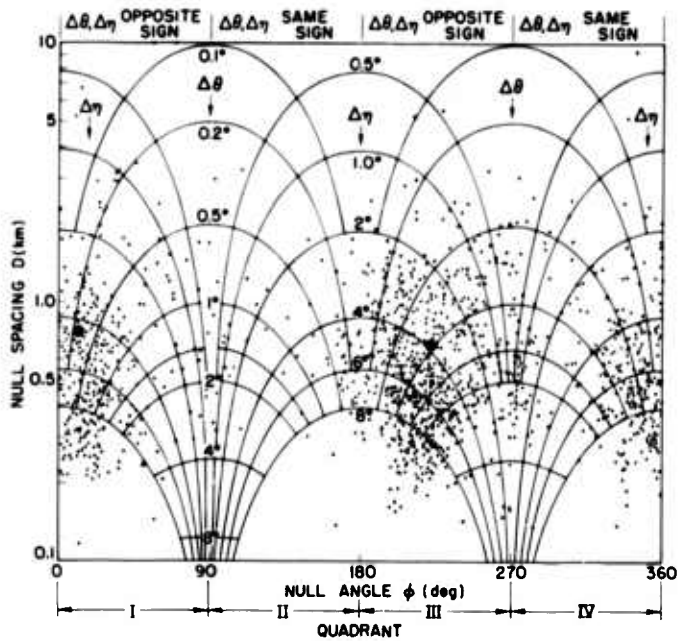

Fig. 25. PREDICTED AND OBSERVED FADING-PATTERN PARAMETERS FOR ALL PROPAGATION (1F) FROM TEXAS.

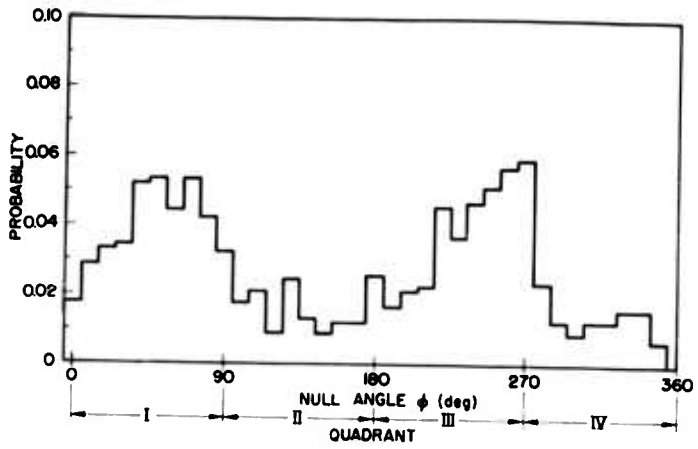

26a. Puerto Rico-to-Stanford Path

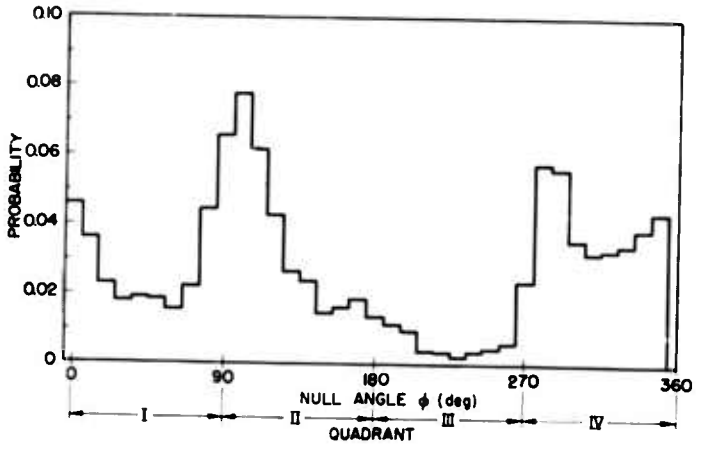

26b. Hawaii-to-Stanford Path

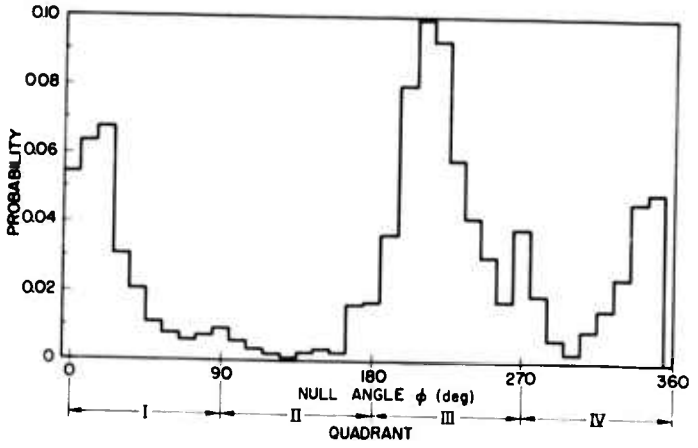

26c. Texas-to-Stanford Path

Fig. 26. DISTRIBUTION OF ALL ϕ MEASUREMENTS.

in the expected quadrants, though some distributions are biased toward one or the other extremity of the expected quadrant.

TABLE 2. PERCENTAGE OF ϕ MEASUREMENTS IN 90-DEG QUADRANTS OVER DIFFERENT PATHS

Quadrant	Percent of ϕ in Quadrants		
	Puerto Rico -SU (expect I,III)	Hawaii -SU (expect II,IV)	Texas -SU (expect I,III)
I	36	24	27
II	15	35	5
III	32	6	47
IV	17	35	21
I and III	68	30	74
II and IV	32	70	26

Note: $\phi = 0$ corresponds to a null lying perpendicular to the great circle between transmitter and receiver and moving toward the transmitter (see Fig. 3).

Symmetrical pairs of quadrants are compared in Table 2 because the fading-pattern model predicts only the orientation and spacing of the null patterns and not their direction of motion. Since the observed values of ϕ describe direction of null motion as well as orientation, data from opposite quadrants are added together for comparison with the model.

2. Null Spacing

a. Mean Value

The overall mean value of null spacing D observed on the fading patterns of signals from Hawaii is 0.88 km, with a standard deviation of 0.98 km. Comparable figures for the signals from Puerto Rico and Texas are shown in Table 3. The difference in numbers of D and V measurements is a result of the presence of fading patterns in which it is possible to find individual nulls that are typical of the

sample but that are not adjacent to a sufficiently similar null for a meaningful measurement of D or F.

TABLE 3. SUMMARY OF FADING-PATTERN MEASUREMENTS

Path	Number of Measurements	Spacing D (km)	
		Mean	Std. Deviation
PR-SU	305	0.755	0.741
Hawaii-SU	3506	0.880	0.984
Texas-SU	1527	0.694	0.674
		Velocity V (km/sec)	
		Mean	Std. Deviation
PR-SU	899	0.382	0.445
Hawaii-SU	3520	0.322	0.329
Texas-SU	1527	0.222	0.195
		Fading Rate F (cps)	
		Mean	Std. Deviation
PR-SU	305	0.644	0.304
Hawaii-SU	3506	0.476	0.351
Texas-SU	1527	0.388	0.262

b. Average Diurnal Variations

Figure 27 shows the average diurnal variation of null spacing for the Hawaii path. The time scale for each of the 27 days included in this curve was normalized so that the time of cw signal fade-in was 0800 PST and of fade-out was 2000 PST. The actual fade-in time varied from 0658 to 1144 PST and the fade-out time varied from 1610 to 2338 PST. Only those days were used on which the equipment operated through fade-in and fade-out.

The spacing had maximum values at initial fade-in and final fade-out. This fact and the 2-km magnitude of the initial and final null spacing imply that this fading was caused by interference between 1F upper and lower rays when the ionized layer was forming and decaying.

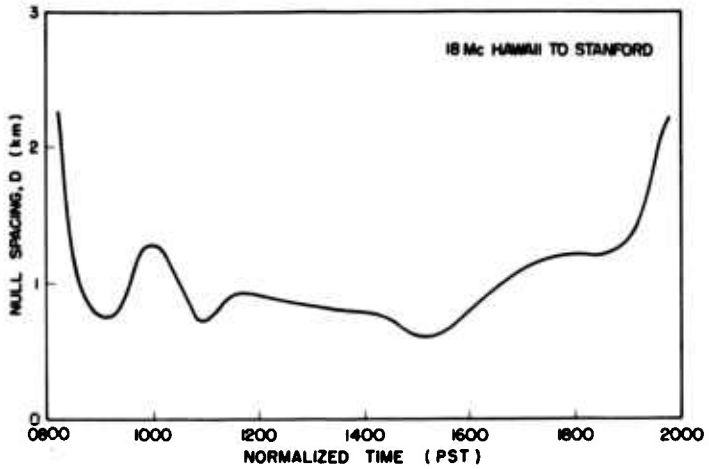

Fig. 27. AVERAGE FADING-NULL SEPARATION (km) AS A FUNCTION OF TIME NORMALIZED TO SIGNAL FADE-IN AND FADE-OUT.

About two hours after fade-in, a smaller peak value of null spacing occurs that is associated with the appearance of the two-hop ray. This peak corresponds to interference between 2F upper and lower rays.

During the middle of the day the time normalization masks any other sharp changes in null spacing, though the dip at 1500 PST occurs at the time of day when the highest-order (usually 3F) modes are possible and so a minimum spacing is expected, because of the high angle of arrival of 3F.

Similar diurnal variation is observed on signals propagated over the Puerto Rico and Texas paths.

E. FADING PATTERN VELOCITY AND FADING RATE

A smoothed curve of the diurnal variation of the mean value of null velocity is shown in Fig. 28. The time is normalized to signal fade-in and fade-out as in Fig. 27, which used the same Hawaii-to-Stanford fading-pattern observations. The mean fading-pattern velocity during the first hour that the signal is present decreases from 0.7 to 0.35 km/sec and remains at about 0.3 km/sec during most of the rest of the day. A slight dip at about 1530 local time indicates the period of

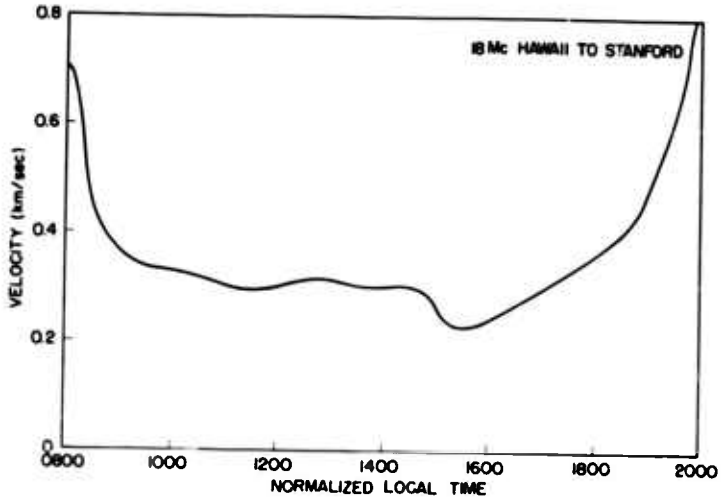

Fig. 28. AVERAGE FADING-NULL VELOCITY AS A FUNCTION OF TIME NORMALIZED TO SIGNAL FADE-IN AND FADE-OUT.

maximum stability of the reflecting layers. Following this, the velocity gradually rises to 0.8 km/sec at fade-out.

The fading rate is defined as the number per second of envelope minima or maxima appearing at a particular antenna. During periods of periodic fading patterns the fading rate is also equal to the null velocity divided by null spacing, $F = V/D$. The diurnal variation of fading rate, derived in this manner from the same observed Hawaii-path data as Figs. 27 and 28, is shown in Fig. 29. The average fading rate is seen to fluctuate much less than either the average null velocity or average spacing; thus the diurnal variation of null velocity can be considered (as discussed in Chapter II-C) to be a result of the diurnal variation of average null spacing.

A clear example of the difference in fading-pattern effect produced by ray geometry and by signal doppler shift is given in Figs. 30 and 31 which show fading-pattern data during a reversal of direction of null motion. During the time shown in the figures, 1F upper and lower rays were interfering to produce the observed fading patterns, which was true of virtually all the Texas data. The ray elevations and

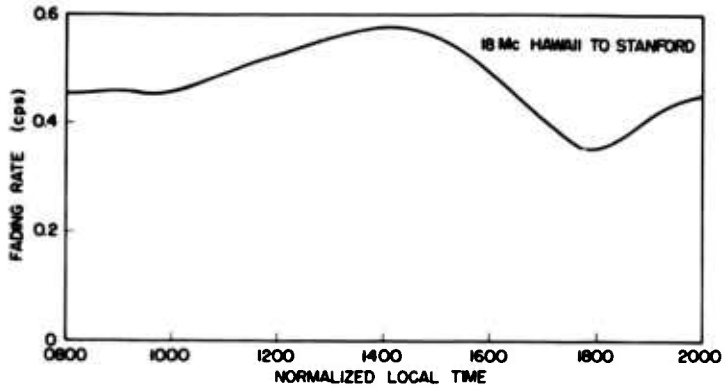

Fig. 29. AVERAGE FADING RATE AS A FUNCTION OF TIME NORMALIZED TO SIGNAL FADE-IN AND FADE-OUT.

bearings remained constant during the period. This constancy is deduced from the fact that the oblique ionograms showed a constant delay time between the 1F upper and lower rays and that the null spacing and orientation, except for the 180-deg shift, remained nearly the same. The fading rate, which is simply the difference in doppler shifts of the two rays, went through a definite zero value at the time of the reversal of null direction.

It can be seen from this sequence of events that, as previously predicted, the orientation and spacing of nulls in a fading pattern is a function of ray geometry, and the null velocity adjusts itself to accommodate the fading rate determined by the difference in doppler shifts of the two interfering waves.

F. FADING PATTERN OBSERVATIONS DURING TWO MAGNETIC STORMS

Routine fading-pattern and mode-identification measurements were in progress on the Hawaii-to-Stanford signal during the moderately severe magnetic storms of 30 April and 6 June 1963. Both storms produced similar effects on the fading patterns and mode structure. These effects are explained in terms of a description of the average morphology of magnetic storms based on observations of over 100 such storms by Matsushita [1959].

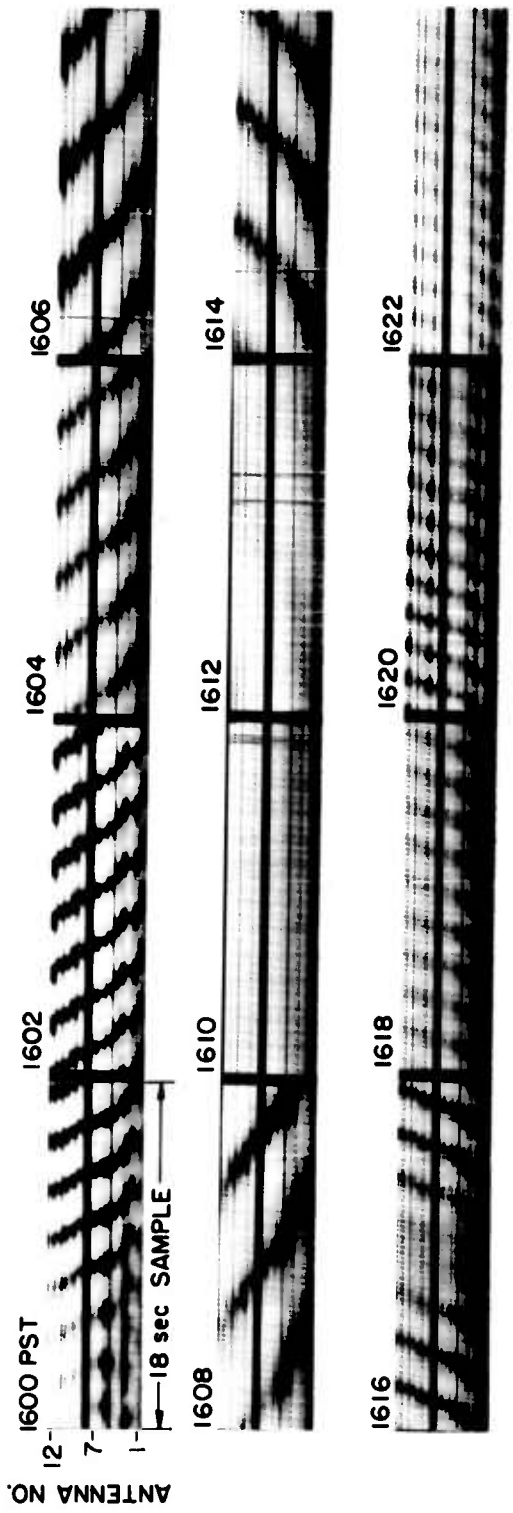

Fig. 30. FADING-PATTERN RECORDS OF 7 OCTOBER 1963 FOR THE TEXAS-STANFORD PATH SHOWING REVERSAL IN DIRECTION OF NULL MOTION.

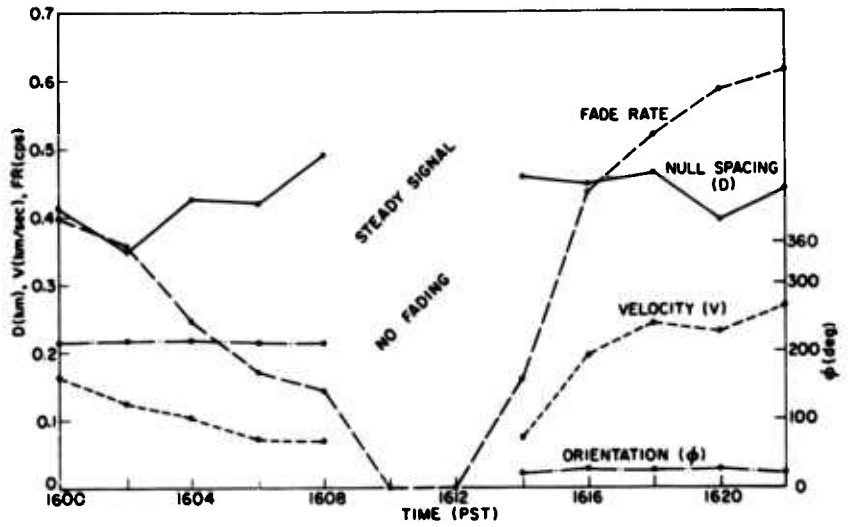

Fig. 31. FADING PARAMETERS DURING REVERSAL OF NULL DIRECTION.

Matsushita shows that, during summer at the latitudes involved in the present experiment (his regions 4, 5, and 6), there is a moderate increase in maximum electron density during the first 9 or 10 hours of the storms at the higher latitudes and less or none at the lower. During the next 40 hours, there is a large decrease in maximum density throughout the region, with the decrease being greater at higher latitudes. There is actually an increase near the geomagnetic equator. The effect of these phenomena on the normally tilted layers of constant ion density is shown in simplified schematic form in Fig. 32 in which it is assumed that an increase in the maximum electron density of a layer lowers the contours of fixed electron density.

Figure 32 shows that, during the first day of a magnetic storm, there should be less than the normal amount of ionospheric tilt and therefore ϕ for the fading patterns should rotate toward 0 and 180 deg. Since, during this period, the ion density is greater than normal, the existence of modes of more than the usual number of ionospheric reflections should be possible with a resulting decrease in null spacing. During the second day of the storm the tilt may be greater

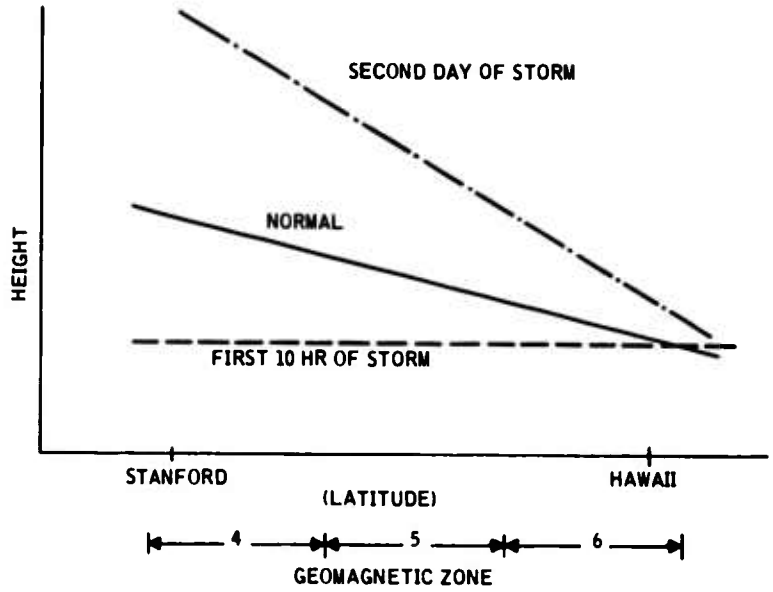

Fig. 32. CHANGE IN HEIGHT AND SLOPE OF A CONTOUR OF FIXED ION DENSITY DURING A MAGNETIC STORM.

than normal, moving ϕ toward 90 and 270 deg. The lower value of electron density will allow fewer ionospheric reflections, resulting in an increase of null spacing above its normal value.

That these effects occur is shown by the contents of Table 4 and Fig. 33.

During both magnetic storms the value of null spacing is reduced below normal the first day and rises above normal the second day. This is clearly a result of the fact that on both first days signals were received that had experienced three F-layer reflections, whereas the highest order mode observed under undisturbed conditions was usually 2F. On both second days most of the signals arrived with only one F-layer reflection and therefore the null spacing was relatively large.

Figure 33 shows that on both first days the null direction was concentrated about 0 and 180 deg and on the second days about 90 and 270 deg, presumably for the reasons discussed above.

The fading rate was higher than normal on both first days and near or below normal on both second days. This is reasonable since the fading rate is equivalent to the difference in doppler shifts of the

Table 4. SUMMARY OF MAGNETIC STORM DATA OVER HAWAII-STANFORD PATH

	Average of Hawaii-Stanford Data 11-2-62 to 6-8-63	Magnetic Storm of 4-30-63		Magnetic Storm of 6-6-63	
		4-30	5-1	6-6	6-7
Null Spacing D (km)					
Mean	0.880	0.780	1.13	0.465	1.27
Std. Dev.	0.984	1.02	1.32	0.722	0.974
Null Velocity V (km/sec)					
Mean	0.322	0.501	0.442	0.246	0.329
Std. Dev.	0.329	0.546	0.405	0.245	0.252
Fading Rate F (cps)					
Mean	0.476	0.859	0.440	0.693	0.282
Std. Dev.	0.351	0.563	0.259	0.408	0.163
Measurable Fades (%)	26	40	34	28	16
Average Value of Kp* During cw Observations	---	5+	3+	6-	2
Highest-Order Propagating Mode	3F	3F	2F (mostly IF)	3F	1F

*Kp is the geomagnetic, planetary, 3-hr, range index prepared by the Committee on Characterization of Magnetic Disturbances, J. Bartels, Chairman, University, Göttingen, Germany. Values regularly appear under "Geomagnetic and Solar Data" in the Journal of Geophysical Research.

two interfering rays and the doppler shift of a ray can be expected to increase with the number of ionospheric reflections.

The fact that the fading during the storm of 30 April 1963 was much more periodic than normal implies that during this storm the total amount of random variation in ionization encountered by the rays was less than normal (see Chapter IV-A).

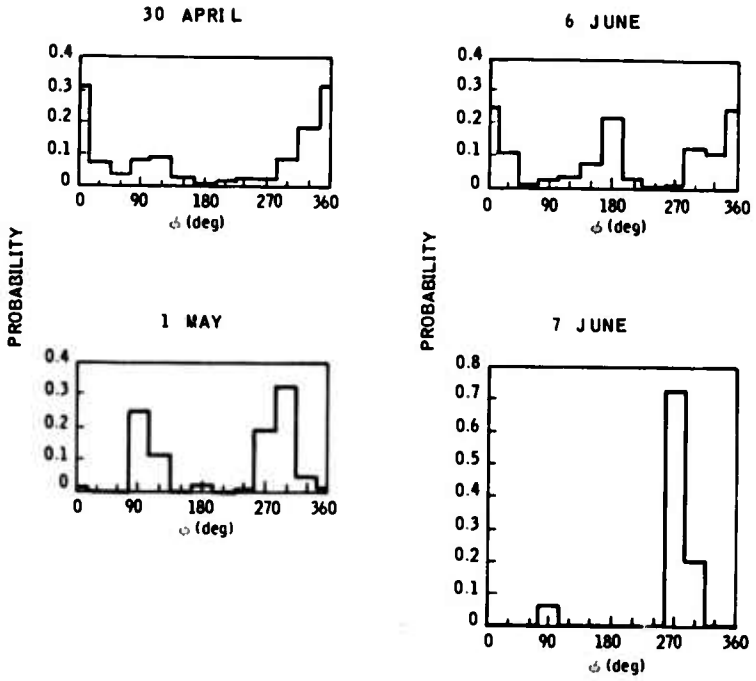

Fig. 33. DISTRIBUTION OF ϕ MEASUREMENTS DURING TWO MAGNETIC STORMS.

An example of the fading patterns observed during the first day of one of the storms is shown in Fig. 34. Note the rapid fading pattern superimposed on the slow one. Both patterns have similar values of ϕ but differ in null spacing and fading rate.

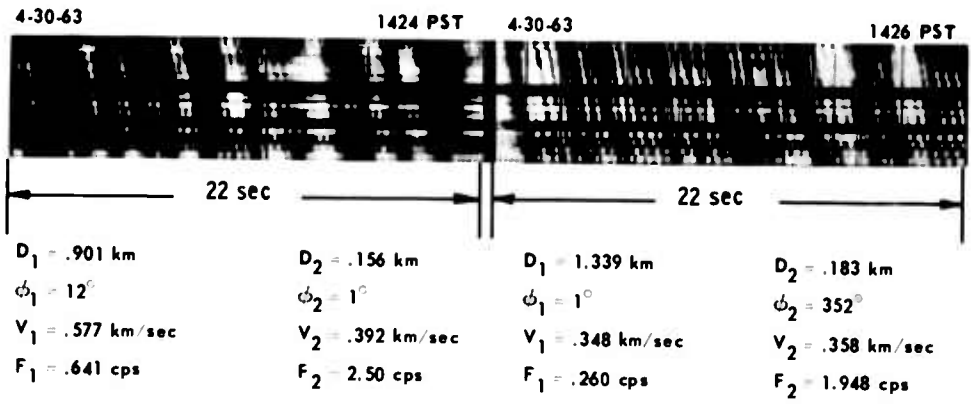

Fig. 34. FADING-PATTERN RECORDS DURING MAGNETIC STORM OF 30 APRIL 1963.

V. POSSIBLE APPLICATIONS OF THE RESULTS OF THIS WORK

A. SPACE DIVERSITY RECEPTION

A well known technique for reducing the harmful effects of fading is the use of two or three receiving antennas spaced a few wavelengths apart, each connected to its own receiver, and with the receivers interconnected in such a way that the one with the strongest signal provides the total output of the system. In this way, if one antenna is in a region of deep fade and is therefore yielding a noisy signal, it is essentially disregarded.

Studies such as those by Van Wambeck and Ross [1951] indicate that it is important to space the different antennas far enough apart but that, for a given spacing, the location relative to the propagation path is unimportant. Since in their experiment they located their antennas only along and across the propagation path, and since the average null direction was probably at an oblique angle to the path, the latter result is understandable. The present experiment shows that there is definitely a preferred direction associated with signal-fading patterns.

It seems reasonable to suppose that the proper use of preferred null-orientation information could lead to some improvement in the layout of space-diversity reception systems. First, the path in question must be examined in order to predict the most likely fading patterns, as is done in Chapter II-C. A hypothetical fading pattern so derived is shown in Fig. 35 superimposed on a typical space-diversity-antenna layout, consisting of three antennas shown as log-periodics, A, B, and C, spaced 300 m apart both along and across the propagation path. The effective diversity is only $300\sqrt{2}$ or 212 m however, because of the orientation of the most likely fading patterns. If B or C is moved to position D, the effective diversity will be doubled to 414 m at no increase in cost. It is probable that some space-diversity systems have been constructed with the A, C, D, layout rather than the A, B, D pattern. This choice seems to have been a matter of chance rather than design, however. There are, in addition, some systems using four antennas in an A, B, C, D pattern, which should, of course,

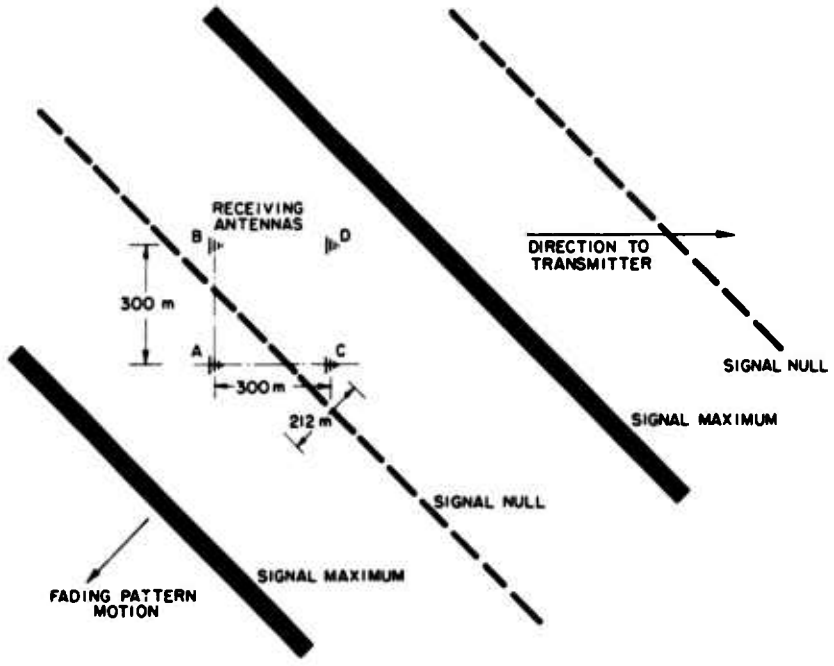

Fig. 35. HYPOTHETICAL FADING PATTERN SHOWING EFFECT OF DIFFERENT SPACE-DIVERSITY-ANTENNA LAYOUTS.

work quite well, though they should work almost as well without either B or C.

Even when the fading nulls do not consist of straight, parallel lines, as is usually the case for propagation over paths in excess of 5000 km, they would be expected to assume an average direction as determined by the ionospheric tilt at the reflection points near the receiver.

B. IONOSPHERIC TILT MEASUREMENTS

It is often desirable in ionospheric research to be able to measure small tilts of the ionized layers. See, for example, Fenwick and Villard [1963] dealing with "Round-the-World" transmissions, or Bramley [1956], who was measuring direction-finder errors. The observations of fading patterns in this experiment are a relatively simple yet very sensitive

means of measuring tilts using a cw transmitter and receiver and several inexpensive antennas.

Direction-finding measurements should be more accurate if made during periods of no ionospheric tilt. Such periods are indicated by values of null direction φ near 0 and 180 deg. Thus the most precise direction-finding measurements should be made during periods when the fading nulls lie approximately perpendicular to the direction to the unknown transmitter as obtained during routine measurements.

VI. DESIRABLE FUTURE STUDIES

A. NORTH-SOUTH PATH

On a north-south path the latitude variations in ion density would not affect the fading-pattern orientation, but diurnal longitudinal variations should make the fading patterns change direction by 90 deg from morning to evening. Such a test would be further evidence of the effect of ionospheric tilts on fading patterns.

B. VERY LONG PATH

Since practical hf communication circuits are sometimes well over 6000 km in length, it would be useful to conduct an experiment similar to the present one over such a path, perhaps 10,000 km or more. Figure 18 indicates that the fading patterns would almost always be irregular, but the tilt of the ionosphere near the receiver might still induce a concentration of null directions even though the nulls did not form straight lines. It is difficult to be quantitative about this question, but observation of the filmed fading-pattern data seems to indicate that for each path the irregular nulls have average bearings and spacings similar to the measurable ones.

VII. CONCLUSIONS

A. NEW EXPERIMENTAL TECHNIQUES EMPLOYED

1. Multiple-Antenna Fading Measurement

The measurements reported here are believed to be the first instance in which the carrier-amplitude fading of obliquely propagated, high-frequency radio waves has been observed in a manner making possible the deduction of its spatial variations. The necessary innovation was the sampling of the instantaneous signal strength on twelve antennas disposed along two perpendicular lines. For the case of fading nulls consisting of straight or nearly straight lines, this antenna arrangement allowed the measurement of the orientation, spacing, and velocity of such nulls. Even though quantitative measurements were made on only the three antennas at the ends and intersection of the two rows, the information from the remaining nine antennas was essential for interpretation of the fading patterns.

2. Simultaneous Measurement of Fading Patterns and Propagation-Mode Structure

Synchronized, oblique, step-frequency, ionospheric sounders were used to identify the propagation modes contributing to the cw signal. Although other hf radio studies have been made using the mode data available from oblique soundings, the work reported here is the first instance of the application of such data to the study of cw fading. Even though the oblique, step-frequency, sounding data are sometimes ambiguous, they are a considerable improvement over previous mode-identification techniques, which varied in accuracy from estimates based on monthly predictions of average ionospheric critical frequencies to single-frequency, oblique, pulse soundings.

B. NEW DATA OBTAINED

It has been shown that the spatial distribution of the carrier amplitude of cw, hf radio signals propagated over moderate length paths, such as studied here, exhibits a degree of periodicity that varies

inversely with path length. Straight line fading null patterns are measurable 33 percent of the time on signals propagated 1840 km and about 10 percent of the time on signals propagated 5724 km. Presumably the "straight" fading nulls are actually curved, but with a radius of curvature much larger than the dimensions of the antenna array.

For a fixed path length the fading-null spacing decreases as the number of ionospheric reflections increases. For the 3741-km, Hawaii-to-Stanford path studied here, the mean value of null spacing for each mode was: 1F hop, 1.4 km; 2F hop, 0.75 km; 3F hop, 0.4 km. The mean velocity of the nulls along the ground varied from about 0.7 km/sec during layer formation and decay to about 0.3 km/sec during midday. The observed null velocity is a product of null spacing and envelope fading rate. The null spacing depends on the ray geometry, as shown above, and the fading rate is equal to the difference in ionospherically induced doppler shifts of the two interfering waves.

The fading nulls tend to lie diagonally across the great circle connecting the transmitter and receiver.

The degree to which the nulls are rotated from lying perpendicular to the great circle is a sensitive indication of the bearing separation of the interfering waves. The bearing separation, in turn, along with the elevation separation deduced from mode information, provides a clear indication of the degree of north-south ionospheric-layer tilt present over the path. The absolute value of the bearing of individual rays cannot be measured by this technique, though it is sensitive to small differences in the bearings of two interfering rays.

Differences of up to about 4 deg in the bearings between rays are commonly deduced from the fading-pattern measurements.

It has been shown that periodic fading is caused by destructive interference both between upper and lower rays of the same mode and between lower rays of different modes. The presence of periodic fading patterns resulting from interference between rays of different numbers of ionospheric reflections implies about 0.003 percent random electron-density variation each 10 sec along the different paths. When the fading patterns become irregular, the random fluctuations in ion density must be greater than 0.003 percent/sec.

Fading pattern measurements made during two magnetic storms indicate that on the first day of both storms the normal north-south ionospheric tilt was reduced, while on the second day it was increased. A marked increase in the periodicity of the fading patterns observed throughout one of the storms indicates a reduction in the random fluctuations of ion density that normally contribute to irregular fading patterns.

C. IMPROVEMENT OF SPACE DIVERSITY RECEPTION SYSTEMS

An improvement in the effectiveness of space-diversity reception systems can be expected if the spacing of the diversity antennas can be maximized in a direction perpendicular to the fading nulls. For paths where transverse-ionospheric-tilt information is available, the predominant fading-null orientation can be derived by the techniques presented here. Two or three antennas can then be properly positioned to maximize the space-diversity effect.

APPENDIX A. REVIEW OF STUDIES OF RADIO-WAVE FADING

Because of the practical effects of fading and the fact that it is a first-order quality of radio waves, the phenomenon of fading has been studied virtually since the inception of the use of radio as a communications technique. Though most of the early experiments were conducted at very low frequencies and over short paths and thus do not have a direct bearing on the fading of waves at high frequencies over long, oblique paths, a complete review of the study of fading must include them because many of the basic mechanisms of fading were discovered using such low-frequency, short paths.

In 1913, De Forest found selective fading between the mark and space frequencies of telegraph transmissions between San Francisco and Hawaii at a wavelength of 3100 meters. He suggested interference between ground and sky waves as the cause and that vertical motion of the layer could cause fading. His deduction is particularly interesting in view of the fact that at that time the existence of a sky wave had by no means been proved.

In 1923, Dellinger, Whitmore, and Kruse, with the assistance of a large number of amateur operators making aural measurements of signal strength, concluded that fading is random and is caused by variations of absorption in the ionosphere.

In 1924, Pickard made a number of fading measurements between 500 and 1500 kc. He found slow fading with relatively small amplitude variations with a period on the order of hours during the day, and fast fading with large changes in amplitude with periods on the order of seconds during the night. By noting the fading on two spaced antennas he found that the fading became uncorrelated with an antenna spacing of more than 600 meters. He made a number of good suggestions to alleviate the harmful effects of fading, such as automatic volume control and single sideband. However, he was not as successful in deducing the cause of fading. He rejected De Forest's interference theory of fading as requiring too much ionization to produce a strong enough sky wave. He suggested that atmospheric weather would influence the collection of

ionization due to solar alpha particles, which would produce non-uniform streams of ionization. These streams would produce a varying absorption that would cause fading.

In 1925, Appleton and Barnett, operating at 770 kc over a 140-km path, found that during the daytime very little fading was caused by frequency modulating their signals by 16 kc. At night this frequency modulation produced very deep, regular nulls, which, when compared with the frequency shift, revealed that one ray path was reflected from a height of about 100 km. This experiment not only helped clarify one cause of fading, but was also a convincing proof of the existence of a reflecting ionized layer.

In 1926, Brown, Martin, and Potter, operating at 610 kc, observed selective fading that they attributed to interference between wave paths. They suggested that fading at a single frequency would be caused by motion of an interference pattern. With three antennas spaced 1/16th of a wavelength apart along and across the path of propagation, they found that fading was similar but showed gradients suggesting a pattern of interference bands moving across the direction of propagation.

While operating facsimile transmissions at 22 meters from New York to England, Eckersley in 1929 noted multipath delays of the order of 1 msec. He related magnetic storms to increased fading rates and noted that diversity reception gives about a 20-to-1 improvement in freedom from fading.

About this time, improvements in equipment made it possible to separate individual rays from a complex, ionospherically propagated signal. Gross separation was accomplished by using pulse transmissions and the magnetoionic components were separated by using polarized receiving antennas. Fading studies then tended to be split into two kinds. Those in which rays were separated measured irregularities and motion of the ionosphere, usually the lower layers. Continuous-wave experiments that recorded the instantaneous strength of the total signal on an antenna were more concerned with the practical effects of fading such as fading rate and depth of fading.

Briefly, the results of measurements of the fading of single components show that this kind of fading is random, following a Rayleigh

amplitude distribution. See for example, Khastgir and Ray [1940], Ratcliffe [1948]. The supposition that this kind of fading is caused by the horizontal motion of irregular clouds of ionization in the E region has led to a large number of experiments designed to measure this horizontal wind motion--the experiments of Pawsey [1935], Munroe [1948], and Banerji [1958] are typical.

The other category of fading studies, in which the present experiment is included, consists of measuring the fading of obliquely propagated, high-frequency signals, usually without separation of modes, as opposed to the low- and medium-frequency, vertical-incidence pulse measurements with which ionospheric winds are studied.

In 1947, Appleton and Beynon described the fading near the maximum observable frequency (MOF) for an oblique high-frequency signal. As the frequency approached the MOF, the fading was first random, corresponding to reception of the lower ordinary ray only. The fading next became periodic, with a relatively long period on the order of 30 sec. This result was explained as being due to interference between the ordinary and extraordinary components of the lower ray. Finally, fading speeded up with a period on the order of a small number of seconds, apparently as a result of the interference of the upper and lower rays of both the ordinary and extraordinary components. They deduced the path differences that led to this interference by calculating equivalent paths from ionograms using standard methods of transmission curves as in Bulletin 462 of CRPL.

In 1950, Khastgir and Das described rapid fading near the MOF similar to that of Appleton and Beynon in 1947 and also a slower, periodic fading of 2 to 10 cycles per minute, which they attributed to vertical movement of the order of 3 to 4 meters/sec of the one- and two-hop F modes.

Periodic fading is generally considered a rather special and occasional effect, with practical communicators usually considering that fading generally follows a random amplitude-probability distribution. In 1951, Van Wambeck and Ross studied diversity reception in the frequency range 7 to 16 Mc over a 900-mile path. They found that improvement in reduction of fading could be gained by separating their antennas

up to about 60 meters, either along or across the path of propagation. Beyond this there was little further improvement. Ladner and Stoner, in a handbook published in 1950, suggest optimum spacings of 300 - 400 meters for space-diversity reception.

The manual for the R-390A/URR, a commonly used military receiver, suggests an optimum separation of 180 meters for space-diversity antennas. Both of these agree with Van Wambeck and Ross in that they mention no preferred relative position for the antennas.

In 1957, Grisdale, Morris, and Palmer performed extensive fading measurements on various oblique paths between 6 and 18 Mc. They found that the signal ampltude followed a Rayleigh distribution, and that the space correlation of the signal strength fell off in a Gaussian manner. Defining structure size as the distance along the ground between points at which the correlation falls to 0.61, they found that structure size was inversely correlated with path length. In particular, they found structure sizes of 300 meters for the path between New York and Great Britain, 210 meters for the path from Delhi to Great Britain, and 150 meters for the path from Australia to Great Britain. They found that these results were independent of frequency.

In 1958, King measured fading between 16 and 2000 kc for obliquely propagated signals. He found that the fading rate in maxima per hour is given by the expression $0.30\, f(kc) \cos i$, where i is the angle of incidence on the ionosphere. He found the fading to be random, caused by possibly flat, circular blobs in the ionosphere that could be described by an autocorrelation function. He did not believe fading to be caused by a constant pattern moving over the ground. In 1960, Singh and Simha performed a similar experiment between 10 and 18 Mc over oblique paths. They found the same expression for the fading rate in maxima per hour.

In 1958, Hedlund and Edwards studied the fading of the vertical and horizontal polarized components of short (100-μsec) pulses transmitted by the F layer over a 1000-mile path at 13 Mc. They found a negative correlation between the fading of the two components and a fading period of the order of 1 min. They attributed this fading to interference between the magnetoionic components of the rays.

Hayden [1961] shows the corrugation of the equiphase surfaces resulting from the interference of two rays coming from slightly different directions. He reports direction-of-arrival measurements on a 5-Mc signal propagated over a distance of 450 km from Columbus, Ohio, to Urbana, Illinois. Using pulse-techniques he shows that E-layer rays have an rms deviation about their mean bearing of 1.6 deg, while the mean bearing is 0.6 deg from the great-circle bearing. He shows that one-hop F rays have a mean deviation of about 2 deg to the north of the great-circle path with an rms deviation about the mean of 4.8 deg. When it was possible to separate the extraordinary from the ordinary components of the one-hop F rays, it was found that the ordinary component shows a definite bias to the north of the great circle while the extraordinary component shows a definite bias to the south, as predicted by the magnetoionic theory. He shows some interesting records taken on the Wullenweber direction-finding antenna. The 10-Mc transmissions from WWV are shown to fluctuate by 30 or 40 deg as the MOF drops through the operating frequency in the evening.

Bowhill [1961] reports an experiment using pulse transmissions at 16 Mc from Ceylon to England, a distance of 8700 km. He finds that the fading of individual short pulses is highly correlated on space diversity antennas 180 meters apart in a line perpendicular to the direction of propagation. He suggests that, when there is only one mode of propagation present, the fading of a cw signal is due to irregularities in the reflecting layer, but when the propagation is complex, with many orders of reflection present, the fading of a cw signal is due principally to phase interference between the orders of reflection.

In 1962, Balser and Smith studied the fading of short (35-μsec), high-frequency pulses transmitted over a 1566-km path. They found that the amplitude-distribution functions fit the Rayleigh distribution. The median fading time for one-hop paths was on the order of 20 sec, often more. They found that the space-correlation distances for the individual rays averaged around 40 wavelengths. Identification of the propagating modes was made by use of synchronized oblique pulse sounders covering the range of 1 to 25 Mc.

APPENDIX B. DERIVATION OF FADING-PATTERN PARAMETERS

Fading-pattern parameters have been derived from a description of the elevations and bearings of two interfering plane waves. The coordinates of a plane wavefront as seen by an observer at the origin are defined in Fig. 2. The range to the nearest point on the wave is ρ, the bearing is θ and the elevation is η. $\eta' = 90 \text{ deg} - \eta$ is introduced in order to conform to the usual spherical coordinates. As is shown in any standard text on analytic geometry, for example Sisam [1946], the point P is described in rectangular coordinates by

$$x = \rho \sin \eta' \cos \theta \qquad y = \rho \sin \eta' \sin \theta \qquad z = \rho \cos \eta'$$

The direction cosines of the line OP are

$$\cos \alpha = \frac{x}{\rho} \qquad \cos \beta = \frac{y}{\rho} \qquad \cos \gamma = \frac{z}{\rho}$$

or, since $\sin \eta' = \cos \eta$ and $\cos \eta' = \sin \eta$ the direction cosines of OP are

$$\begin{aligned} A &= \cos \alpha = \cos \eta \cos \theta \\ B &= \cos \beta = \cos \eta \sin \theta \\ C &= \cos \gamma = \sin \eta \,. \end{aligned} \tag{9}$$

The equations of two plane wavefronts of different directions are

$$\begin{aligned} \rho_1 &= xA_1 + yB_1 + zC_1 \quad \text{and} \\ \rho_2 &= xA_2 + yB_2 + zC_2 \,. \end{aligned} \tag{10}$$

The intersection of these two planes defines a line. If the two wavefronts are considered to have the same electrical phase, a plane of maximum field strength is generated by the motion of their line of intersection as the wavefronts move forward. The line of intersection is defined by the simultaneous equations

$$A_1x + B_1y + C_1z = \rho$$

and

$$A_2x + B_2y + C_2z = \rho \qquad (11)$$

where the wavefronts are arbitrarily assumed to be equidistant from the origin.

The equation

$$A_1x + B_1y + C_1z + \rho + k(A_2x + B_2y + C_2z + \rho) = 0$$

defines a family of planes all of which contain the line defined in Eq. (11); k is chosen to satisfy one additional point and thus define one plane of the family. For simplicity, the point chosen is the origin and $k = -1$. Therefore the plane of maximum field strength generated by the forward motion of the two wavefronts is defined by the equation

$$(A_1-A_2)x + (B_1-B_2)y + (C_1-C_2)z = 0.$$

The intersection of this plane with the ground $(z = 0)$ defines a line of maximum field strength as observed on the antenna array of the present experiment. The equation

$$(A_1-A_2)x + (B_1-B_2)y = 0 \qquad (12)$$

gives the null direction but not the null spacing of an interference fading pattern.

$$y = -\frac{(A_1-A_2)}{(B_1-B_2)}x = mx,$$

or, as defined in Fig. 3, and using values from Eq. (9)

$$\Phi_A = \tan^{-1} m + \frac{\pi}{2}$$

$$\Phi_A = -\tan^{-1}\left[\frac{\cos\eta_1 \cos\theta_1 - \cos\eta_2 \cos\theta_2}{\cos\eta_1 \sin\theta_1 - \cos\eta_2 \sin\theta_2}\right] + \frac{\pi}{2},$$

which is the same as Eq. (5).

To find the spacing between signal maxima, one point in the next parallel signal maximum, as observed at the ground, must be obtained. This adjacent signal maximum is defined by the intersection of one of the original wavefronts with a wavefront advanced one wavelength from the other original one.

$$A_1x + B_1y + C_1z = \rho$$

$$A_2x + B_2y + C_2z = \rho - \lambda \tag{13}$$

Let $z = 0$, and $\rho = 0$; then

$$B_2y - B_1 \frac{A_2}{A_1} y + \lambda = 0$$

$$y_1 = \frac{-A_1\lambda}{A_1B_2 - B_1A_2}, \qquad x_1 = \frac{+B_1\lambda}{A_1B_2 - B_1A_2}.$$

The spacing between signal maxima is given by the distance between the point (x_1, y_1) and the line

$$(A_1-A_2)x + (B_1-B_2)y = 0.$$

$$D = \frac{(A_1-A_2)x_1 + (B_1-B_2)y_1}{\left[(A_1-A_2)^2 + (B_1-B_2)^2\right]^{1/2}}$$

$$D = \frac{\frac{(A_1-A_2)B_1\lambda}{A_1B_2-B_1A_2} - \frac{(B_1-B_2)A_1\lambda}{A_1B_2-B_1A_2}}{\left[(A_1-A_2)^2 + (B_1-B_2)^2\right]^{1/2}}$$

$$D = \lambda \Big/ \left[(A_1-A_2)^2 + (B_1-B_2)^2\right]^{1/2}$$

and from Eq. (9)

$$D = \lambda \Big/ \left[(\cos\eta_1 \cos\theta_1 - \cos\eta_2 \cos\theta_2)^2 + (\cos\eta_1 \sin\theta_1 - \cos\eta_2 \sin\theta_2)^2\right]^{1/2}$$

APPENDIX C. COMPLEXITY OF VERY LONG PATH, ONE-HOP MODES

The technique of ray tracing and the use of step-frequency sounders demonstrate some interesting phenomena involved in the propagation of waves to extreme one-hop ranges, such as from Hawaii to Stanford, 3741 km.

At 1300 PST on 24 April 1963, vertical-incidence ionograms were obtained at Hawaii and Stanford. Using the method of Croft and Gregory [1963], computations using the data from the ionograms were performed that described the trajectories of rays leaving the transmitter in ½-deg increments and also the trajectories of all rays reaching the receiver. The results of the first computation appear in Fig. 36, which, incidentally, was plotted in about 15 min by a machine connected to the computer. The bending of rays in the E region resulted in the darker area at a height of about 120 km. Figure 37 is a simplified reproduction of Fig. 36 that also shows the specific rays reaching the receiver. Note that these rays follow paths separate from the bulk of the energy, shown by the shaded areas. Figure 38, which shows ground range as a function of take-off angle for the rays of Fig. 36, aids in the interpretation of these results. It shows that most of the energy reflected from the E region comes to earth at about 2400 km and most of that from the F region returns at a range of about 3300 km. The first two (lower-angle) rays reaching the receiver at 3741 km can be considered a transition between E and F rays, influenced strongly by partial bending in the E region. The third ray is a typical F-layer upper or Pederson ray. One would expect, and indeed the computer results predict, that the two lower-angle rays would arrive close together in time, followed after some delay by the third ray.

Figure 39 shows a portion of an oblique step-frequency ionogram taken at the same time as the data for the previous figures. It clearly shows two pulses at 17.8 Mc close together in time of arrival, followed, after additional delay, by a third.

Such effects as described above demonstrate the frequent difficulty encountered in the routine examination of oblique step-frequency

ionograms. Since it is not practical to conduct such an analysis for large amounts of data, only those oblique ionograms that are relatively unambiguous are analyzed.

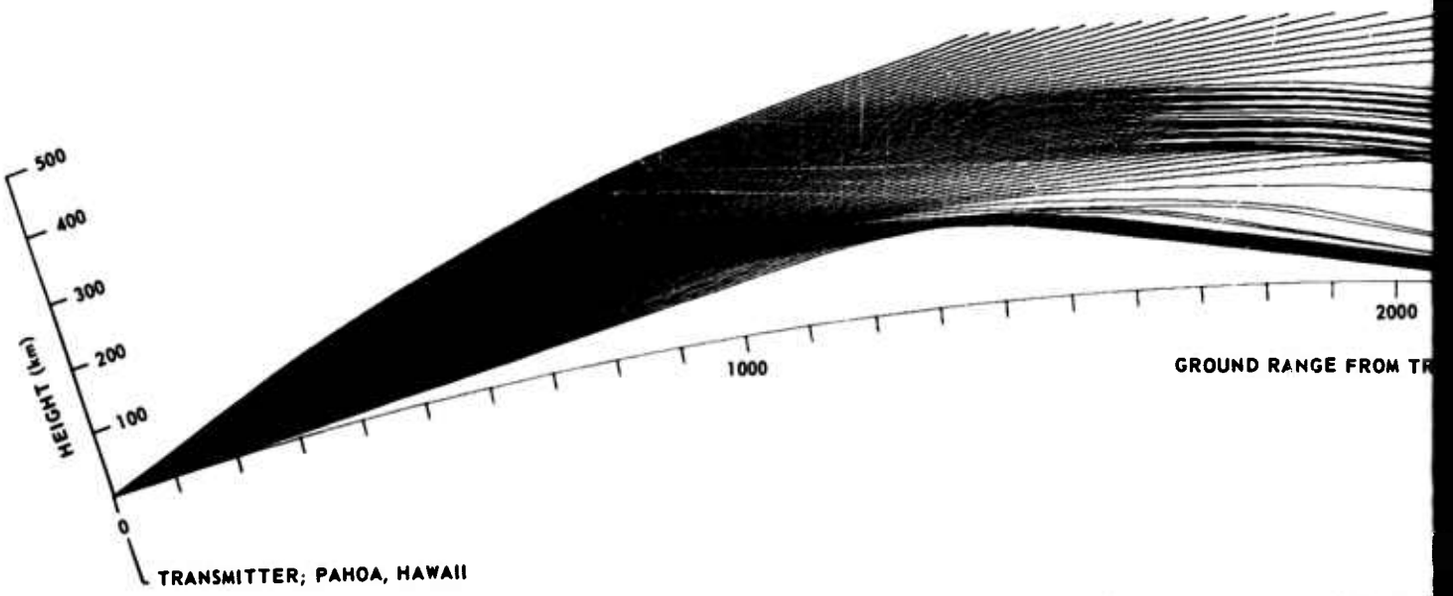

Fig. 36. RAY TRAJECTORI

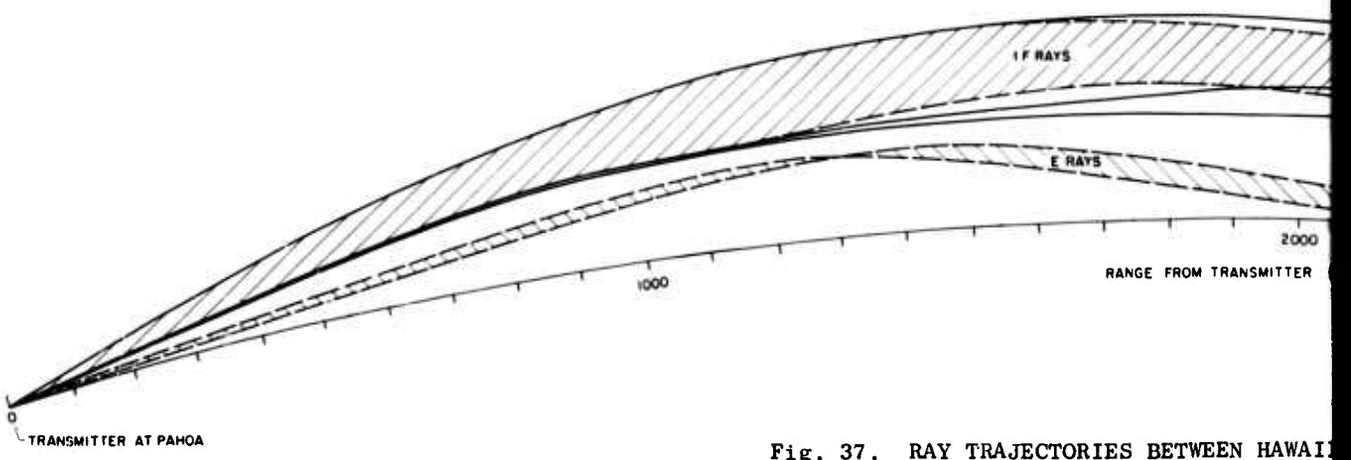

Fig. 37. RAY TRAJECTORIES BETWEEN HAWAI

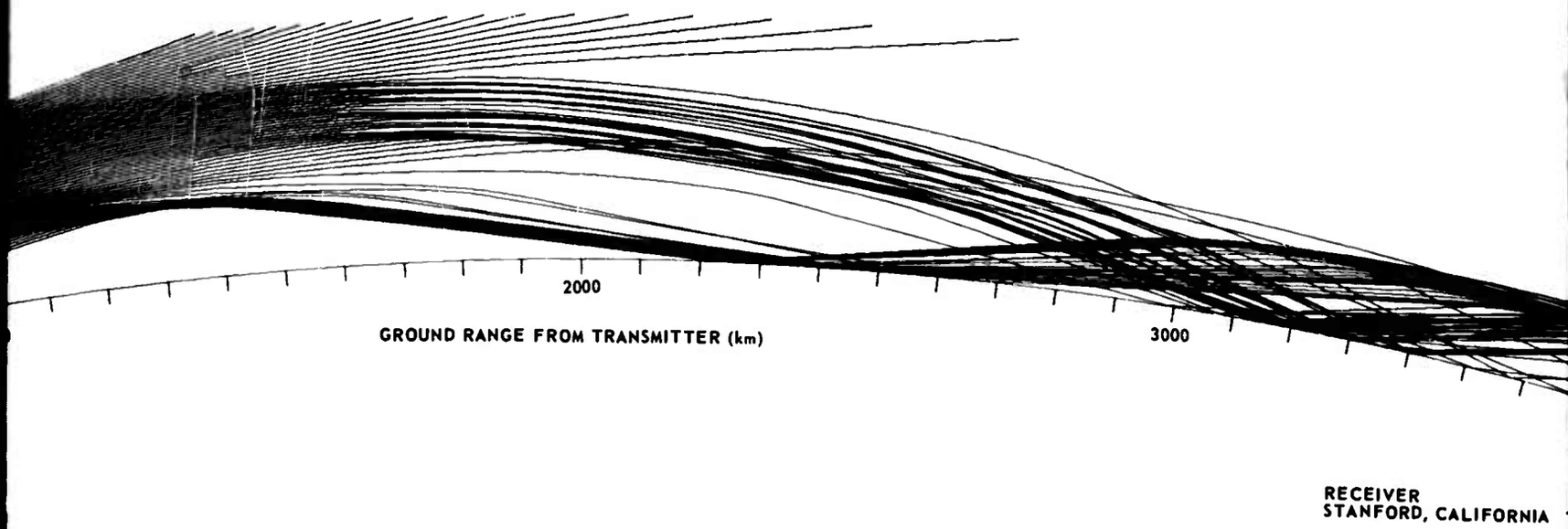

Fig. 36. RAY TRAJECTORIES

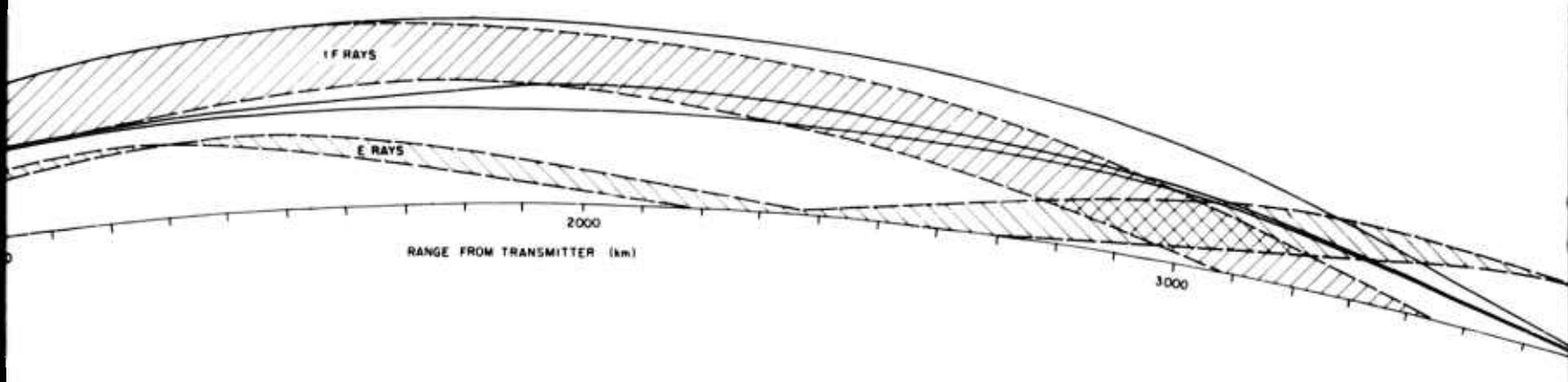

Fig. 37. RAY TRAJECTORIES BETWEEN HAWAII AND STANFORD

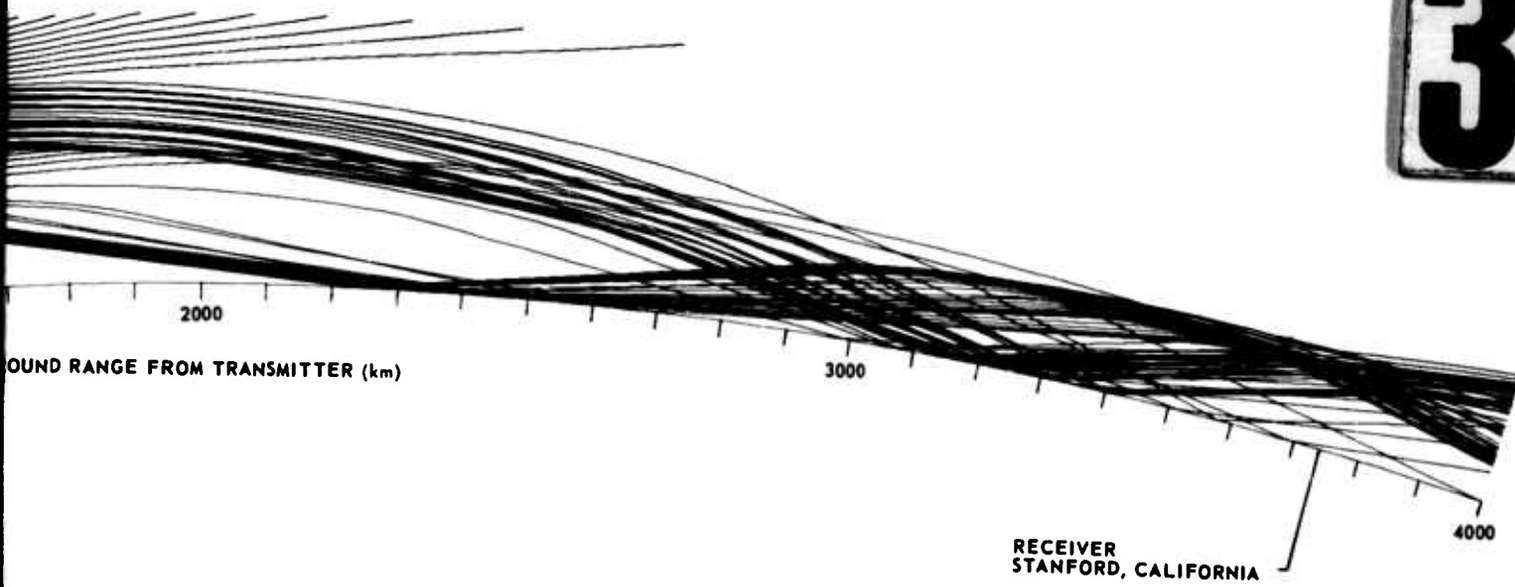

OUND RANGE FROM TRANSMITTER (km)

. RAY TRAJECTORIES

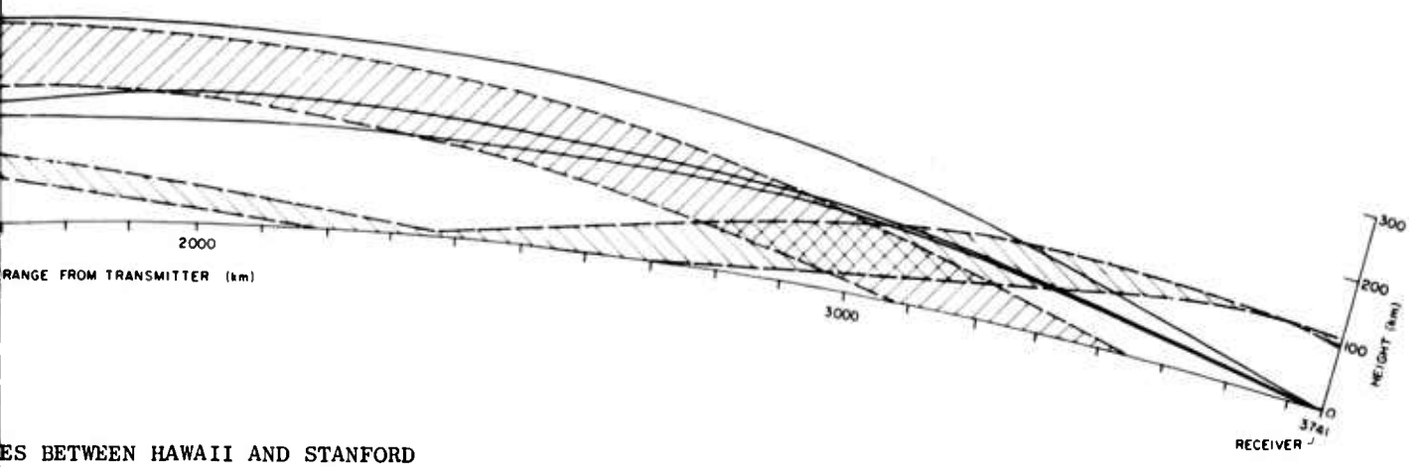

RANGE FROM TRANSMITTER (km)

ES BETWEEN HAWAII AND STANFORD

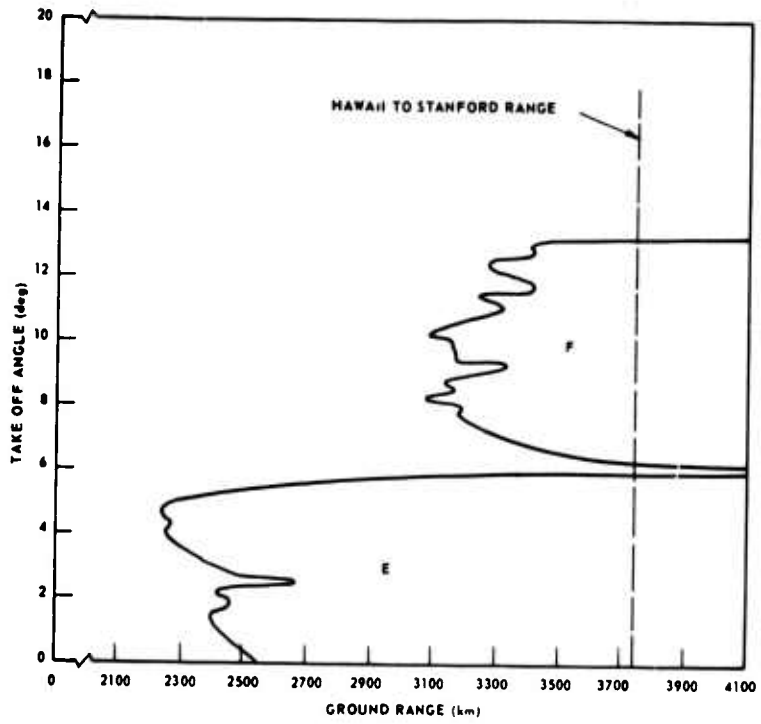

Fig. 38. TAKE-OFF ANGLE VS GROUND RANGE FOR RAYS OF FIG. 36.

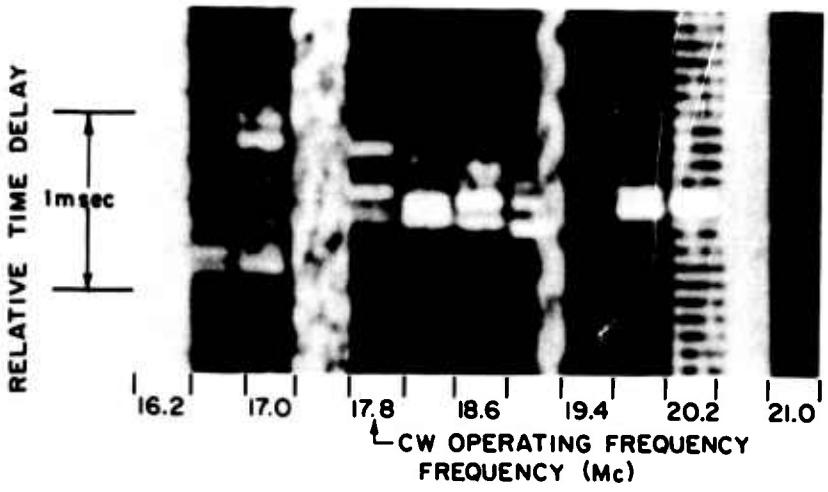

Fig. 39. PORTION OF OBLIQUE IONOGRAM.

BIBLIOGRAPHY

Appleton, E. V., and M. A. F. Barnett, "Local Reflection of Wireless Waves from the Upper Atmosphere," Nature, 115, pp. 333-334. 1925.

Appleton, E. V., and W. J. G. Beynon, "The Application of Ionospheric Data to Radio Communication Problems," PT II, Proc. Phys. Soc., 59, pp. 58-76, 1947.

Balser, M., and W. B. Smith, "Some Statistical Properties of Pulsed Oblique HF Ionospheric Transmissions," J. of Res. of the Nat. Bur. of Stds., Radio Propagation, 66D, 6, pp. 721-730, Nov-Dec 1962.

Banerjee, S. S., and G. Mukerjee, "Fading of Short Wave Radio Signals and Spaced Diversity Reception-Part I," Philo. Mag., 39, p. 697, 1948.

Banerji, R. B., "Method of Measuring Ionospheric Winds by Fading at Spaced Receivers," J. Atmos. Terr. Phys., 12(4), pp. 248-257, 1958.

Bixby, L. H., "Calculation of High Frequency Radio Field Intensity Over a 4000 Km Ionospheric Path," Radio Propagation Laboratory, Stanford University, Stanford, Calif., May 15, 1953.

Booker, H. G., J. A. Ratcliffe, and D. H. Shinn, "Diffraction From an Irregular Screen With Applications to Ionospheric Problems," Roy. Soc. Philo. Trans., 242A, pp. 579-609, 12 Sep 1950.

Bowhill, S. A., "Diversity Effects in Long Distance High Frequency Radio Pulse Propagation," J. of Res. of the Nat. Bur. of Stds., 65D, 3, pp. 213-223, May-Jun 1961.

Bramley, E. N., "Directional Observations on H.F. Transmissions Over 2100 Km," Proc. IEE, 103B, pp. 295-300, May 1956.

Brown, R., D. K. Martin, and R. K. Potter, "Some Studies in Radio Broadcast Transmission," Bell Sys. Tech. J., 5, pp. 143-213, 1926.

Budden, K. G., Radio Waves in the Ionosphere, Cambridge University Press, Cambridge, England, 1961.

Croft, T. A. and L. Gregory, "A Fast, Versatile Ray-Tracing Program for IBM 7090 Digital Computers," Rept SEL-63-107 (TR No. 82), Stanford Electronics Laboratories, Stanford, Calif., Oct 1963.

Davies, K., J. M. Watts, and D. H. Zacharisen, "A Study of F_2 Layer Effects as Observed With a Doppler Technique," J. Geophys. Res., 67, 2, pp. 601-609, Feb 1962.

DeForest, L., "Recent Developments in the Work of the Federal Telegraph Company," Proc. IRE, 1, Pt 1, pp. 37-51, 1913.

Dellinger, J. H., L. E. Whittemore, and S. Kruse, "A Study of Radio Signal Fading," Sci. Papers of NBS, 19, pp. 193-230, 1923.

Eckersley, T. L., "An Investigation of Short Waves," JIEE, 67, pp. 992-1032, 1929.

Fenwick, R. B., and O. G. Villard, Jr., "A Test of the Importance of Ionosphere--Ionosphere Reflections in Long Distance and Around the World High Frequency Propagation," J. Geophys. Res., 68, 20, pp. 5659-5666, 15 Oct 1963.

Fenwick, R. C., "On the Doppler Shifts of Standard-Frequency Signals Transmitted Via the Ionosphere," TR No. 13, Contract Nonr 225(33), Stanford Electronics Laboratories, Stanford, Calif., Jun 1960.

Fenwick, R. C., and O. G. Villard, Jr., "Continuous Recordings of the Frequency Variation of the WWV-20 Signal After Propagation Over a 4000 Km Path," J. Geophys. Res., 65, 10, pp. 3249-3260, Oct 1960.

Grisdale, G. L., J. G. Morris, and D. S. Palmer, "Fading of Long Distance Radio Signals and a Comparison of Space and Polarization Diversity Reception in the 6-18 Mc/s Range," Proc. IEE, 104B, pp. 39-51, 1957.

Hayden, E. C., "Propagation Studies Using Direction Finding Techniques," J. of Res. of NBS, 65 D, 3, pp. 197-212, May-Jun 1961.

Hedlund, D. A., and L. C. Edwards, "Polarization Fading Over an Oblique Incidence Path," IRE Trans. on Antennas and Propagation, pp. 21-25, Jan 1958.

Kanellakos, D. P., "Origin and Location of Ionospheric Perturbations Affecting the Frequency and Bearing of H-F Radio Waves," Rept SEL-62-139 (TR No. 43), Stanford Electronics Laboratories, Stanford, Calif., Nov 1962.

Kanellakos, D. P., K. L. Chan, and O. G. Villard, Jr., "On the Altitude at Which Some Solar-Flare-Induced Ionization is Released," J. Geophys. Res., 67, 5, pp. 1795-1804, May 1962.

BIBLIOGRAPHY (Continued)

Khastgir, S. R., and P. M. Das, "Periodic Fading of Short-Wave Radio Signals," Proc. Phys. Soc., 63B, 371, pp. 924-930, 1950.

Khastgir, S. R., and A. K. Ray, "On the Intensity Variations of the Down-Coming Wireless Waves From the Ionosphere," Indian J. Phys., 14, pp. 283-293, 1940.

King, J. W., "The Fading of Radio Waves Reflected at Oblique Incidence," J. Atmos. Terr. Phys., 12, pp. 26-33, 1958.

Ladner, A. W., and C. R. Stoner, Short Wave Wireless Communication, John Wiley, New York, 5th Ed., 1950.

Manning, L. A., Bibliography of the Ionosphere, (an Annotated Survey through 1960), Stanford University Press, Stanford, Calif., 1962.

Matsushita, S., "A Study of the Morphology of Ionospheric Storms," J. Geophys. Res., 64, 3, pp. 305-321, Mar 1959.

Munroe, G. H., "Short-Period Changes in the F Region of the Ionosphere," Nature, 162, pp. 886-887, 1948.

National Bureau of Standards, "Ionospheric Radio Propagation," NBS Circular 462, U. S. Govt. Printing Office, 25 Jun 1948.

Nupen, Wilhelm, "Bibliography on Ionospheric Propagation of Radio Waves (1923-1960)," Technical Note No. 84, Boulder Laboratories of the U. S. Nat. Bur. of Stds., 1960. U. S. Dept. of Commerce, OTS, Washington 25, D. C.

Pawsey, J. L., "Further Investigations of the Amplitude Variations of Downcoming Wireless Waves," Proc. Camb. Philo. Soc., 31, pp. 125-144, 1935.

Pickard, F. W., "Short Period Variations in Radio Reception," Proc. IRE, 12, pp. 119-158, 1924.

Ratcliffe, J. A., "Diffraction from the Ionosphere and the Fading of Radio Waves," Nature, 162, pp. 9-11, 3 Jul 1948.

Ratcliffe, J. A., The Magneto-Ionic Theory and its Application to the Ionosphere, London, Cambridge University Press, 1959.

Salaman, R. K., "Historical Survey of Fading at Medium and High Radio Frequencies," Technical Note No. 133, Boulder Laboratories of the U. S. Nat. Bur. of Stds., 1962. U. S. Dept. of Commerce, OTS, Washington 25, D.C.

BIBLIOGRAPHY (Continued)

Scott, J. C. W., "The Poynting Vector in the Ionosphere," Proc. IRE, 38, pp. 1057-1068, 1950.

Singh, B. N., and O. P. Simha, "The Variation of the Rate of Fading With Frequency," J. Atmos. Terr. Phys., 19, pp. 141-143, 1960.

Sisam, C. H., Concise Analytic Geometry, Henry Holt and Co., New York, 1946.

Van Wambeck, S. H., and A. H. Ross, "Performance of Diversity Receiving Systems," Proc. IRE, 39, pp. 256-264, 1951.

Waterman, A. T., and J. W. Strohbehn, "Reflection of Radio Waves from Undulating Tropospheric Layers," J. of Res. of the Nat. Bur. of Stds., Radio Propagation, 67D, 6, Nov-Dec 1963.

Wright, J. W., L. R. Wescott, and D. J. Brown, "Mean Electron Density Variations of the Quiet Ionosphere 4-June 1959," Technical Note No. 40-4, Boulder Laboratories of the U. S. Nat. Bur. of Stds., May 1961.

DISTRIBUTION LIST
for
PROJECT TEPEE REPORTS

(Revised by ONR August 1963)

No. of Copies

Air Force Activities

Headquarters
North American Air Defense Command
Ent AFB
Colorado Springs 12, Colo.
1 Attn: NELC-AP

Air Force Unit Post Office
Los Angeles 45, Calif.
1 Attn: SSD (SSOCE)

Foreign Technology Division
Wright-Patterson AFB, Ohio
1 Attn: TDEED, Mr. W. L. Picklesimer
1 Attn: TDATA, Mr. G. A. Long, Jr.
1 Attn: TDCE, Mr. M.S.J. Graebner

Hq., AFCRL
L. G. Hanscom Field
Bedford, Mass.
1 Attn: Dr. G. J. Gassman(CRUP)
1 Attn: Mr. W. F. Ring(CRUI)

HQ., USAF
Office of Asst. Chief of Staff,
Intelligence
Policy and Programs Group, AFNINC
1 Washington 25, D.C.

Hq., Rome Air Dev. Center
AFSC, USAF
Griffiss AFB, N.Y.
1 Attn: RAUEL-3, Mr. G.R. Weatherup

Army Activities

CO, U.S.Army Munitions Command
Picatinny Arsenal
Dover, N.J.
1 Attn: SMUPA-VA6

CO, U.S.Army Materiel Command
Washington 25, D.C.
1 Attn: AMCRD-D

No. of Copies

* CO, U.S.Army Electronics
Research Unit
P.O. Box 205
1 Mt. View, Calif.

Navy Activities

Chief of Naval Operations
Dept. of the Navy
Washington 25, D.C.
1 Attn: Op-723E
1 Attn: Op-07TE

CO and Director
U.S.Navy Electronics Lab
San Diego, Calif. 92152
1 Attn: Library

Director, Special Projects
Dept. of the Navy
Washington 25, D.C.
1 Attn: Code SP-204
1 Attn: Code SP-2041

Commander
U.S. Naval Air Test Ctr.
Weapons Systems Test Div.
Patuxent River, Md.
1 Attn: Code 32
1 Attn: Code 323

Commander
Pacific Missile Range
Pt. Mugu, Calif.
1 Attn: Code 3215

Commander
Naval Missile Center
Pt. Mugu, Calif.
1 Attn: Code NO3022

Director, Naval Res. Lab
Washington 25, D.C.
1 Attn: Code 5320, Mr. J. M.
Headrick
1 Attn: Code 2027

*Classified only.

No. of Copies

CO, U.S.Naval Ordnance Test Unit
Atlantic Missile Range
Patrick AFB, Fla.
1 Attn: SPPO02

Department of Defense Activities

*Defense Documentation Center
Cameron Station
20 Alexandria, Va.

Director
Advanced Research Projects Agency
Washington 25, D.C.
1 Attn: Mr. Alvin Van Every

Director
Weapons Systems Evaluation Group
Office of the Director of Defense
Res. and Engineering
1 Washington 25, D.C.

Other

National Bur. of Standards
Boulder Labs
Boulder, Colo.
1 Attn: Mr. L. H. Tveten, 85.20

Director
National Security Agency
Ft. George G. Meade, Md.
1 Attn: C3/TDL

Raytheon Company
Box 155
1415 Boston-Providence Turnpike
Norwood, Mass.
1 Attn: Mr. L. C. Edwards

**HQ., AFCRL
Office of Aerospace Research
USAF, L. G. Hanscom Field
Bedford, Mass.

No. of Copies

Pickard and Burns, Inc.
103 Fourth Ave.
Waltham 54, Mass.
1 Attn: Dr. John C. Williams, Res. Dept.

**USA Electronics Materiel Agency
Ft. Monmouth Procurement Office
Ft. Monmouth, N.J.

The RAND Corp.
1700 Main St.
Santa Monica, Calif.
1 Attn: Library

**Director, USAF Project RAND
Dept. of the Air Force
Hq., USAF, Wash.25,D.C.

Electronic Defense Labs
P.O. Box 205
1 ***Mt. View, Calif.

Rensselaer Polytechnic Inst.
Plasma Res. Lab
Troy, N.Y.
1 ***Attn: Mr. E. Howard Holt, Director

Electro-Physics Labs
AFC Electronics Division
3355 Fifty-Second Ave.
Hyattsville, Md.
1 Attn: Mr. W. T. Whelan

**Inspector of Naval Material
401 Water St.
Baltimore 2, Md.

*All requests for this report shall be approved by the Office of Naval Research, Field Projects Branch, Washington 25, D.C.

**When the document is classified, send a copy of the receipt form to this addressee.

***Unclassified reports only.

No. of Copies

General Electric Co.
Heavy Military Electronics Dept.
Syracuse, N.Y.
1 Attn: Mr. G. R. Nelson

**Rome Air Development Center
Griffiss AFB, Rome, N.Y.
Attn: Mr. W. L. Wasser
Contracting Officer

RCA, Aerospace Communications and Controls Division
Burlington, Mass.
1 Attn: Mr. J. Rubinovitz

**Hq., AFCRL
L. G. Hanscom Field
Bedford, Mass.

Inst. of Science and Technology
The University of Michigan
P.O. Box 618
Ann Arbor, Mich.
1 Attn: BAMIRAC Library

**Hq., Central Contract Management Region
Wright-Patterson AFB, Ohio

MIT - Lincoln Lab
Lexington 73, Mass.
1 Attn: Dr. J. H. Chisholm

**Navy Representative
MIT - Lincoln Lab
Lexington 73, Mass.

Westinghouse Electric Corp.
Air Arm Division
Box 746
Baltimore 3, Md.
1 Attn: Mr. David Fales

**Baltimore Air Procurement Office
c/o Westinghouse Electric Corp.
Box 1693, Baltimore 3, Md.
Attn: Mr. J. G. Green, AF
Contracting Officer

No. of Copies

University of California
Dept. of Mathematics
Berkeley 4, Calif.
1 Attn: Dr. Edmund J. Pinney

**CO, ONR Br. Office
1000 Geary St.
San Francisco 9, Calif.

Aero Geo Astro Corp.
13624 Magnolia Ave.
Corona, Calif.
1 Attn: Mr. A. W. Walters

**Inspector of Naval Material
929 So. Broadway
Los Angeles, Calif.

Dr. J. V. Harrington
Director, Center for Space Research
MIT, Bldg. 33-109
1 ***Cambridge, Mass.

Battelle Memorial Inst.
505 King Ave.
Columbus 1, Ohio
1 Attn: RACIC

(ACF Reports ONLY)
**Director, Advanced Res. Proj. Agency
Pentagon, Wash.25,D.C.

HRB Singer, Inc.
Science Park
P.O. Box 60
1 State College, Pa

**Inspector of Naval Material
10 N. 8th St.
Reading, Pa.

**When the document is classified, send a copy of the receipt form to this addressee.
***Unclassified reports only.

No. of
Copies

Astrophysics Res. Corp.
2444 Wilshire Blvd., Rm. 512
Santa Monica, Calif.
1 Attn: Dr. Alfred Reifman

**Inspector of Naval Material
292 So. Broadway
Los Angeles 15, Calif.

**When the document is classified, send a copy of the receipt form to this addressee.

UNCLASSIFIED